EUROPEAN ORGANIZATION FOR NUCLEAR RESEARCH
European Laboratory for Particle Physics

Internal Note/ZDC
ALICE reference number
ALICE-INT-2002-08 V 1.0
Institute reference number

Date of last change
2002-03-05

Centrality measurement in the ALICE experiment with the Zero Degree Calorimeters

Author:

C. Oppedisano

Università degli Studi di Torino, Torino, Italy

Università degli Studi di Torino
Facoltà di Scienze M.F.N.
Dipartimento di Fisica Sperimentale

Dottorato di Ricerca in Fisica
XIV Ciclo

Centrality measurement in the ALICE experiment with the Zero Degree Calorimeters.

Tesi di dottorato
di
Chiara Oppedisano

Relatore:
Prof. M. Gallio

Contro-Relatore:
Dott. A. Morsch

Co-Relatore:
Dott. E. Scomparin

Coordinatore:
Prof. R. Garfagnini

Dicembre 2001

A Mate,
Alberto
e a nonna Anna,
che racconta
della sua nipote
“scienziata”.

Acknowledgements

I would like to thank Federico Carminati, Jiri Chudoba and Massimo Masera for all the help they gave me, for the useful discussions and for the patience they had in answering the great amount of my questions (starting from basic doubts like "What is C++ and what can I do with it?").

A special thanks goes to Andreas Morsch, whose help has been fundamental for this work. I would also like to thank him since he accepted to be the external member of the committee of my thesis.

Ed infine...

Devo ringraziare di cuore tutti (ma proprio tutti!) i "Pinottiani" che hanno reso piacevole il lavoro anche durante quest'ultimo faticoso periodo.

Ringrazio Mauro Gallio per il tempo che ha sempre trovato, tra i suoi mille impegni urgenti, per rispondere a tutte le mie domande e per il costante incoraggiamento a non disperare quando mi sentivo persa in un labirinto di oggetti e puntatori (nonstante la sua scarsa fiducia iniziale in tutto ciò che è scritto in C++!).

Grazie ad Enrico per avermi guidato ed aiutato nel lavoro, per avermi insegnato molte cose e per aver sempre valorizzato il mio lavoro. Credo di doverti ringraziare anche per avermi fatto tuffare a capofitto nell'oceano sconfinato del C++...perchè alla fine non è poi cosí male (basta avere fede e non farsi troppe domande quando tutto funziona!).

Ringrazio Emilio Chiavassa per gli utilissimi consigli e per l'incoraggiamento che mi ha dato quando mi sembrava tutto molto difficile.

Grazie di cuore a Beppe per aver ascoltato tutti i miei sfoghi (scientifici e non!) e per avermi trasmesso il suo entusiasmo per gli esperimenti "raffazzonati"!

Un grazie grandissimo a Roberta per l'incoraggiamento e l'instancabile ottimismo che mi ha regalato in questi mesi, anche quando io ero insopportabile, acida e musona. La tua amicizia e la tua allegria hanno riempito le mie giornate e mi hanno incoraggiato tantissimo!

Come non ringraziare l'altro mio collega d'ufficio, nonchè compagno di questa lunga avventura?! Grazie Alessandro, per il tuo sorriso e per l'ironia con cui abbiamo vissuto la scrittura della tesi...anche se non proprio in coincidenza di orari!

Grazie Federica, per essermi stata vicina e per avermi accolto nella tua comoda poltrona di velluto marrone nelle mie pause di cinque minuti degli ultimi giorni! Ringrazio Pietro per avermi dimostrato l'anno passato che tutto è possibile quando si tratta di scrivere la tesi!

Grazie ad Alfredo per aver illuminato la via di ritorno verso casa, la sera, alle otto passate con la mia sfrecciante bicicletta rossa! Ringrazio anche Nora, Anna ed Ermanno.

Grazie infine a Pier Luca, compagno di nuotate, a Giovanna e ai suoi "pasticciotti", ad Alberto e Raffaella per l'allegria con cui attraversano il nostro ufficio! Grazie a Paolo "Merò" per tutti i TCP/IP che mi ha chiesto! Grazie a Luisella anche se passa a trovarci troppo raramente!

Ringrazio Paolo Merlatti per le utili discussioni nelle quali mi ha fatto capire che è inutile disperare (anche se non ho colto proprio bene il succo del discorso e mi sono agitata un sacco lo stesso!). Grazie a Francesco ed Elisabetta perchè condividere è bello (però sarebbe stato ancora più bello se Francesco avesse condiviso con noi almeno uno dei suoi 35 capitoli!).

Sommario

L'esperimento ALICE al collider LHC sarà dedicato allo studio della materia nucleare in collisioni nucleo-nucleo. L'obiettivo della fisica degli ioni pesanti è lo studio della transizione di fase dalla materia adronica ordinaria ad un plasma in cui quark e gluoni sono liberi. La teoria QuantoCromoDinamica (QCD) prevede che la formazione di tale stato avvenga alle elevate densità di energia raggiunte nelle collisioni centrali di ioni pesanti accelerati ad energie ultra-relativistiche.

La densità di energia può essere stimata misurando la centralità della collisione. All'esperimento ALICE la centralità della collisione sarà determinata in maniera indipendente da rivelatori diversi. L'osservabile più direttamente correlata alla geometria della collisione è l'energia trasportata in avanti dai nucleoni spettatori. Tale energia sarà misurata da un sistema di calorimetri posti a zero gradi rispetto all'asse del collider, i cosiddetti calorimetri a zero gradi (ZDC).

L'accettanza e la risoluzione di questi rivelatori è stata studiata in dettaglio con simulazioni, considerando tutti i fattori che potrebbero in linea di principio incidere sulla rivelazione degli spettatori. Per effettuare questi studi è stato sviluppato un nuovo codice basato su tecniche "Object-Oriented" che fornisce uno strumento per la simulazione, la ricostruzione e l'analisi per gli ZDC. Le prestazioni dei rivelatori, inseriti nell'apparato sperimentale complessivo dell'esperimento ALICE, sono state studiate utilizzando il codice sviluppati ed i risultati ottenuti sono ampiamente discussi.

Questo lavoro propone inoltre due metodi per la stima del parametro d'impatto e del numero di nucleoni partecipanti dall'energia misurata nei calorimetri a zero gradi. I risultati ottenuti con i due metodi sono accordo; infatti in entrambi i casi i valori simulati del parametro d'impatto sono riprodotti con un'accuratezza inferiore al 9% su tutto l'intervallo di centralità. La risoluzione sul parametro d'impatto e sul numero di partecipanti è stata valutata anche in funzione della centralità ed è emerso che si ottiene una migliore risoluzione sugli eventi centrali dalla ricostruzione del numero di partecipanti piuttosto che dalla stima del parametro d'impatto. È stata anche investigata la dipendenza dei risultati ottenuti dal modello usato per descrivere l'interazione, verificando che la misura della centralità non è in prima approssimazione influenzata dal modello utilizzato.

Abstract

ALICE is a dedicated heavy ion experiment, designed to study the physics of strongly interacting matter in nucleus-nucleus collisions at the LHC collider, foreseen to start in 2006. The aim of heavy ion physics is to study the phase transition from hadronic matter to a plasma of quarks and gluons, the so called Quark Gluon Plasma (QGP). Statistical QCD predicts that this transition occurs at the extreme energy density values reached in the collisions of heavy ions at ultra relativistic energies.

The energy density can be estimated through a measurement of the centrality of the collision. This latter quantity will be measured by ALICE in different independent ways, by means of different detectors. The measurable quantity most directly correlated to the geometry of the collision is the energy carried in the forward direction by spectator nucleons. This energy will be measured by means of a system of calorimeters placed at zero degree with respect to the LHC axis, the Zero Degree Calorimeters (ZDC).

The acceptance and the resolution of these detectors have been studied in detail through simulations, taking into account all the factors that could affect spectators detection. A new code for the simulation of the ZDC in the frame of the ALICE experimental setup has been developed with Object-Oriented techniques. This code provides a tool for simulation, reconstruction and analysis for the ZDC. Using this code the physics performances of the detector in the overall ALICE setup have been studied and the obtained results are reported.

For the evaluation of the impact parameter and of the number of participant nucleons from the energy measured in the ZDC two different methods are proposed and discussed. It is shown that the results obtained with these two methods are in relatively good agreement; in fact in both cases the simulated value of the impact parameter is reproduced within 9% over the whole centrality range. The resolution on the impact parameter and on the number of participants has been calculated as a function of centrality and it has been pointed out that a better resolution for the most central events is obtained from participants reconstruction rather than from the estimate of the impact parameter. The dependence of the results on the model used to describe the interaction has been evaluated and it has been verified that the centrality estimation is not strongly affected by the used model.

Contents

List of Figures

List of Tables

Introduction

The aim of heavy ion physics is the study of nuclear matter at the extreme energy density values reached in the collisions of heavy nuclei accelerated at ultra-relativistic energies. QCD theory predicts that if the macroscopical variables describing the interacting system reach values higher than the calculated critical ones ($\epsilon_c \sim 1-3$ GeV/fm^3 and T$_c \sim$ 150-200 MeV), the hadronic matter will melt into a new state in which its partonic constituents are no more confined by color interaction. This deconfined state is the so called Quark Gluon Plasma (QGP).

A coherent picture of the collision dynamics has emerged from fixed target experiments with heavy ions performed at the CERN SPS synchrotron. Results collected by the SPS experiments (namely NA44, NA45, NA49, NA50, WA97/NA57 and WA98) in more than 10 running years, have led to the conclusion that a new state of matter has been produced in Pb-Pb collisions at 158 A GeV. The properties of this state are not reproduced by ordinary hadron dynamics but are rather consistent with a deconfined state in which quarks and gluons are free.

The conditions for the formation and the study of QGP are more favorable at collider experiments, where the available energy in the center of mass is strongly increased. The colliders will allow the study of strongly interacting matter in a qualitatively new region characterized by very high energy densities. The Relativistic Heavy Ion Collider (RHIC) at Brookhaven Laboratory is the first heavy ion collider, presently running at its full designed collision energy, accelerating Au nuclei at 200 A GeV. Relative to SPS, the center of mass energy is improved of a factor 10. The CERN Large Hadron Collider (LHC), foreseen to start in 2006, will accelerate Pb ions at 2.76 A TeV. The improvement in center of mass value is about a factor 14 with respect to RHIC. ALICE (A Large Ion Collider Experiment) is the dedicated heavy ion experiment at LHC.

Nucleus nucleus interactions can be characterized through the centrality of the collision. The more central is the collisions, the higher is the number of participant nucleons and, consequently, the energy density reached. Moreover, some QGP signatures should show a threshold behavior in the correlated observables as a function of the energy density, estimated through the centrality of the collision. The event by event determination of centrality of the collisions plays therefore a fundamental role in heavy ion physics. The forward energy carried by non interacting spectators is the measurable quantity most directly related to the centrality of the collision; in fact it allows a direct estimate of the number of participants. Spectators energy is measured by means of hadronic calorimeters placed at zero degrees with respect to the beam direction, the so called Zero Degree Calorimeters (ZDC).

This thesis concerns the ZDC detectors for the ALICE experiment. The ZDC project includes two hadronic calorimeters and an electromagnetic device. The magnetic elements of the LHC beam line, used to deflect circulating ion beams, will also separate spectator neutrons from protons. This allows the use of two distinct calorimeters for the measurement of non interacting energy. A third calorimeter will detect the electromagnetic energy carried by neutral particles produced in the collision.

The existent technical design for such devices has been reconsidered in order to improve the resolution on centrality achievable with a measurement of the zero degree energy. For this reason the rapidity range covered by the electromagnetic calorimeter has been changed. Detector performances have been carefully studied through numerical simulations in order to optimize their response. Test on prototypes with particle beams have then been performed at the CERN SPS accelerator and the obtained results have been compared to simulations in order to evaluate the reliability of these latter. From such comparisons it has come out that the simulations predict the correct beam energy dependence for detectors response and resolution.

Once the design of the ZDC system has been completed, it has emerged the need of simulations in the frame of the overall ALICE experimental setup; taking therefore into account all the detectors and the machine element that could in principle affect ZDC responses. For this purpose a new simulation package has been developed. It is conceptually inserted in the Object-Oriented framework designed by the ALICE collaboration for simulation, reconstruction and analysis. The necessity to migrate towards Object-Oriented techniques, due to the high amount of data to be processed and stored, allows the use of fundamental properties of the C++ implementation language like intrinsic modularity, reuse of code and maintanability. The developed simulation code has allowed the study of the ZDC performances and it has demonstrated that the proposed design for the ZDC system ensures a reliable estimation of the centrality of the collision.

Chapter 1 is dedicated to heavy ion physics. After a very brief description of the objectives and the methods of this research field, the probes used to investigate the system formed in the collision are described on the basis of SPS experimental results. First RHIC results on centrality dependence of charged particle multiplicity and transverse energy are presented. Then the improvements and the new physics aspects that will derive from increasing further the colliding beams energy are introduced. Finally an overview of the main ALICE detectors is given.

In chapter 2 the centrality determination with the ZDC is discussed. It is shown that this measurement does not depend strongly on the model used to describe the collision. In fact the number of participants nucleons as a function of centrality evaluated from the Glauber theory is in agreement with the one obtained by means of the HIJING event generator. The motivations that lead to quartz fibre calorimetry as detection technique are explained. The characteristics of the designed detector and their energy resolution are presented and the possibility to use the ZDC as a luminosity monitor is introduced. Then the achievable resolution on centrality is discussed. In principle two factors can affect this resolution: the intrinsical fluctuations in the number of participants at fixed impact parameter and the detector experimental resolution. The influence of these factors on centrality resolution is evaluated. Furthermore the measurement of the zero degree energy can also be strongly affected if not all spectators reach the hadronic ZDCs (that are placed at 116 m from the interaction point). Spectator losses can be due to magnetic fields of the beam line (for protons) and to the production of nuclear fragments (for both protons and neutrons). The effect of magnetic fields on spectator protons trajectories has been carefully studied. Concerning the nuclear fragmentation a model for its evaluation has been worked out and the obtained results are presented. Finally it is shown that the production of nuclear fragments introduces an ambiguity in centrality determination that can be solved using the information provided by the electromagnetic calorimeter.

The electromagnetic detector is the subject of chapter 3, where the studies done in order to optimize its response are presented. The results of the test beam performed on a prototype of the ALICE electromagnetic calorimeter are discussed.

In chapter 4 the code developed for simulation and reconstruction of the ZDC system is described. The general ALICE framework is introduced, then the architecture of the classes implemented for the ZDC is drawn and some general results obtained with this code are shown.

Chapter 5 provides the guidelines for the determination of the centrality of the collision with the ZDCs. Starting from simulated events, the results obtained reconstructing the global variables that characterize the event are shown. The accuracy that can be reached in the reconstruction of these variables is evaluated. Finally I will show that the ZDC can provide a reliable definition of centrality classes. These classes can be used for the study of the observables that are expected to follow a threshold behavior, such as quarkonia or multistrange particle production, to study the onset values for deconfinement.

Chapter 1

Heavy ion physics and the ALICE experiment

1.1 Ultra-relativistic heavy ion collisions: motivations and objectives

The main aim of ultra-relativistic heavy ion collisions is the study of strongly interacting matter at high energy densities. The theory that describes strong interactions, the quantum chromodynamics (QCD), is based on quarks intrinsic color charge. Quarks are confined to form hadrons by a binding potential that increases linearly with the quarks distance:

$$V_0(r) \sim \sigma r, \tag{1.1}$$

the string tensor σ accounts for the energy per unit separation distance. Hadrons are color singlet states of colored quarks; therefore ordinary nuclear matter is a color insulator.

In a medium of electric charges a transition from electric insulator to conductor occurs when the electric charge density is increased over a critical value. This is due to the Debye screening of the interaction potential between charges that shortens the interaction length. The Debye screening radius r_D depends on the medium charge density; once it becomes less than the atom binding radius, the electrons can move freely and the medium becomes a plasma of unbound electric charges [1]. In analogy to this transition, QCD predicts that for high nuclear densities color charge is screened and quarks are no longer confined into hadrons. The medium is then transformed from insulator to color conductor and hadronic matter turns into a plasma of deconfined quarks and gluons; this state is the so-called Quark-Gluon Plasma (QGP).

Therefore at sufficiently high color charge density the interaction potential between two quarks includes a screening term, becoming:

$$V(r) \sim \sigma r \left[\frac{1 - e^{-\mu r}}{\mu r}\right] \tag{1.2}$$

where the screening mass μ corresponds to the inverse of the Debye screening radius r_D Hadrons whose dimensions are of the order of the μ parameter are melted.

Primary objective of the ultra-relativistic heavy ion collisions is the production of the deconfined state, to study both the phase transition from hadron gas to QGP and the characteristics of the deconfined state theoretically predicted. Furthermore the QCD phase transition is the only one of the standard model within reach of experimental physics.

The field of heavy ion physics has also a cosmological interest, since the universe has undergone the inverse phase transition, from QGP to an hadron gas, about 10^{-5} s after the Big Bang. Global features of the universe like matter-antimatter asymmetry and large scale structure (that is to say galaxies distribution) could be correlated to the properties of this phase transition. There is also an astrophysical impact of heavy ion experiments; in fact at LHC the top energy will correspond to about 10^{17} eV in the laboratory reference system. These extreme energies may contribute to the understanding of cosmic ray interactions. Moreover heavy ion physics might be also of relevance for the understanding of neutron stars physics that depends on the nuclear equation of state, since their core is supposed to consists of cold nuclear matter at extreme densities.

1.2 QCD phase diagram

The theoretical basis for the QGP search is given by lattice-QCD calculations that predict a critical energy density value ϵ_c for the transition of the order of 1-3 GeV/fm^3. High energy densities can be obtained either by increasing temperature or the net baryon number density. The critical deconfinement temperature T_c at baryon chemical potential $\mu_B = 0$ is about 170 MeV [2, 3]. Therefore ultra-relativistic heavy ion collisions allow the exploration of the QCD phase diagram (shown in fig. 1.1).

The transition is accompanied by a sudden increase in energy density and pressure as a function of temperature (see fig. 1.2). For $T \sim T_c$, ϵ/T^4 increases by more than a factor 10, reaching a value of about 80% of the Stefan-Boltzmann limit for an ideal gas of non-interacting quarks and gluons.

Furthermore lattice QCD predicts also that in a quark-gluon plasma chiral symmetry is restored and quark masses are reduced from the large constituent values to the small bare ones. Therefore the threshold for a quark-antiquark pair production is sensibly lowered in a QGP.

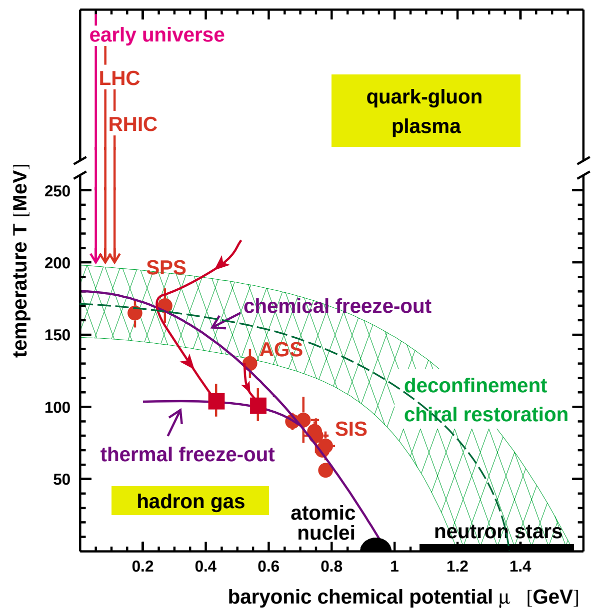

Figure 1.1. QCD phase diagram in the (T, μ_B) plane. The green region indicates the expected phase transition region within its present uncertainty. Transitions provided by various heavy ion experiments are indicated.

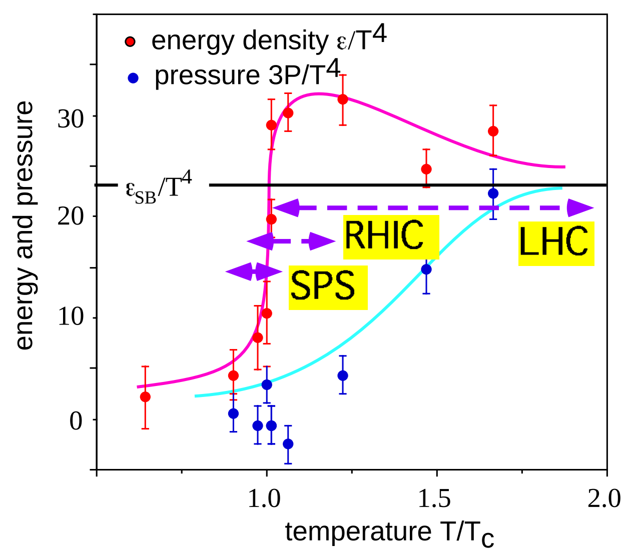

Figure 1.2. Temperature dependence of energy density and pressure in units of T^4. Temperature ranges accessible at SPS accelerator and at RHIC and LHC colliders are also indicated.

1.3 Initial conditions and collision evolution

Nucleus-nucleus collisions cannot be explained by a simple superposition of individual nucleon-nucleon interactions. In fact rescattering of partons and of secondary particles changes the particle production and eventually leads to a local thermal equilibrium. The evolution of the very dense system formed in the collision can be described by hydrodynamic models [4].

Impact of the nuclei takes place almost instantaneously ($\tau_c \sim 1$ fm/c), in this short time interval constituent quarks and gluons scatter with each other. The rescattering processes result in thermodynamic pressure and therefore in the expansion of the hot and dense system, the so called "fireball". If the system is dense enough, partons multiple scattering leads to kinetic equilibrium and it will further evolve collectively towards QGP if the scattering time of quarks and gluon is much less than the expansion rate. If the deconfined medium is produced, it expands and cools until its density falls below the critical transition value, at which point hadronization processes begin. The hadron gas decouples, or as it is commonly said it "freezes out", once the average distance between hadrons exceeds the range of strong interaction. The hydrodynamical, locally thermal, model ceases to be valid at this point. The decoupling is not an instantaneous process but it is determined by the expansion rate and hadronic rescattering cross sections.

The initial energy density reached by the interacting system can be evaluated through the Bjorken estimate [5]:

$$\epsilon_0 = \frac{1}{2\pi R_A^2 \tau_0} \left(\frac{dE_T}{dy} \right)_{y=0} \tag{1.3}$$

where π R_A^2 is the overlap area of the two colliding nuclei (π $R_{Pb}^2 = 63$ fm^2 for Pb nuclei at null impact parameter [3]), $\tau_0 \sim 1$ fm/c and $(dE_T/dy)_{y=0}$ is the measured transverse energy emitted at central rapidity. The initial energy density can also be expressed as a function of the measured multiplicity (dN/dy) and of the average energy at zero rapidity (p_0), since $(dE/dy)_{y=0} = p_0$ $(dN/dy)_{y=0}$. In fig. 1.3 the dependence of the initial energy density on the number of participant nucleons is shown for Pb-Pb collision at 158 A GeV for SPS energies; ϵ_0 goes from about 1.3 GeV/fm^{-3} in peripheral collisions to 3.5 GeV/fm^{-3} in the most central ones [2].

1.4 SPS experimental results

The different states of evolution require different probes for their investigation since the associated length scales are very different. The probes for the deconfined state need to be hard in order to resolve sub-hadronic scales (of the order of 1 fm). They

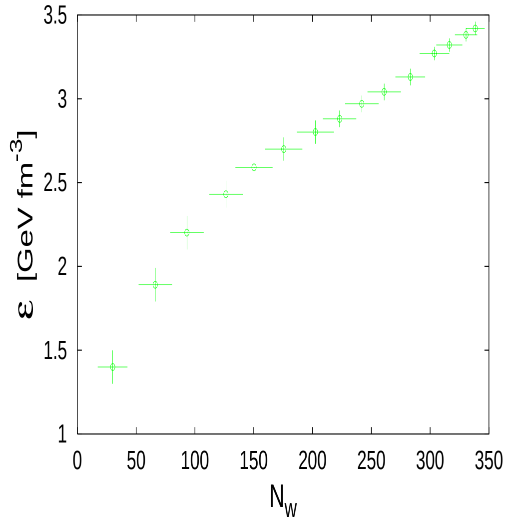

Figure 1.3. Initial energy density versus participants nucleons number for Pb-Pb system at 158 A GeV at the SPS fixed target experiments.

must be able to distinguish sharply between confined and deconfined state and they also have to retain their information throughout the whole interaction. Hadronic state probes are softer since the scale length to be resolved is of the order of the hadronic size; they have to probe the final state of the medium but they can also give indirect information about the previous states.

Direct hard probes of QGP are hard thermal dilepton and photon emission, jet quenching and charmonium suppression. The hadronic intermediate medium can be characterized by in-medium modification of resonances, while proposed soft probes of the hadronic final state are the transverse momentum broadening, the flow and the strangeness enhancement predicted as a consequence of the QGP formation.

In the following I will briefly resume the present status of knowledge and investigation of these probes summarizing the SPS experimental results. I will also try to underline the implications and the conclusions that have be drawn from the SPS experimental programme concerning the system conditions reached after the collision.

1.4.1 Probes for deconfinement

Low mass dilepton enhancement

In heavy ion collisions at the SPS an enhancement of the low mass dilepton spectra has been observed in Pb-Au collisions at 158 A GeV by the NA45 (CERES) experiment [6]. In proton-nucleus collisions the invariant mass spectrum is quite well reproduced by the sum of the known sources of e^+e^- pairs (as can be seen fig. 1.4, left panel). On the contrary both in S-Au and in Pb-Au collisions there is an excess in the mass range 250 MeV $\leq m_{e^+e^-} \leq$ 700 MeV (fig. 1.4, right panel).

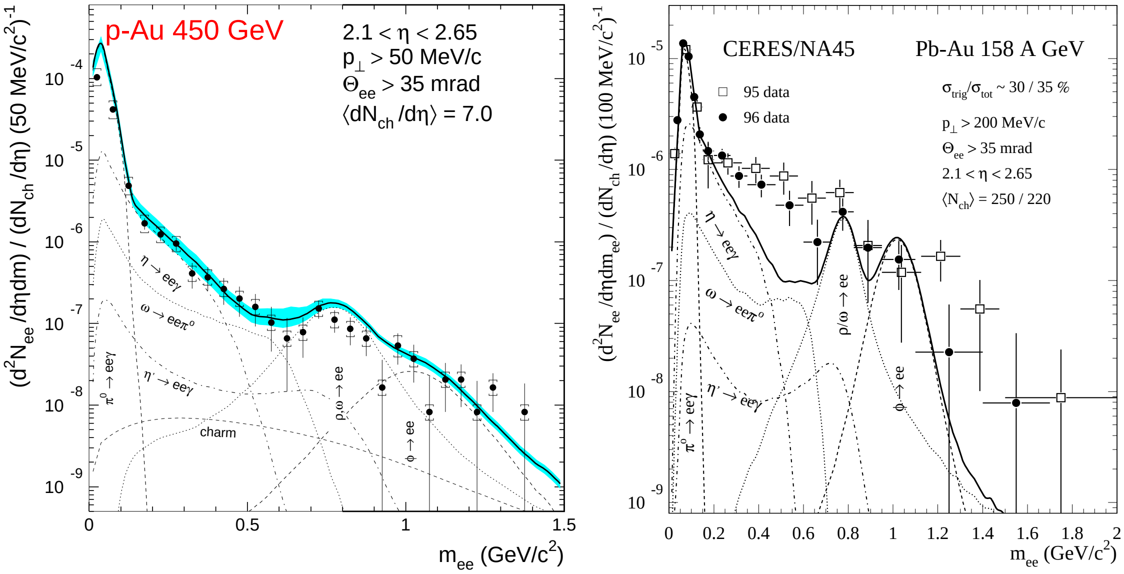

Figure 1.4. Dilepton invariant mass spectrum in p-Au (left) and in Pb-Au (right) collisions, compared to the expected yield (solid line) from known sources [6].

A possible and consistent explanation of the effect is that the strong rescattering in a dense hadronic medium modifies the ρ resonance spectral function, leading to a collisional broadening in the mass spectrum. This implies that pions (that are the most abundant species at the SPS energies) undergo intense rescattering before freeze-out and thus the fireball could reach an approximate local thermal equilibrium.

Transverse flow and momentum broadening

Rescattering among the fireball constituents results in thermalization and in a strong collective transverse flow caused by the thermodynamic pressure. At freeze-out the system emits particles from the decoupling surfaces according to the thermal distribution corresponding to the values locally assumed by the freeze-out temperature and the baryon chemical potential. Since the flow is a collective phenomenon, particles with different masses will be produced with the same velocity, thus heavier particles will acquire a higher transverse momentum. The transverse flow therefore produces a broadening in the secondaries transverse momentum. In fig. 1.5 is shown the mass dependent broadening in transverse momentum distribution of secondary hadrons reported by NA49 [8].

The shapes of all hadronic spectra in case of collective transverse flow can be characterized by only two parameters: the temperature T and the transverse flow

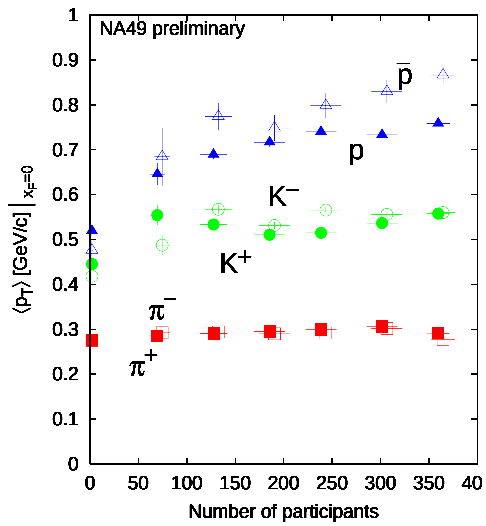

Figure 1.5. Average transverse momentum of different hadronic species in Pb-Pb collisions at the SPS as a function of the number of participating nucleons [8].

velocity at freeze-out v_t. In transverse mass distributions $dN/dm_t^2 \sim \exp[-m_t/T_{slope}]$, the inverse slope parameter T_{slope} can be expressed in the non-relativistic region ($p_t \ll m$) as

$$T_{slope} = T_f + \frac{1}{2} m < v_t^2 > \tag{1.4}$$

and in the relativistic region ($p_t \gg m$) by the blue-shift formula (since the expansion is observed from outside the fireball) [9]:

$$T_{slope} = T_f \sqrt{\frac{1 + < v_t >}{1 - < v_t >}}. \tag{1.5}$$

In fig. 1.6 the measured transverse mass distribution is plotted for many hadronic species; the dependence of the temperature is linear as predicted by equation (1.4). Assuming that particles freeze-out at about the same temperature, T_{slope} should increase with the rest mass, as it is effectively observed with the exception of Ξ and Ω. It has been suggested that these particles freeze-out earlier because of their low interaction cross section [10].

Evidently it is not easy to separate the different contributions in momentum broadening; in fact it can be due to the final collective state, but also to multiple scattering of the initial partons. Moreover such a phenomenon is already present in proton-proton collisions, where an increasing of p_t as a function of hadron multiplicity was observed [11].

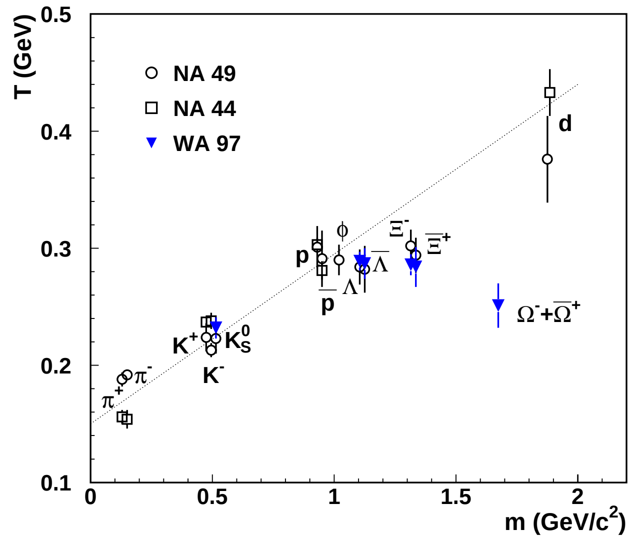

Figure 1.6. Transverse mass dependence of the inverse slope measured in Pb-Pb collisions at 158 A GeV at the SPS for various hadronic particles.

Particle ratios

Transverse flow is also expected to change the momentum distributions of final state hadrons. However flow effects drop out from the total yields of each hadron species if the freeze-out occurs at constant temperature T and baryon chemical potential μ_B values. Therefore 4π integrated yields are not sensitive to the collective fireball dynamics and can then be described with purely thermal models. Obviously the basic assumption of unique freeze-out T and μ_B values for the whole system is not much realistic, but as a first approximation global average values can be used instead of the local ones. Thermal model results are compared to the measured ratios in Pb-Pb collisions at 158 A GeV in fig. 1.7. The observed hadron yields are quite well reproduced by a system in thermal and chemical equilibrium. This implies that the the thermal model approach can be used to extract the freeze-out parameters. Fitting the SPS experimental results the found values are: T = 168 MeV and μ_B = 266 MeV [12].

The observables discussed so far let emerge the picture of a collective strongly interactive system created in Pb-Pb interactions at 158 A GeV. New features of ultra-relativistic heavy ion interactions, such as the low dilepton mass enhancement or the transverse flow, have been observed, but no specific signal of QGP formation has been discussed. Two QGP signatures have been studied in detail at the SPS: the strangeness enhancement and the J/Ψ suppression.

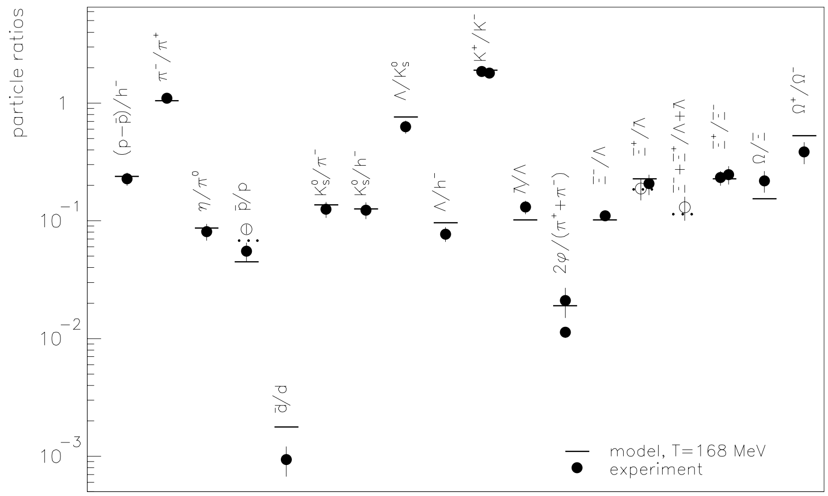

Figure 1.7. Particle ratios measured from NA44, NA49, WA97, WA98 and NA50, compared to the ratios obtained in a thermal model with T = 168 MeV and μ_B = 266 MeV [12].

Strangeness enhancement

Strangeness enhancement is expected in a QGP medium since the strange quark mass is lowered to $m_s \simeq 120$ MeV by the restoration of chiral symmetry and the Pauli blocking of u and d quark states favors the formation of strange quarks [19]. Therefore in ultra-relativistic heavy ion collisions a global enhancement of strangeness production relative to elementary particle and proton-nucleus interactions is expected. A global enhancement factor of about 2 is in effect observed for central Pb-Pb collision relatively to e^+e^-, pp, p$\bar{\text{p}}$ and pA (see fig. 1.8). A strangeness enhancement is also reported with increasing centrality (fig. 1.9), but it is already present in lighter ion collisions and has no onset behavior.

However the most interesting result is the multistrange baryon production at midrapidity studied first by WA97 and then by NA57. In fig. 1.10 the multistrange hadron yield is plotted as a function of the number of participant nucleons, reference data are provided by p-Be interactions. The yield of strange hadrons per participant nucleons is higher for particles with higher strangeness content: the enhancement factor for Ω and $\bar{\Omega}$ is of about 15 [16]. This behavior cannot be explained by hadronic rescattering processes where multistrange baryon and anti-baryon production would be suppressed relative to K and Λ due to their higher threshold. On the contrary, the strangeness increase must have origin at the partonic level, before hadronization.

Recently NA57 reported a drop by a factor 2.6 in $\bar{\Xi}^+$ yield and by a factor 1.8 in Ξ^- production with decreasing centrality [17]. Such a drop is not predicted by any known model and, moreover, models that correctly reproduce the enhancement measured by WA97 fail to explain the centrality dependence observed by NA57.

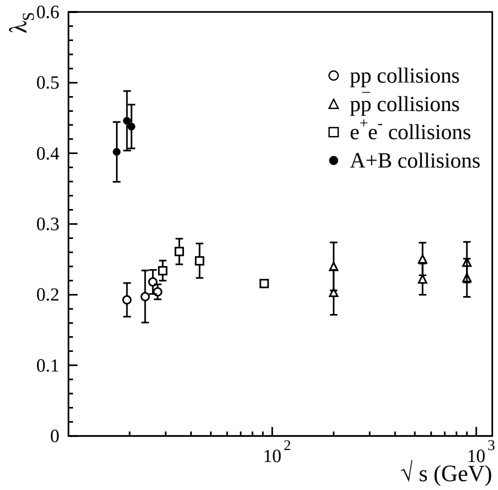

Figure 1.8. Global strangeness enhancement factor λ_S measured in S+S and S+Ag collisions at 200 A GeV by the NA35 experiment and in Pb-Pb collisions at 158 A GeV by NA49 relative to e^+e^-, pp and p$\bar{p}$ collisions [13].

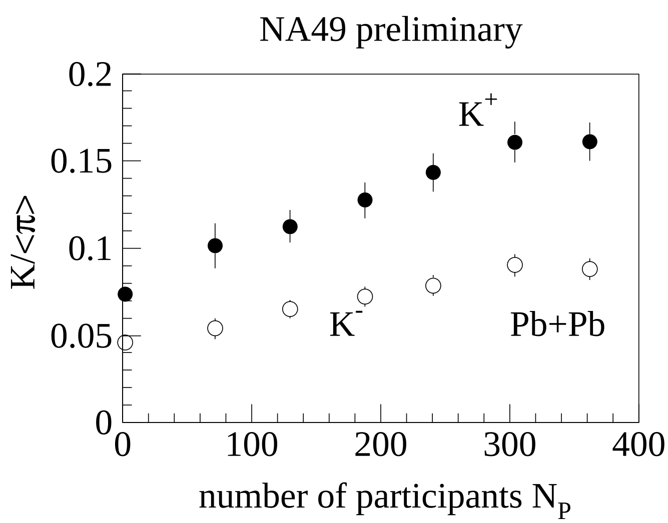

Figure 1.9. K/π ratio as a function of the number of participant nucleons in Pb-Pb collision as measured by the NA49 collaboration [14].

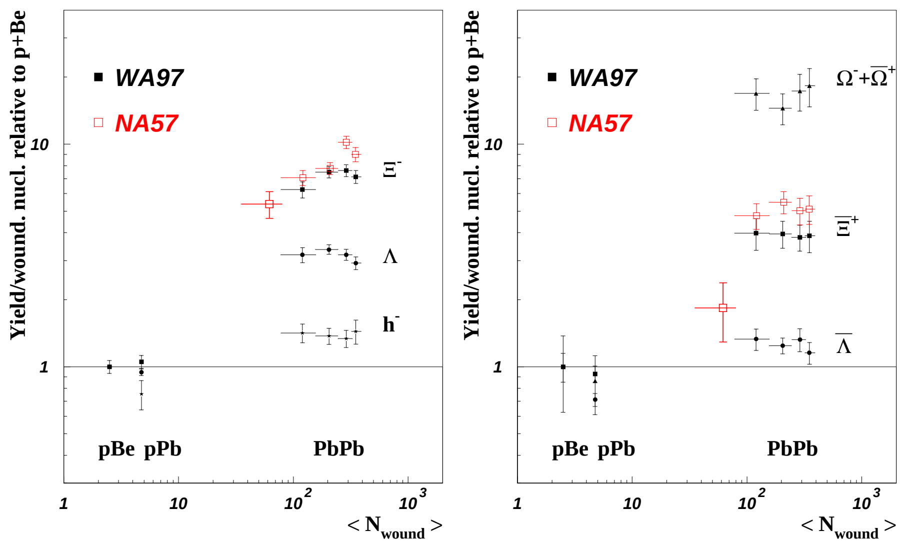

Figure 1.10. Multistrange baryon yields per wounded nucleon relative to p-Be measured by WA97 [15] (closed black symbols) and by NA57 [17] (open red symbols).

J/Ψ suppression

At SPS energies charmonium dissociation has demonstrated to be a very good probe to test deconfinement. The formation of quark-antiquark bound states is prevented in a deconfined medium by the screening of the color field [20]. The screening potential described by equation (1.2) indicates that, once the Debye radius $r_D = \mu^{-1}$ becomes shorter than the characteristic length of the bound state, the latter can no longer exists. With increasing temperature, a deconfined medium will therefore lead to successive melting of quarkonium states as a function of their binding energy. The suppression of specific quark-antiquark bound states can be used as an indicator of the medium temperature. A suppression in the J/Ψ production was observed at SPS energies already in proton-nucleus collisions relative to proton-proton ones. This indicates a strongly interacting medium and implies that J/Ψ suppression generally does not univocally mean deconfinement.

Charmonium hadroproduction is based on hard perturbative processes of gluon fusion into a $c\bar{c}$ pair, generally formed in a color octet state. The following color neutralization is presently explained by different models involving non-perturbative features (among them the color octet model). All these models lead to the formation of a pre-resonant $c\bar{c}$ state that has the same characteristics (size, lifetime) for the different states ψ', χ_c and J/Ψ. At SPS conditions (J/Ψ is produced with a momentum of about 30 GeV/c [11]) the nuclear medium of the target only sees the pre-resonant state. Therefore the absorption should be the same for ψ' and J/Ψ, as it was indeed reported by the NA38 collaboration (see fig. 1.11). The same degree of attenuation for such different states is explainable only as an effect of the pre-resonant absorption of the charmonium state in nuclear matter.

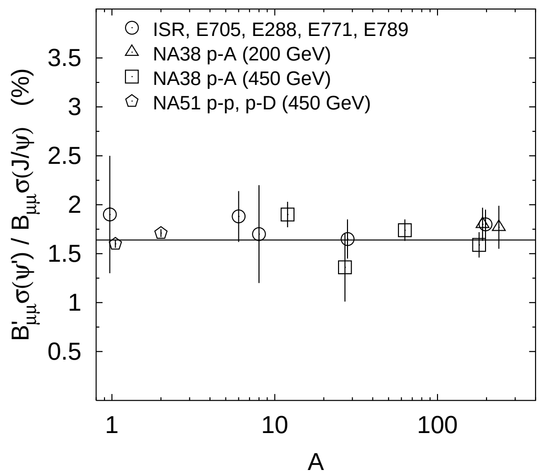

Figure 1.11. Attenuation in rate production for ψ' and J/Ψ as a function of A in pA and AA collisions [21].

The J/Ψ production suppression in nuclear collisions from pA to peripheral Pb-Pb ones perfectly fits in the picture of such a pre-resonant "normal" absorption. In fig. 1.12 the ratio of J/Ψ over Drell-Yan is plotted as a function of the L variable that measures the mean nuclear matter thickness transversed by the $c\bar{c}$ pair, obviously the most central is the collision the more dense is the created system and the higher is the value assumed by the L variable. For central Pb-Pb collisions a suppression of J/Ψ beyond the expected pre-resonant absorption is observed both as a function of the L variable and as a function of the transverse energy E_T (see fig. 1.12 and 1.13).

This "anomalous" suppression shows two important features. First of all it shows an onset as a function of the centrality; in fact for peripheral Pb-Pb collisions the normal pre-resonant behavior is followed. Secondly the suppression pattern has two successive drops: the first one for $E_T \simeq 40$ GeV, the second for $E_T \simeq 100$ GeV. This characteristic two step pattern reflects the sequential melting of χ_c and J/Ψ; in fact only a 67% of J/Ψ is directly produced while the remaining 33% derives from χ_c decays.

The J/Ψ suppression pattern is thus the one predicted by deconfinement; on the other hand "conventional" mechanisms, such as the absorption by secondary hadrons (hadronic comovers models), are not able to reproduce the NA50 data since they have a smooth behavior rather then a two-step pattern as a function of the centrality.

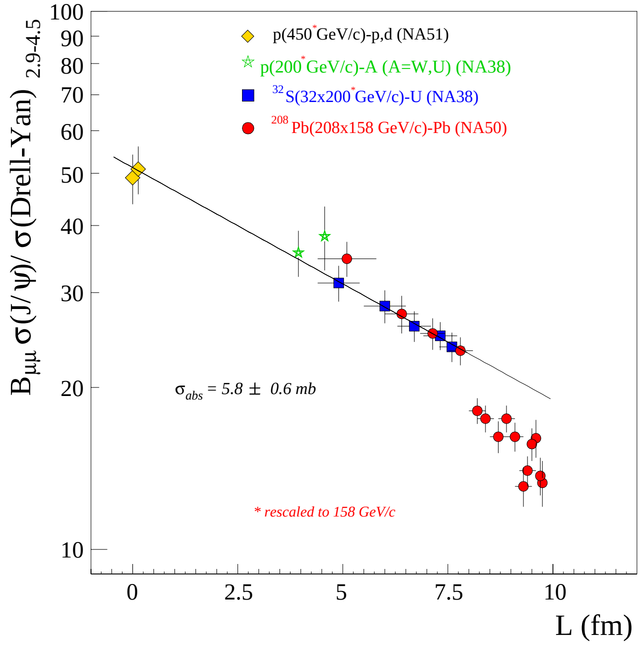

Figure 1.12. J/Ψ over Drell-Yan production ratio as a function of the mean path L in nuclear matter of the $c\bar{c}$ pair.

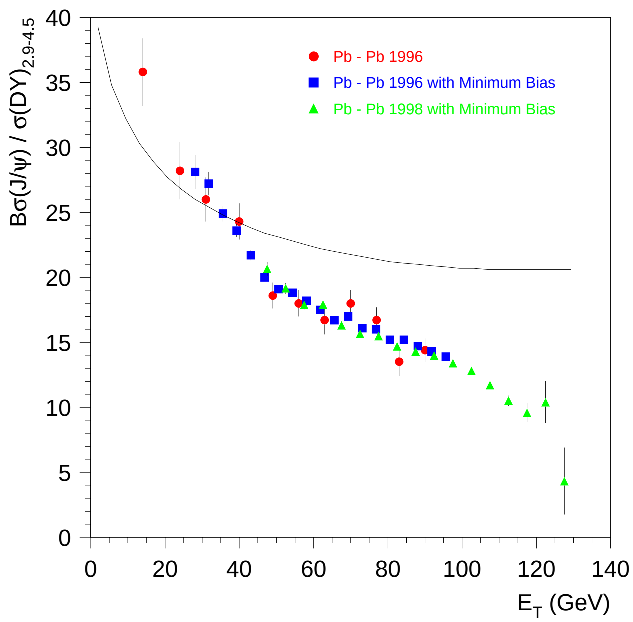

Figure 1.13. J/Ψ over Drell-Yan as a function of the transverse energy for Pb-Pb collisions as measured by the NA50 experiment. The solid line represents the "normal" pre-resonance absorption [22].

1.4.2 Conclusions from the SPS experimental programme

From the analysis of several different observables independently measured by the SPS experiments a picture of a strongly interacting medium has emerged. The system formed in Pb-Pb central interaction at 158 A GeV reaches initial energy densities of about 3.5 GeV/fm^3 and temperatures around 210-220 MeV [3]; these values are well above the theoretically predicted ones for a phase transition towards the QGP.

Evidence of collective behavior and a large degree of thermalization due to intense rescattering among the constituents in the final hadronic stage comes from the low mass $e^+ e^-$ enhancement, from measured momentum spectra and hadron yields. Strangeness production is globally enhanced with respect to pp and pA interactions and a strong enhancement is found for multistrange baryons production. This last observation suggests that the system is indeed thermalized already before the hadronic phase. The best candidate to probe deconfinement at SPS energies is found to be the J/Ψ suppression since the reference provided by pp and pA is well understood, there is a clear onset of the phenomenon and the suppression pattern is in complete agreement with a deconfinement prediction, while it can not be reproduced by conventional models.

In February 2000 CERN announced officially that from all these results evidence for the formation of a new state of matter has emerged: "this state exhibits characteristic properties which cannot be understood with conventional hadron dynamics but which are qualitatively consistent with expectations from the formation of a state of matter in which quarks and gluons no longer feel the constraint of color deconfinement" [23].

1.5 First results from RHIC experiments

With the advent of RHIC (Relativistic Heavy Ion Collider) at the Brookhaven National Laboratory a new era in heavy ion physics has begun. The highest center of mass energy at the SPS fixed target experiments, reached in Pb-Pb collisions, is $\sqrt{s} \sim 17$ A GeV. At RICH Au ions are accelerated at $\sqrt{s} \sim 200$ A GeV, entering thus in a new energy and density regime.

Very briefly RHIC consists of four experiments for the study of the QGP state measuring independent observables: STAR measures global variables on a event by event basis, PHENIX concentrates in detecting photons, dileptons and hadrons, BRAHMS and PHOBOS will measure particle production as a function of centrality, single particle spectra, and particles correlations.

Charged particle multiplicity at midrapidity

Charged particle density at midrapidity is one of the global observables that provides information on the initial conditions of the collision. It is sensitive to the mechanisms that determine particle production; therefore measured multiplicities can contribute to test different theoretical models describing particle production.

Among these models two different approaches have been compared and are widely used to reproduce RHIC experimental results: HIJING and EKRT saturation model. In the HIJING model [26] two components account for particle production: soft interactions that scale linearly with the number of participating nucleons N_{part} ($\sim$ A) and hard processes that scale with the number of binary collisions N_{coll} ($\sim A^{4/3}$). HIJING has the possibility to consider jet quenching and nuclear shadowing. The EKRT model [27] introduces a saturation in the gluon density due to the large production of semi-hard gluons in a small volume at RHIC energies; the saturation scale depends both on $\sqrt{s}$ and on A. In fig. 1.14 charged particle densities per participating nucleon measured both in pp and AA collisions are compared with HIJING and EKRT calculations. Both the models seem to agree with the first PHOBOS results.

Recently the PHOBOS collaboration has published the result of charged particle multiplicity at $\sqrt{s}$=200 GeV. The measured value, normalized per participant pair, is: $(dN_{ch}/d\eta)_{\eta=0}/0.5N_{part}$=3/78±0.25(syst) [28]. The increase observed going from 130 to 200 GeV is not so large as predicted by the HIJING model when jet quenching is considered.

The dependence of $dN_{ch}/d\eta$ at midrapidity on the centrality of the collision shows a critical difference between the two models (see fig. 1.15). The HIJING model leads to an increase in the normalized multiplicity $(dN_{ch}/d\eta)_{\eta=0}/0.5N_{part}$ as a function of centrality, while EKRT saturation model predicts a slightly decreasing dependence.

The results obtained by PHOBOS experiment cannot be used to distinguish between the two models. On the other hand more recent results from PHOBOS are in agreement with the calculations by Kharzeev and Nardi (KN) [29]. In fig. 1.16 PHOBOS data are shown together with the prediction from the three models (similar results has been reported by the PHENIX collaboration [30]). The KN model assumes, like HIJING, that particle production at high energy is partly due to soft and partly to hard interactions. The fraction of multiplicity originated from hard processes is extracted from PHOBOS first results to predicts the centrality dependence of $(dN_{ch}/d\eta)/0.5N_{part}$.

Midrapidity transverse energy distribution

Transverse energy measurement provides a characterization of the geometry of the collision. The midrapidity transverse energy distribution has been measured at

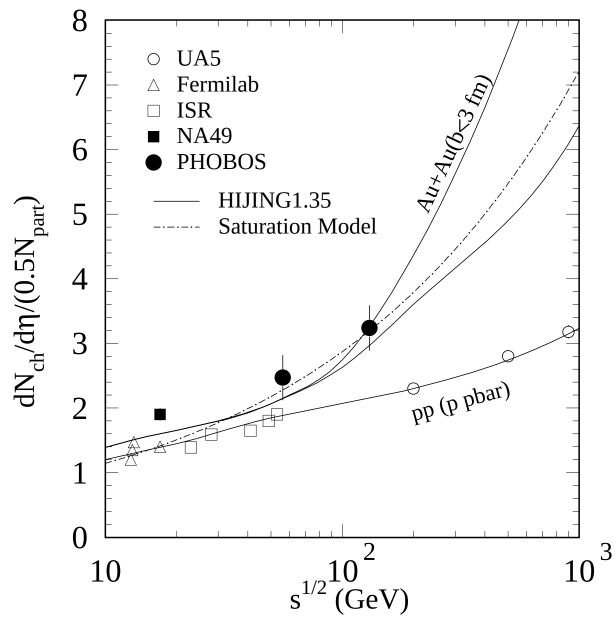

Figure 1.14. Energy dependence of the charged particle rapidity density per participant pair in pp, $p\bar{p}$ and AA. PHOBOS data refers to 6% most central Au-Au collisions [24]. The two solid curves corresponds to HIJING prediction with (upper) and without (lower) jet quenching, the dot-dashed one to EKRT calculations.

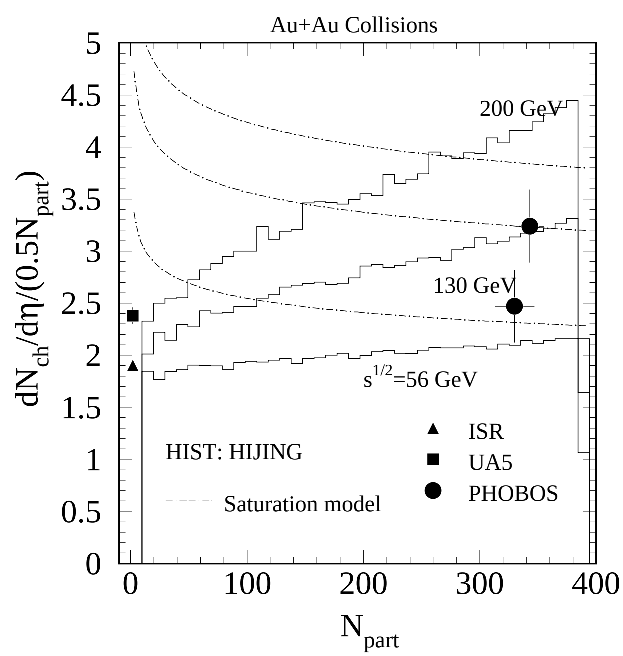

Figure 1.15. Charged particle pseudorapidity distribution per participant nucleon pair as a function of N_{part} for central (b<3 fm) Au-Au collisions at $\sqrt{s} = 130$ A GeV. Calculations for HIJING (solid) and EKRT (dot-dashed) are also shown.

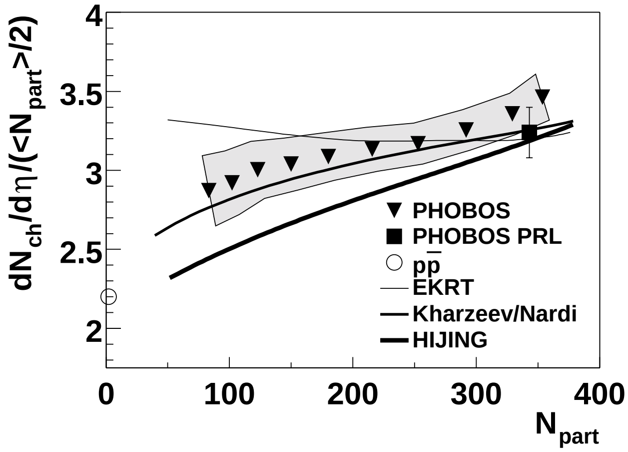

Figure 1.16. Centrality dependence of the measured charged particle pseudorapidity density per participant pair. HIJING, EKRT and KN predictions are compared.

RHIC by the PHENIX experiment. The measured increase in E_T distribution with increasing centrality (reported in fig. 1.17) has been compared to WA98 data relative to SPS energies.

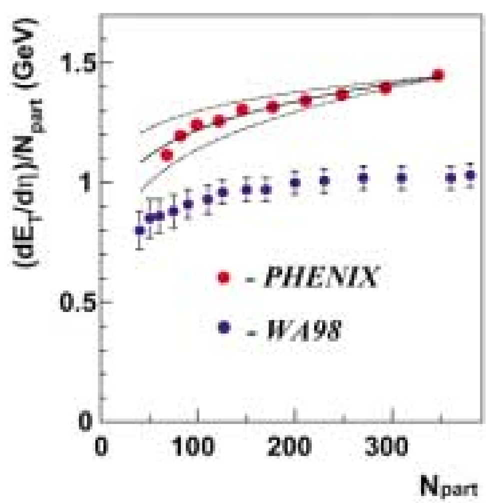

Figure 1.17. Transverse energy density per participant as a function of the number of participants in Au-Au collisions at $\sqrt{s} = 130$ GeV [31], compared to WA98 results for Pb-Pb collisions at $\sqrt{s} = 17$ GeV [32].

The transverse energy at midrapidity measured by PHENIX is about 40% larger. Parameterizing $(dE_T/d\eta)_{\eta=0}$ as a function of N_{part}^{α}, WA98 finds for the parameter the value $\alpha = 1.08 \pm 0.06$ [32], while PHENIX obtains $\alpha = 1.13 \pm 0.05$ [31].

From the measured E_T spectra the initial energy density can be estimated through the Bjorken formula (1.3). For central Pb-Pb collisions at the SPS a value around 3.5 GeV/fm^3 is obtained, while PHENIX has calculated $\epsilon = 4.6$ GeV/fm^3 in central Au-Au interactions [31], corresponding to an increase of 30% relative to the SPS. A very interesting result is that both experiments find, as a function of centrality, a constant value (of about 0.8 GeV) for the ratio $(\mathrm{dE}_T/\mathrm{d}\eta)_{\eta=0}/(\mathrm{dN}_{ch}/\mathrm{d}\eta)_{\eta=0}$. This indicates that the larger amount of energy density at RHIC results in an increase in particle production rather than in higher transverse energy per particle.

1.6 New aspects for heavy ion physics at LHC

Initial conditions and global observables

The following step in heavy ion collision will be the ALICE experiment at the LHC collider, where Pb beams will be accelerated at an energy of 2.76 A TeV. The LHC energy will exceed that available at RICH by a factor of about 30, opening thus new perspectives and giving accessibility to a completely new energy regime in which hard processes dominate. In table 1.1 some quantitatively changes at LHC relative to SPS and RHIC are reported.

	SPS	RHIC	LHC
$\sqrt{s}/A$ (GeV)	17	200	5500
dN_{ch}/dy	400	1000	$3-8\cdot 10^3$
τ_0^{QGP} (fm/c)	1	0.2	0.1
$\epsilon(\tau_0^{QGP})$ (GeV/fm^3)	3	35	500
τ_{QGP} (fm/c)	$\lesssim 2$	$2-4$	$\gtrsim 10$
τ_{fo} (fm/c)	10	$20-30$	$30-40$
V_{loc} (fm^3)	few 10^3	few 10^4	few 10^5

Table 1.1. Values reached by global observables for SPS fixed target, RHIC and LHC collider experiments.

Concerning the number of charged particles per rapidity unit (dN_{ch}/dy), The predictions for LHC energies are still debated since for these high energies there are uncertainties about phenomena like jet quenching, gluon shadowing and final parton state saturation. The thermalization time of the QGP (τ_0^{QGP}) is strongly reduced at LHC energies leading thus to higher initial energy densities. The time spent by the system in the QGP phase (τ_{QGP}), the freeze-out time (τ_{fo}) and the final local freeze-out volume (V_{loc}) are strongly increased with respect to SPS and RHIC conditions. Therefore the system will be denser and hotter, the QGP will be formed earlier and it will remain thermalized for a longer time; these features make the LHC conditions more favorable for QGP study.

New accessible probes

The study of quarkonium suppression to probe deconfinement can be extended at LHC to the Υ family. Open charm and beauty productions can be measured and will provide a normalization respectively for $c\bar{c}$ and $b\bar{b}$ production (and suppression). They will also help on distinguish between different production stages: initial, pre-equilibrium, thermalization and final hadronization.

Thermal lepton pairs and photons emitted from the hot initial reaction volume do not interact strongly but decouple immediately, hence they can provide information about the medium at their emission time. In principle thermal emission can be used to determine the temperature at the time the signal was emitted. The functional form of the spectra for photon momentum k_γ is the same for QGP or for hadronic medium:

$$dN/dk_\gamma \sim e^{-k_\gamma/T};$$

therefore it cannot be used to distinguish between confined and deconfined phase. Furthermore, thermal emission has to compete with other sources of background (mainly Drell-Yan mechanism and hadronic electromagnetic decays). For these reasons at SPS energies there is no unambiguous evidence for thermal dilepton and photons production. In fact hard photons produced by Drell-Yan process in hard parton collision dominate the spectrum for high momenta, while at low momenta the contribution is almost completely due to hadronic decays. Since thermal photons production increases strongly with the plasma temperature (it is proportional to T^4), energy density and lifetime it might be observable at LHC energies. Moreover the background could be reduced by thermalization and jet quenching, thus the conditions for their detection are very promising.

Hard jets are produced through hard partonic interactions in the very early stages of the collision. Jets produced with high transverse momentum pass through the surrounding medium and interact with it losing their energy. The energy loss in a deconfined medium was predicted to be much higher than in ordinary nuclear matter [33]. An estimate of the radiative energy loss per unit length gives an average loss dE/dx of 3 GeV/fm in a QGP and of 0.2 GeV/fm in nuclear matter [11]. Jet quenching in a deconfined medium is an hard probe, not accessible at SPS energy, it might be visible already at RHIC but it will be definitively more evident at LHC.

New physics aspects

The big jump in energy corresponds to a very different evolving system. Not only probes and observables are accessible in a very different range, but also new physics aspects of heavy ion reactions seem to emerge from the present theoretical picture.

The slowing down of the incoming nuclei leads to a vanishing net baryon density at midrapidity (at SPS there was a high baryon density and at RICH it seems lower but still not null). Therefore at LHC the null baryon chemical potential μ_B provides conditions that are very similar to those of the primordial universe.

At LHC energies particle production is almost dominated by hard processes that scale proportional to the number of binary collisions. The density of low momentum partons in the initial state are so high that the quark phase space density saturates. Gluon merging becomes important so that the interaction is described as a collision between two gluon "walls" [25]. Moreover gluon saturation implies very large occupation numbers and therefore the following evolution can be described by classical chromodynamics. This relevant characteristic is verified only at LHC conditions.

A unique feature of heavy ion collisions is the possibility to measure a number of observables on a event by event basis. Event by event physics is a fundamental tool to study the critical phenomena, the transition phase and anomalous events that can be indicated by non statistical fluctuations in the measured observables. The accuracy of such measurements increases with the number of observed particles, therefore LHC will provide very precise results.

1.7 ALICE experiment

ALICE (A Large Ion Collider Experiment) is a dedicated heavy ion experiment, designed to study the quark-gluon plasma in Pb-Pb interaction at $\sqrt{s} = 5.5$ TeV per nucleon at the LHC collider. In addition lower mass ions, proton-nucleus and proton-proton collisions will be studied to provide reference data.

The detector (see fig. 1.18) consists essentially of the central barrel for hadrons and dielectrons detection, that is placed in a solenoidal magnetic field and covers the pseudo-rapidity range $|\eta| < 1$. A forward spectrometer ($2.5 < \eta < 4$) measures muon pair production and very forward detectors ($\eta > 4$) provide both neutral and charged particle multiplicities and the centrality of the collision.

In the following I will give a very brief overview of the ALICE detectors and of the observables they will measure. Further details can be found in the ALICE Technical Proposal [34] or in Technical Design Reports of each detector.

Detectors and observables

The inner tracking system (ITS) covers the central rapidity range ($|\eta| < 0.9$). It will be made by six barrels of high resolution detectors (silicon pixel, silicon drift and silicon micro-strip). It is designed to provide secondary vertex reconstruction for hyperons and charm decays, particle identification and tracking of low p_t particles (down to ~ 20 MeV/c) and will improve momentum resolution of higher p_t particles. The main tracking system is supplied by a time projection chamber (TPC), chosen for its high efficiency and dE/dx resolution ($< 10\%$).

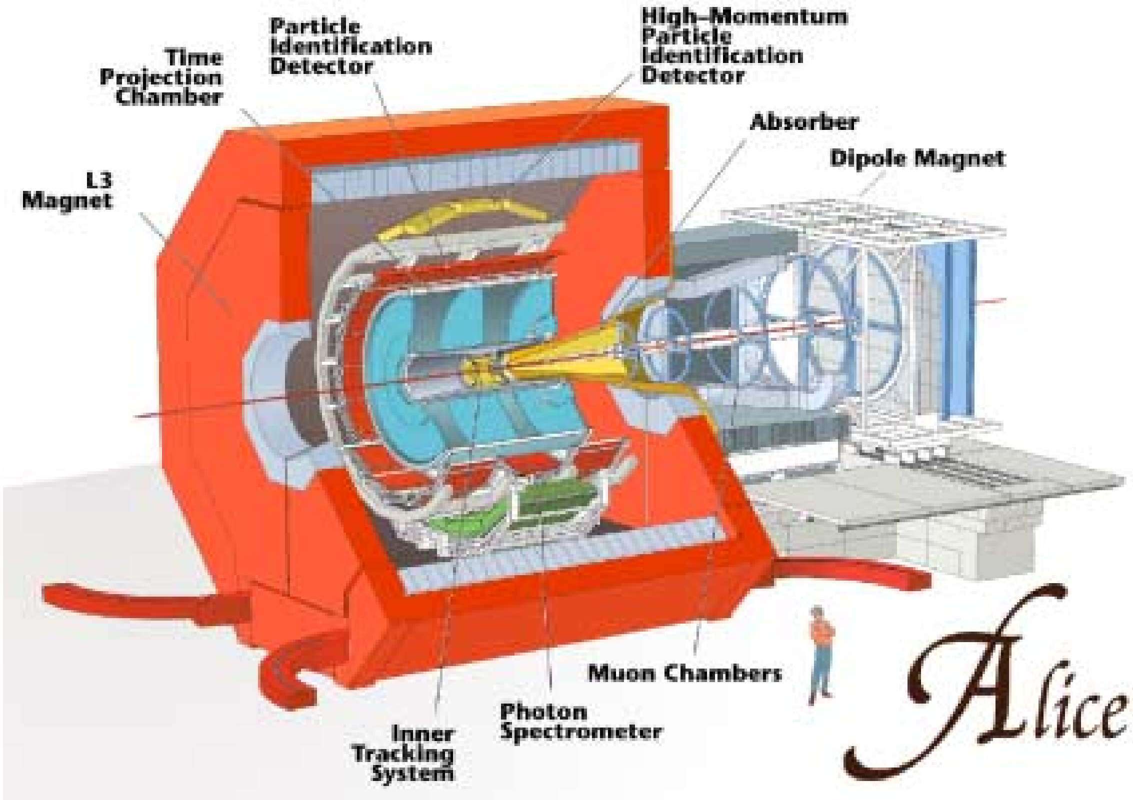

Figure 1.18. View of the ALICE detector.

Particle identification will be provided by different detector systems. A large acceptance (the covered area is more than 100 m^2) time of flight (TOF) will identify particles with momenta in the range 0.5 GeV/c $< p_t <$ 2.5 GeV/c. For that purpose multigap resistive plate chambers will be used for their very good time resolution ($<$ 100 ps). A Ring Imaging Cerenkov (RICH) detector of smaller acceptance will provide identification for particles of very high momenta (1.5 GeV/c $< p_t <$ 5 GeV/c). Finally a transition radiation detector (TRD) will identify electrons with $p_t >$ 1 GeV/c, improving the e/π rejection power and providing information about heavy quark production in the central acceptance.

A single arm electromagnetic calorimeter, or photon spectrometer (PHOS), will be used to measure energy released by prompt photons, π^0 and η in the pseudorapidity range $|\eta| < 0.12$. It will be made of a scintillating crystal ($PbWO_4$) in order to reduce the occupancy and optimize the light yield.

The forward dimuon arm will measure mouns resulting from the decays of the heavy quark resonances (ψ and Υ families) and also from the semileptonic decays of charm and beauty hadrons. The mass resolution achievable is suitable for the separation of all the states. The dimuon arm consists of an absorber made by alternate layers of high and low Z materials, a dipole magnet for momrntum measurement, 10 thin and high granularity stations for tracking (cathode strip and cathode pad chambers), an iron wall and then four planes of resistive plate chambers for the dimuon trigger.

Between the forward detectors, the photon multiplicity detector (PMD) is designed to measure collective flow and transverse energy of neutral particles with $1.8 < \eta < 2.6$. The forward multiplicity detector (FMD) will measure charged particle multiplicity in the pseudorapidity interval $1.5 \leq \eta \leq 5.5$. A set of calorimeters put at zero degree relative to the collider axis, the so called Zero Degree Calorimeters (ZDC), will provide information on collision centrality by measuring event by event the energy carried by spectator nucleons.

References

[1] N. F. Mott, Proc. Phys. Soc. (London) A **62** (1949) 416.

[2] H. Satz, Bielefeld Univ. Fak. Phys., 8 Sep 2000, [hep-ph/0009099].

[3] U. Heinz, Nucl. Phys. A **685** (2001) 414.

[4] K. Eskola, Proc. of the International Europhysics Conference on High-energy Physics, EPS-HEP '99, Tampere, Finland, [hep-ph/9911350].

[5] J. D. Bjorken, Phys. Rev. D **27** (1983) 140.

[6] CERES Collaboration, Nucl. Phys. A **661** (1999) 23c.

[7] R. Rapp, J. Wambach, [hep-ph/9909229], to appear in Adv. Nucl. Phys.

[8] NA49 Collaboration, Nucl. Phys. A **638** (1998) 91c.

[9] K. S. Lee, U. Heinz, E. Schnedermann, Z. Phys. C **48** (1990) 525.

[10] H. van Hecke, H. Sorge, N. Xu, Phys. Rev. Lett. **81** (1998) 5764.

[11] H. Satz, Rep. Prog. Phys. **63** (2000) 1511.

[12] P. Braun-Muzinger, I. Heppe, J. Stachel, Phys. Lett. B **465** (1999) 15, [nucl-th/9903010].

[13] F. Becattini, M. Gazdzicki, J. Sollfrank, Eur. Phys.J C **5** (1998) 143.

[14] NA49 Collaboration, Nucl. Phys. A **661** (1999) 485c.

[15] WA97 Collaboration, Nucl. Phys. A **661** (1999) 130c.

[16] WA97 Collaboration, Phys. Lett. B **449** (1999) 401.

[17] NA57 Collaboration, Proceedings of XXXVIth Rencontres de Moriond, QCD and High Energy Hadronic Interactions , 17-24 March 2001, Les Arcs 1800, France.

[18] U. Heinz, Nucl. Phys. A **661** (1999) 140, [nucl-th/9907060].

[19] J. Rafelsky, B. Muller, Phys. Rev. Lett. **48** (1982) 1066.

[20] T. Matsui, H. Satz, Phys. Lett. B **178** (1996) 416.

[21] NA38 Collaboration, Phys. Lett. B **220** (1989) 471.

[22] NA50 Collaboration, Phys. Lett. B **450** (1999) 456.

[23] CERN Press Release, 10 Feb. 2000.

[24] PHOBOS Collaboration, Phys. Rev. Lett. **85** (2000) 3100, [hep-ex/0007036].

[25] K. J. Eskola, K. Kajantie, P. V. Ruuskanen, K. Tuominen, Nucl. Phys. B **579** (2000) 370.

[26] X. Wang, M. Gyulassy, Phys. Rev. Lett. **86** (2001) 3496, [nucl-th/0008014].

[27] K. J. Eskola, K. Kajantie, P. V. Ruuskanen, K. Tuominen, Nucl. Phys. B **570** (2000) 379, [hep-ph/9909456].

[28] PHOBOS Collaboration, submitted to Phys. Rev. Lett. (August 2001), [nucl-ex/0108009].

[29] D. Kharzeev, M. Nardi, Phys. Lett. B **507** (2001) 121, [nucl-th/0012025].

[30] PHENIX Collaboration, Phys. Rev. Lett. **86** (2001) 3550, [nucl-ex/0012008].

[31] PHENIX Collaboration, Phys. Rev. Lett. **87** (2001) 052301, [nucl-ex/0104015].

[32] WA98 Collaboration, Eur. Phys. J. C **18** (2001) 651.

[33] J. D. Bjorken, Fermilab-Pub-82/59-THY (1982).

[34] ALICE Technical Proposal, CERN/LHCC/95-71.

[35] ALICE Collaboration, ZDC Technical Design Report, CERN/LHCC 99-5.

Chapter 2

Centrality determination with ALICE Zero Degrees Calorimeters

2.1 Centrality measurement in heavy ion collisions

The phase transition to QGP can be observed with the presence of a threshold effect in some signatures (i.e., charmonia, bottomonia and strangeness production) as a function of the energy density. It is therefore crucial to estimate event by event the centrality of the collision and to compare energy density onset values for different probes.

The centrality of a nucleus-nucleus collision is generally defined through the so-called impact parameter b, defined as the distance between the geometrical centers of the colliding nuclei in the plane transverse to their direction. A good resolution on centrality measurement is essential in order to observe the existence of a threshold, that otherwise could be smeared out. It is moreover important to have different detectors providing in independent ways a characterization of the event geometry. In order to provide a reliable result, a good centrality estimator needs to be almost model independent.

Some observables correlated with centrality depend on physics processes and do not therefore reflect simply the geometry of the collision. For example the event geometry can be characterized through a measurement of the produced particle multiplicity or of the transverse energy carried by participants and secondary particles. The more central is the collision, the higher are particle multiplicity and transverse energy.

In the ALICE experiment, the ITS will measure charged particle multiplicity at midrapidity ($|\eta| \leq 0.9$) while the PHOS will detect the neutral transverse energy carried by photons ($|\eta| \leq 0.12$). In the forward rapidity region the FMD will detect charged particle multiplicity with $1.5 \leq \eta \leq 5.5$, while the PMD will measure the neutral energy in the range $1.8 \leq \eta \leq 2.6$.

2.1.1 Centrality determination with the ZDC

The observable most directly related to the geometry of the collision is the number of participant nucleons, that can be estimated measuring the energy carried in the forward direction (at zero degree relative to the beam direction) by non interacting (spectator) nucleons. The zero degree forward energy decreases with increasing centrality. The measurement of the zero degree energy relies on the detection of spectator nucleons that will be made in ALICE by means of Zero Degree Calorimeters (ZDC). In the ideal case, in which all spectators are detected, the estimate of the number of participants would be simply provided by the following relationships:

$$E_{ZDC}[TeV] = 2.76 \cdot N_{spectators}$$

$$N_{participants} = A - N_{spectators}.$$

where 2.76 TeV is the energy of the Pb nucleon at LHC. We will see that the ALICE experimental conditions do not allow such a simple estimate and I will then discuss in the following how the zero degree energy measurement will provide the impact parameter of the collision.

Glauber model

The number of participating nucleons, N_{part}, can be correlated to the impact parameter of the collision in the framework of the Glauber theory [1]. This is a purely geometric model in which the number of participants at a fixed impact parameter b can be evaluated through the relation:

$$\begin{aligned} N_{part}(\vec{b}) &= \int d^2s \left\{ AT_A(\vec{s}) \left[1 - [1 - \sigma_N T_B(\vec{b} - \vec{s})]^B\right] \right. \\ &\quad \left. + BT_B(\vec{b} - \vec{s}) \left[1 - [1 - \sigma_N T_A(\vec{s})]^A\right] \right\} \end{aligned} \tag{2.1}$$

where A and B are the mass numbers of the colliding nuclei. N_{part} depends on the nuclear profile functions, T_A and T_B ($T_{A,B} = \int dz \rho_{A,B}(z, \vec{s})$), and on the nucleon-nucleon inelastic cross section, σ_N. The number of participants obtained within this model for Pb-Pb collisions at $\sqrt{s} = 5.5$ TeV as a function of centrality is plotted in fig. 2.1. The nucleon-nucleon inelastic cross section has been extrapolated from proton-proton reference data [2] and found to be of the order of 60 mb.

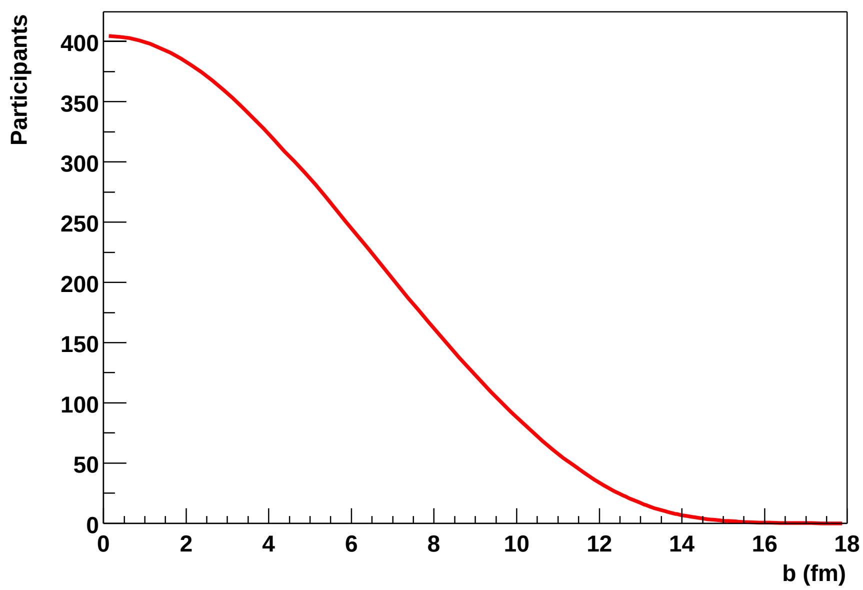

Figure 2.1. Number of participant nucleons as a function of the impact parameter calculated from Glauber theory (eq. (2.1) for Pb-Pb collisions at $\sqrt{s} = 5.5$ TeV.

Event generators

Centrality dependence of the number of participants obtained with the Glauber geometrical model can be compared with the one given by a nucleus-nucleus event generator, such as VENUS [3] or HIJING [4]. Event generators introduce intrinsic fluctuations in the number of participants (spectators) at fixed impact parameter. As it will be shown in the following, these fluctuations affect the resolution that can be achieved measuring centrality with the ZDC.

In fig. 2.2 results obtained with HIJING are compared with Glauber calculations (for the same σ_N value). It can be seen that the two calculations are in agreement and similar results can be obtained with VENUS. Therefore centrality determination through spectators energy measurement is largely model independent. On the contrary, the measurement of charged particle multiplicity strongly depends on the model used to describe particle production, as has emerged from the interpretation of RHIC data (see section 1.5).

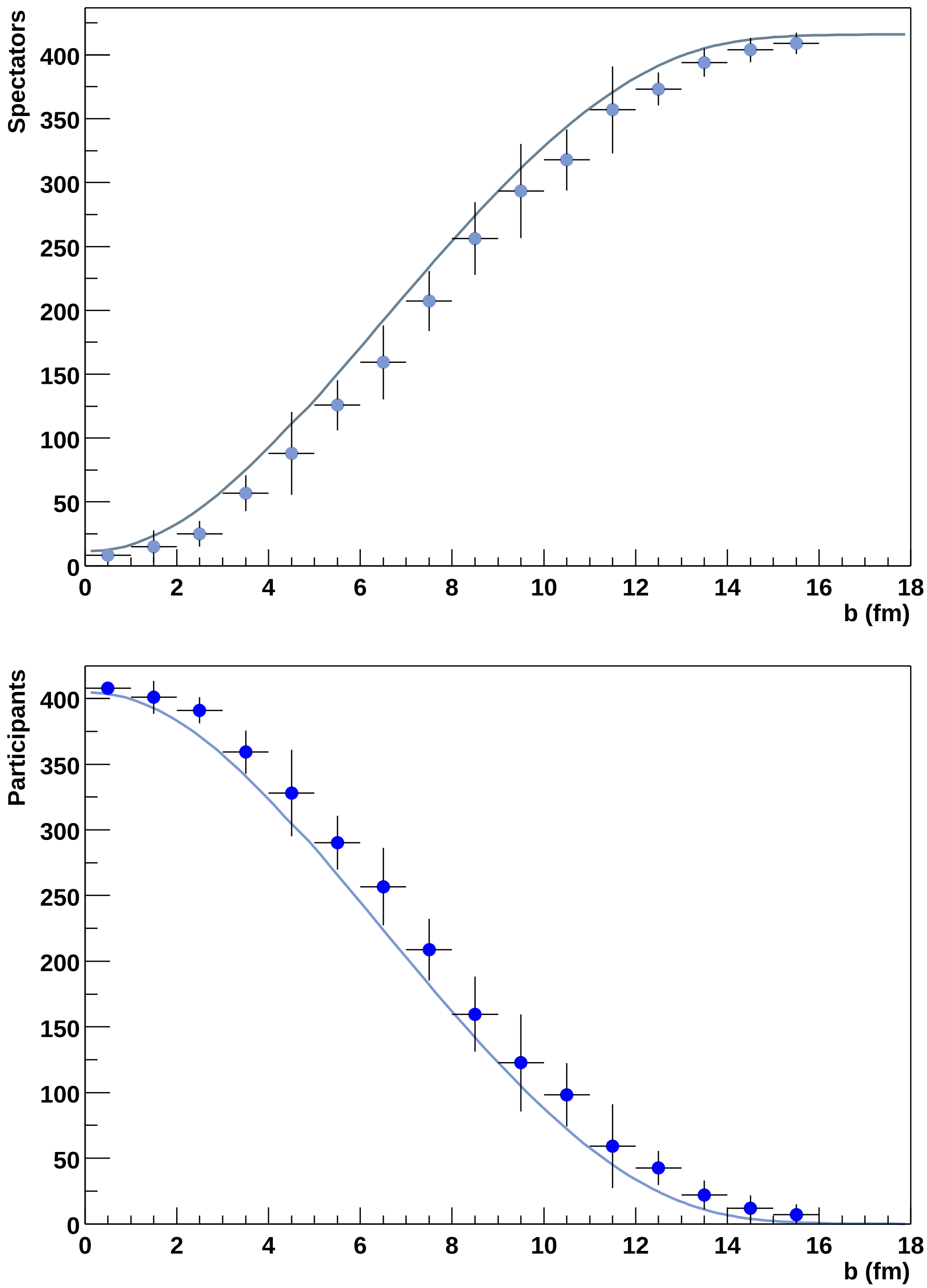

Figure 2.2. Number of spectators as a function of the impact parameter in Pb-Pb collision at 2.7 TeV per nucleon: Glauber model (solid line) and HIJING (points) are compared.

2.2 Zero Degree Calorimeters for the ALICE experiment

Detector characteristics and detection technique

Detection of zero degree energy at colliders is available where the two circulating beams are deflected by means of the separation dipoles of the beam line. This is the reason why the ALICE ZDCs will be placed at 116 m from the Interaction Point (IP), where the distance between the beam pipes (∼8 cm) allows the insertion of a detector (see fig. 2.3).

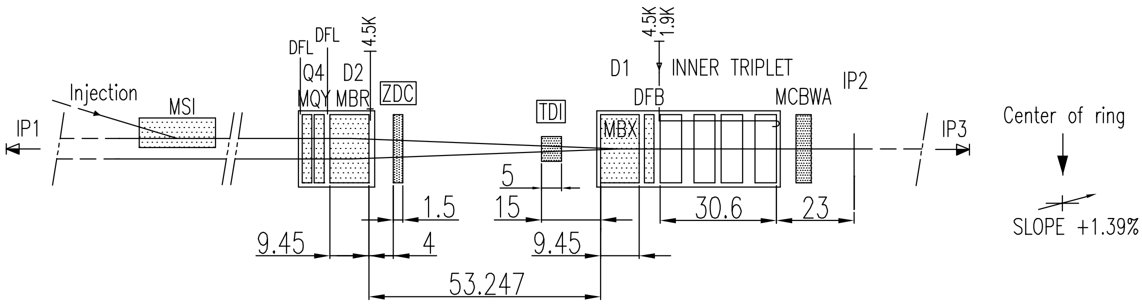

Figure 2.3. Schematic view of the beam line from ALICE interaction point (IP2) till the ZDC location.

At this distance from IP, spectator protons are spatially separated from neutrons by the magnetic elements of the LHC beam line. Therefore two distinct detectors will be used: one for spectator neutrons, placed at zero degrees relative to the LHC axis, and one for spectator protons, placed externally to the outgoing beam pipe on the side where positive particles are deflected (see fig. 2.4). In the ALICE TP [5] a third calorimeter for negative particles was proposed whose aim was to estimate and subtract the background due to participants from the proton ZDC signal. But further studies have shown that this contribution is negligible (see [6] pag. 43) and therefore this detector is no more foreseen in the ZDC project.

The detection technique adopted for the ALICE Zero Degree Calorimeters is the quartz fibres calorimetry [7]. The shower generated by incident particles in a dense absorber (the so called "passive" material) produces Cerenkov radiation in quartz fibres ("active" material) interspersed in the absorber. This technique has been chosen because it fulfills two fundamental requirements. Firstly, due to the small amount of space available (particularly for the neutron calorimeter), the detectors need to be compact and therefore a very dense passive material should be used as absorber in order to contain the shower. Secondly, the ZDC will operate in a very high radiation environment (about 10^4 Gy/day is the estimated dose for the neutron calorimeter at a luminosity of 10^{27} cm^{-2} s^{-1}) and radiation hardness is guaranteed by radiation resistance of quartz fibres [8, 9]. Furthermore the Cerenkov effect gives two more advantages: a very fast signal due to the intrinsic speed of the emission process and a very low sensitivity to induced radioactivation thanks to its threshold behavior.

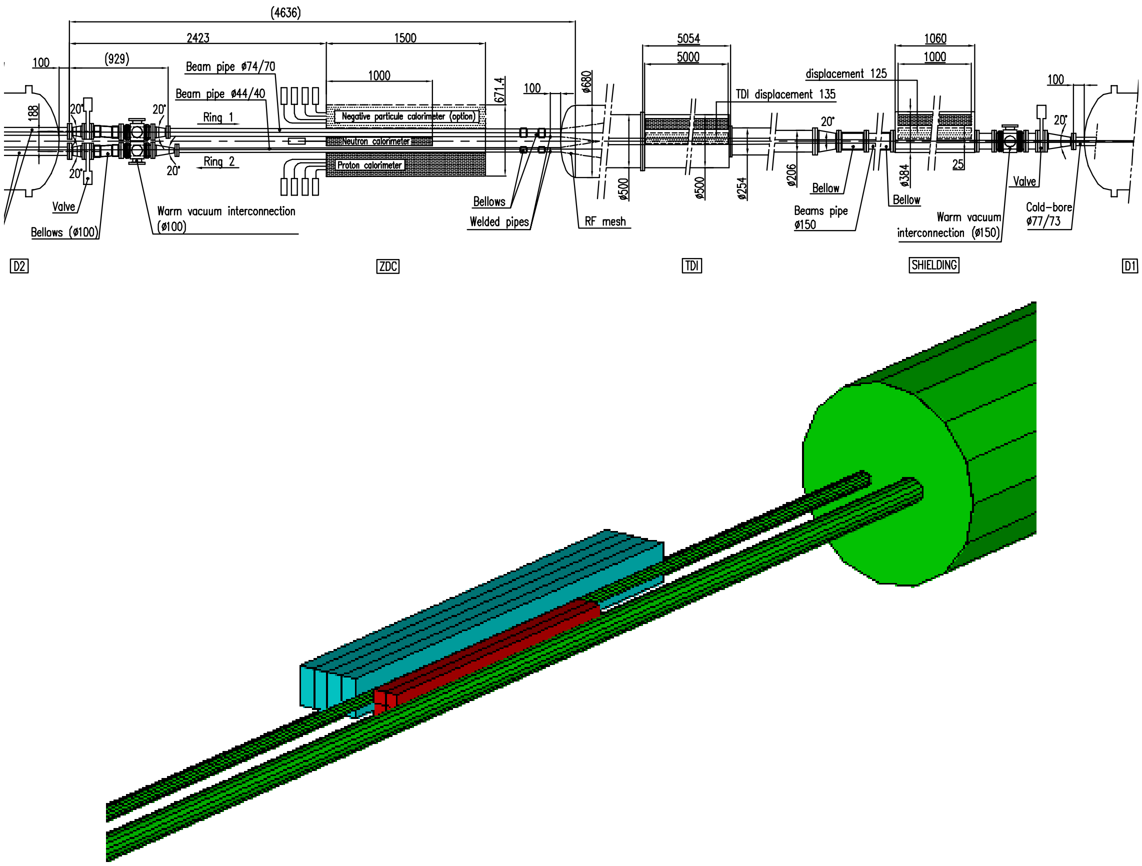

Figure 2.4. View of the ZDC in the LHC beam line.

As it has already said, the neutron ZDC (ZN) has the most severe geometrical constraint and therefore detector transverse dimension should not be greater than 7 cm (1 cm is left for the box containing the detector). For this reason a very dense passive material must be used to maximize containment of showers generated by neutrons of 2.76 TeV. For the proton calorimeter (ZP) there are no such stringent space constraints and, moreover, spectator protons spot has a large spatial distribution (as will be shown in section 2.4). Then a larger detector made of a less dense material can be used. Another important characteristic for these detectors is the fibre spacing that should not be greater than the radiation length of the absorber in order to avoid electron absorption in the passive material. Table 2.1 contains a summary of the main characteristics for the two detectors (further details can be found in [6]).

	ZN	ZP
Dimensions [cm^3]	$7.04 \times 7.04 \times 100$	$12 \times 22.4 \times 150$
Absorber	tungsten alloy	brass
$\rho_{absorber}$ [g cm^{-3}]	17.61	8.48
Fibre core diameter [μm]	365	550
Fibre spacing [mm]	1.6	4
Filling ratio	1/22	1/65

Table 2.1. Dimensions and main characteristics of absorber and quartz fibres for neutron and proton calorimeters.

Energy resolution

In principle the resolution on the centrality determination depends both on the intrinsic fluctuations in the number of participants at fixed b and on the energy resolution achieved by the ZDC. Simulation performed with the GEANT 3.21 package [10] for a single nucleon of 2.76 TeV impinging in the center of the front face gives a resolution value equal respectively to $(8.3 \pm 0.2)\%$ for the neutron calorimeter and to $(9.1 \pm 0.2)\%$ for the proton one (plots in fig. 2.5).

Neglecting as a first approximation the momentum smearing due to nucleon Fermi motion and supposing that all spectators are detected by the ZDC, the expected energy spread for N_s incident nucleons can be approximated as:

$$\sigma_{N_s}(E) = \sqrt{\sum_{i=0}^{N_s} \sigma_i^2(E)} = \sqrt{N_s}\, \sigma_i(E),$$

where σ_i is the width of the i^{th} energy distribution. For an impact parameter of 2 fm, for example, there are about 15 expected spectators for each nucleus (see fig. 2.2) and the resolution is 2.6%. This value, as will be shown in next paragraph, is well below the expected intrinsic fluctuations in the number of spectators at fixed b deduced from a nucleus-nucleus event generator, that gives a value above 15% for comparable impact parameters (see fig. 2.7).

Detector prototypes

The ZDC calorimeter used by the NA50 experiment can be considered as the ALICE neutron calorimeter prototype. In fact dimensions, passive material and filling ratio are comparable (a detailed description of the NA50 ZDC can be found in [9]). Furthermore the operational conditions in NA50 experiment are more severe than they will be in ALICE. In fact the whole beam energy is deposited in the detector, corresponding to 33 TeV per beam ion with an intensity of 10^7 Pb/s, leading to a maximum absorbed dose of the order of few Grad. The detector has shown a very

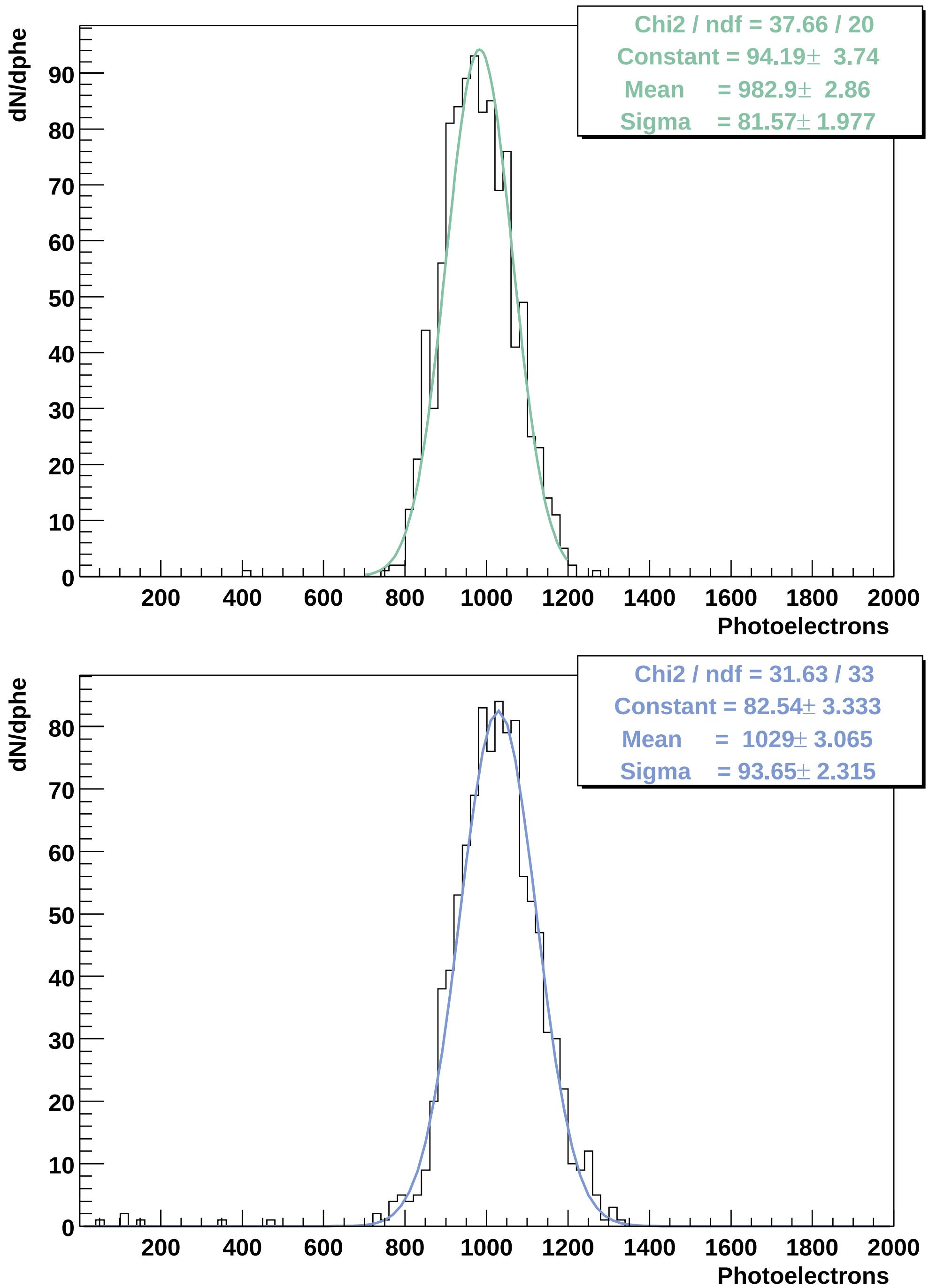

Figure 2.5. Resolution of neutron (up) and proton (down) calorimeters for a single nucleon of 2.7 TeV impinging in the center of detector front faces. The resolution is calculated from the superimposed gaussian fit.

high radiation hardness: the lead peak resolution as a function of the maximum dose suddenly deteriorated from the initial 6 % to 9%, but then remained almost stable (see fig. 2.6). On the contrary a worsening of the ZDC signal amplitude with increasing absorbed dose was observed, but the response lowering can be easily corrected by increasing the photomultiplier gains. On the other hand the detector has shown to be almost insensitive to induced radioactivation.

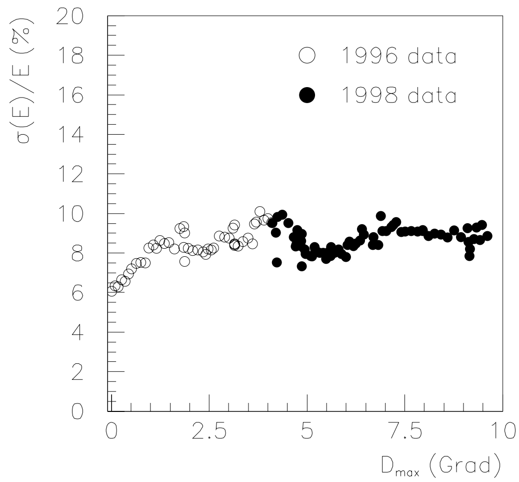

Figure 2.6. Resolution on the lead peak measurement as a function of the absorbed dose for the NA50 ZDC during 2 years of data taking [9].

A prototype of the proton calorimeter was built and tested with hadron beams at the CERN SPS accelerator. It had different dimensions relative to the ALICE one since its front face was square (16×16×150) cm^3 and also plastic fibres were used instead of the more expensive quartz ones (the main difference between the two is the numerical aperture that is 0.22 for the quartz fibres and 0.50 for the plastic ones). The prototype showed a good linearity as a function of the incident energy (beam energy ranged from 50 to 180 GeV), with an energy resolution $\sigma/\mathrm{E} = 240/\sqrt{\mathrm{E(GeV)}}$ that would lead to a value of the order of 5% at LHC energies. The response of the detector as a function of the particle impact point over the calorimeter front face was uniform. Results of the proton prototype beam test can be found in [11].

Therefore the proposed detectors for zero degree energy measurement at ALICE have demonstrated to fulfill the requirements needed in terms of radiation hardness and energy resolution.

ZDC for luminosity monitoring

Apart from their use for the determination of centrality collisions, the ZDC can also be used to monitor the LHC luminosity. The cross section for electromagnetic dissociation of heavy nuclei at LHC exceeds the nuclear one by several orders of magnitude and this will limit the beam lifetime. LHC luminosity can be monitored by the ZDC measuring the rate of mutual electromagnetic dissociation in one neutron channel. The interaction rate is in fact proportional to the luminosity $\mathcal{L}$:

$$\frac{dN^{EMD}_{1n,1n}}{dt} = \sigma^{EMD}_{1n,1n} \cdot \mathcal{L}.$$

Therefore the luminosity can be deduced from the measured rate if the cross section for mutual electromagnetic dissociation, $\sigma^{EMD}_{1n,1n}$, is known with good precision. The cross section for mutual dissociation in one neutron at LHC energies can be calculated in the framework of the Weizsäcker-Williams method. The estimated value for Pb-Pb collisions at 2.76 TeV per nucleon is ∼0.5 barn ([12], [13]). This process has been chosen since it can be easily identified by the simultaneous detection of one neutron on both sides with respect to the interaction point. Furthermore this reaction is almost background free and is detected with full acceptance by neutron ZDCs, assuring a rather precise measurement of the interaction rate.

2.3 Resolution on centrality

Intrinsic fluctuations and resolution on impact parameter

The intrinsic fluctuations in the number of spectators at fixed impact parameter are strong and they limit the resolution that can be achieved on centrality through a measurement of spectators energy. Moreover these fluctuations depend on the impact parameter value and they are higher for the most central collisions. To improve the resolution on centrality, statistical fluctuations on the number of spectators can be reduced, measuring spectators energy for both colliding nuclei. For this purpose, two system of ZDC will be placed on each side with respect to the IP to measure centrality in the ALICE experiment.

Fig. 2.7 shows the achieved resolution on impact parameter when only statistical fluctuations in the number of spectators are considered; results for one nucleus and for both nuclei are compared. $\sigma(\mathrm{b})/\mathrm{b}$ is $\gtrsim$ 20% for very central collisions (b $\lesssim$ 2 fm) where the fluctuations are very important due to the low number of spectators. For very peripheral collisions (b $\gtrsim$ 11 fm) the number of spectators remains approximatively constant over a wide b range. This causes a worsening in impact parameter resolution, as can be inferred from fig. 2.8, where the error made on b estimation is plotted as a function of centrality.

However, since the number of spectators on two sides are correlated, measuring non interacting energy on both sides the improvement on b resolution is of the order of 4%. Moreover it allows the rejection of events due to interactions between beam nuclei and residual gas particles.

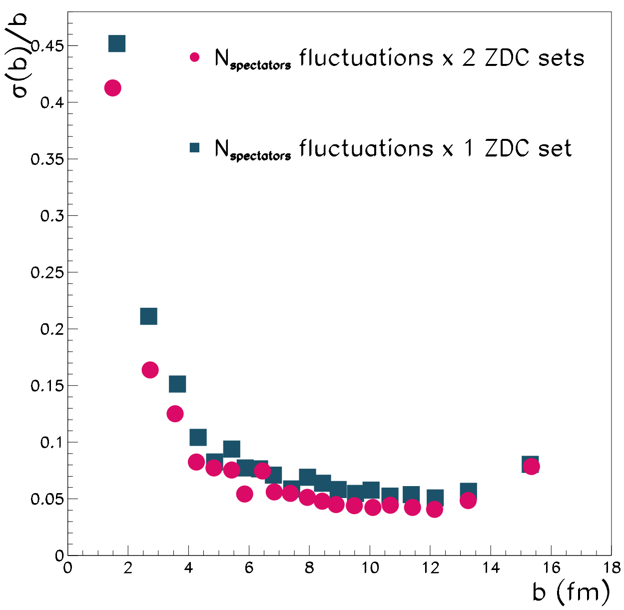

Figure 2.7. Resolution on the impact parameter for a measurement of spectators for one nucleus (in blue) and for both nuclei (in red), only statistical fluctuations on the number of spectators are considered.

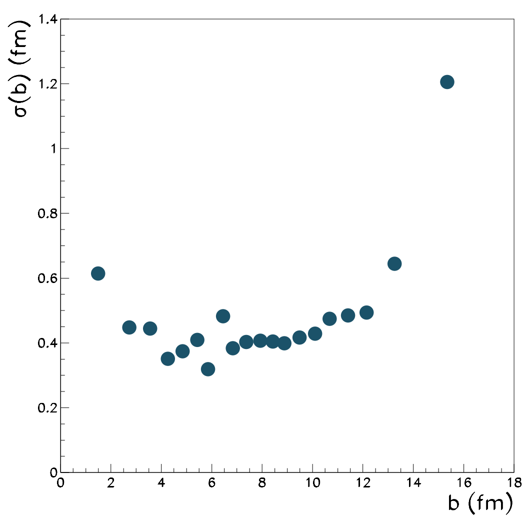

Figure 2.8. Centrality dependence of the absolute error made on impact parameter estimation from zero degree energy measurement for both colliding nuclei.

Detector response and resolution on impact parameter

Event generators give the number of spectators and of secondary particles produced for each b value; then GEANT package is used to track particles through the setup till the ZDC. Spectators are generated taking into account beam divergence and crossing angle as well as the Fermi motion (approximated with a two gaussian function [14]). Then the shower development inside the detectors is followed, energy losses and Cerenkov light yields are calculated. In this way the correlation between energy detected in the ZDC and impact parameter can be established taking into account detector resolutions.

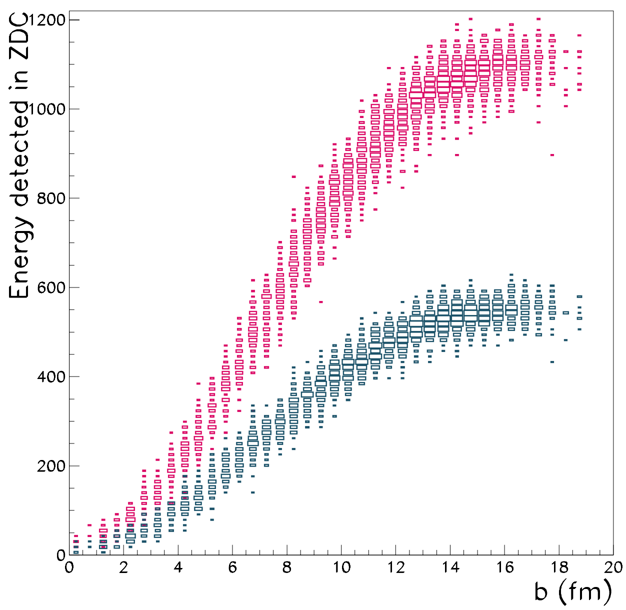

Figure 2.9. Correlation between total energy measured in ZDCs and impact parameter when spectators energy is measured for one nucleus (in blue) or for both colliding nuclei (in magenta).

In fig. 2.9 results obtained for 3000 HIJING minimum bias events are shown for one and two ZDC sets. The width of the correlation is due to intrinsic fluctuations and to detector energy resolution. In fig. 2.10 the resolution on impact parameter due both to statistical fluctuations and detector resolutions is compared with the one given only by intrinsical fluctuations. It can be seen that for central collisions the resolution is not strongly affected if detectors resolutions are considered. For very peripheral collision detector resolution is worsened by the fact that the number of spectators saturates and therefore for b $\gtrsim$ 11 fm the energy detected by the ZDC remains practically constant while b is still increasing (as can be seen in fig. 2.9).

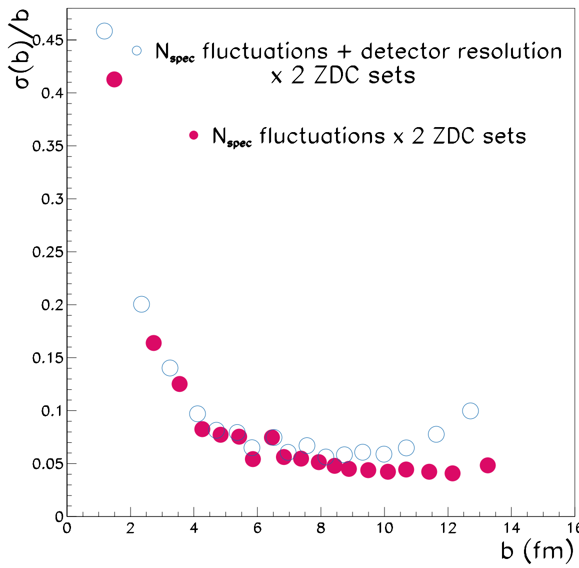

Figure 2.10. Resolution on b due to statistical fluctuations (red fill symbols) and when also detector resolutions are considered (blue open symbols). Spectators energy is measured for both interacting nuclei.

In conclusion the resolution on centrality measurement with the ZDC is not deteriorated by detector resolutions since it is widely dominated by the intrinsic fluctuations in the number of spectators at fixed impact parameter.

Resolution on the number of participants

Since the zero degree energy provides a direct measurement of the number of participants, the correlation between energy measured in ZDC and number of participating nucleons is narrower than the one between E_{ZDC} and impact parameter (see fig. 2.11).

Also the resolution on the number of participants is better compared to the impact parameter one; as can be seen in fig. 2.10. In very central collisions (b $\lesssim$ 2 fm) more than 350 participants are estimated from the Glauber model, the resolution is well below the 5% and it remains under the 10% until the number of participants is about 125, corresponding to an impact parameter of about 9 fm. For $N_{part} \lesssim 50$ the resolution is strongly worsened, but this corresponds to very peripheral events with b $\gtrsim$ 11.5 fm.

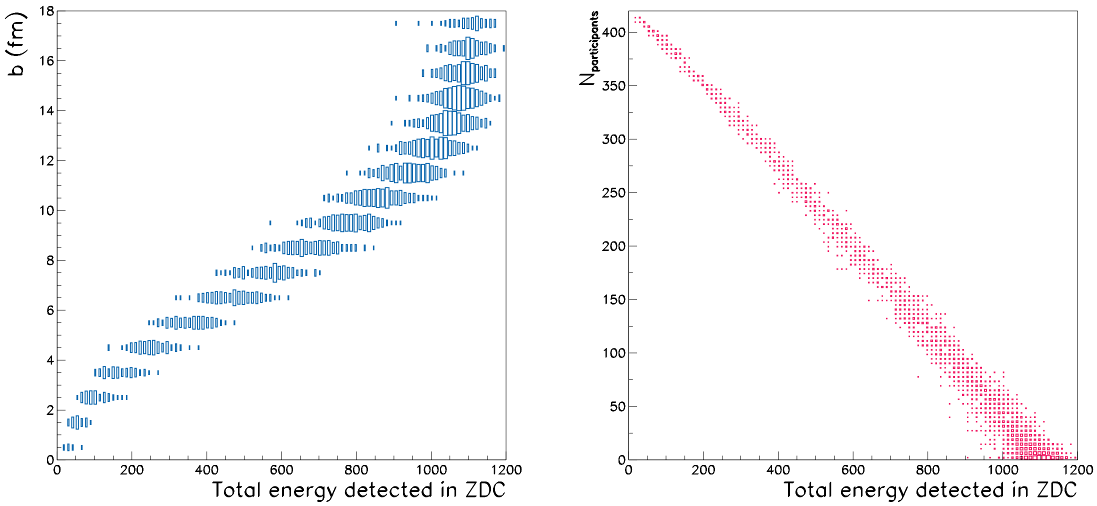

Figure 2.11. Left: correlation between E_{ZDC} and the impact parameter. Right: correlation E_{ZDC} versus the number of participants.

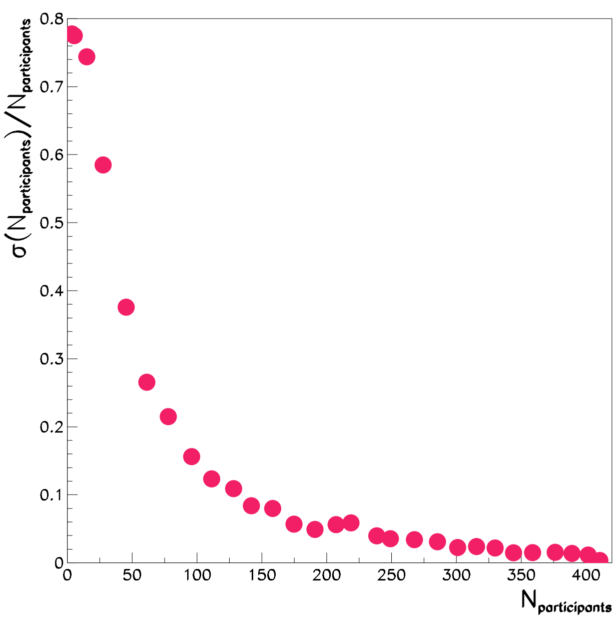

Figure 2.12. Resolution in the number of participants deduced from ZDC.

2.4 Spectator proton losses

GEANT simulations give evidence of spectator proton losses along the beam line due to the magnetic fields whose aim is to deflect and focalize the ion beams. The spatial distribution of spectator protons strongly depends both on LHC optics and on momentum broadening due to Fermi motion. The longitudinal component of Fermi momentum is crucial since it is Lorentz boosted and it gives a spread of the order of 500 GeV/c for the longitudinal momentum of spectators (see fig. 4.7). Therefore any magnetic field encountered by protons gives a kick to their trajectories and some of them are lost along the beam. In table 2.2 the magnetic elements of the beam line from IP to the ZDC and their main characteristics are reported, field values refer to version 6.2 of LHC optics. The first magnetic element is a dipole needed to compensate the field of the dimuon arm dipole. It is followed by a quadrupole triplet that squeezes the beams and bring them into collision. The last magnetic element before the ZDCs is a superconducting dipole that separates the two beams. After this dipole a large horizontal dispersion of spectator protons is observed.

Magnetic element	Distance from IP (m)	Magnetic length (m)	Nominal field
Corrector dipole	19.216	1.7	-0.914 T
1^{st} quadrupole	23.0	6.3	-204.43 T/m
2^{nd} quadrupole	31.8	5.5	204.43 T/m
3^{rd} quadrupole	38.3	5.5	204.43 T/m
4^{rth} quadrupole	47.3	6.3	-204.43 T/m
Separator dipole D1	58.383	9.45	3.796 T

Table 2.2. Parameters of the beam line magnetic elements (LHC optics v6.2).

Other relevant parameters of LHC optics that affect protons detection are: the displacement of the closed beam orbit, the aperture of the dipole D1 and the radiofrequency screen in the design of the removable dump (indicated as TDI) that, during beam injection, remains closed to avoid the quenching of the superconducting magnet D1. In fig. 2.13 a top view of the ALICE setup from the IP to the ZDC can be seen; the red superimposed tracks represent 40 spectator protons of 2.7 TeV. Dimuon absorber, beam shielding and magnetic dipole are included in the geometry; they are followed by the quadrupole triplet, the D1 dipole and the TDI element. Summary of proton losses in the various elements of beam optics and in the insertion region are reported in table 2.3. The current configuration foreseen for the D1 aperture is the main limitation on the acceptance for spectator protons; furthermore a not negligible amount of proton arrives at ZP location but is outside its acceptance.

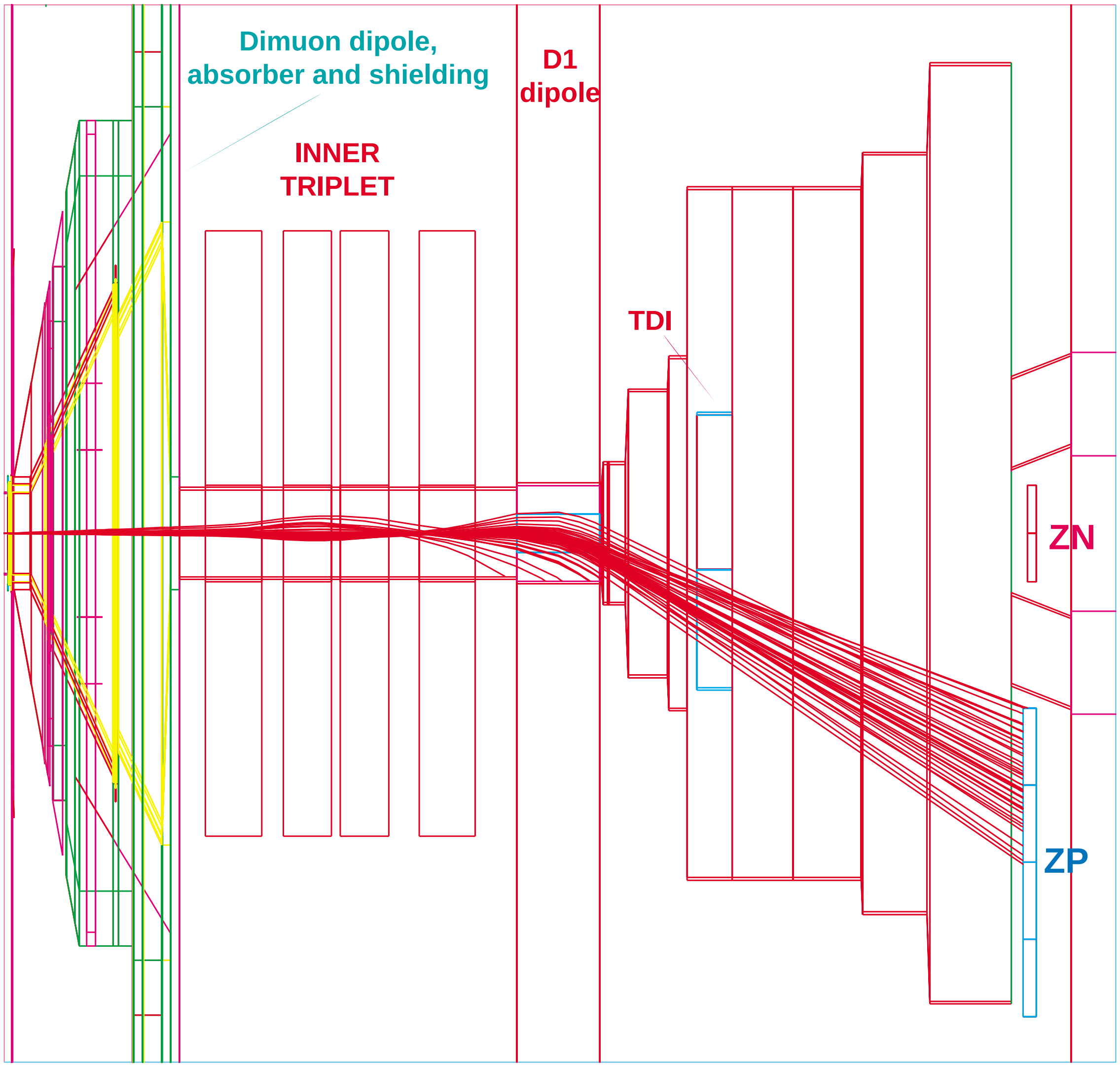

Figure 2.13. Tracking of spectator protons from the IP to the proton ZDC (results obtained with version 6.2 of LHC optics). Draw is not to scale; it is in fact strongly compressed in the beam direction since from IP to the ZDCs the distance is 116 m, while the transverse dimension of the proton calorimeter is 22.4 cm.

Volume	Proton lost (%)
Inner triplet	0.2%
Dipole D1	13.8%
TDI volume	0.11%
Outside ZP acceptance	8.5%
Detected in ZP	77.4%

Table 2.3. Percentages of spectator proton losses along the beam line. Version 6.2 of LHC beam optics has been used.

Protons that reach the calorimeter will have a spot rather enlarged in the horizontal coordinate, mainly because of D1 fields: 90% of detected protons will hit a (12.6×2.8) cm^2 area (see fig. 2.14). This explains the reason why a rather large device has been designed.

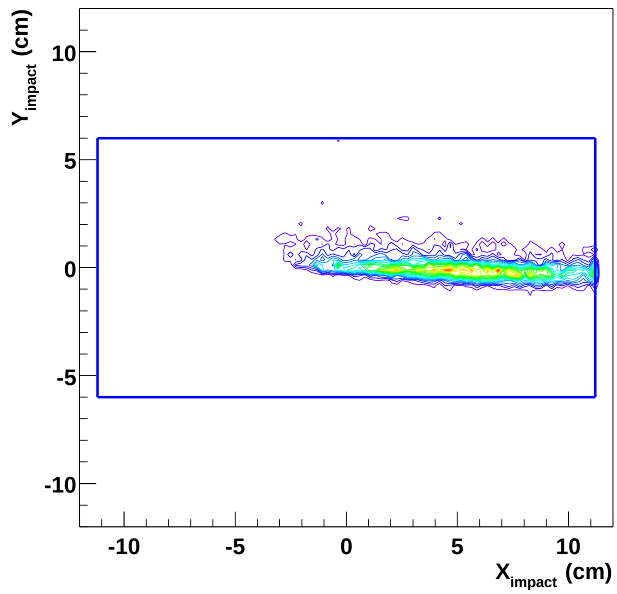

Figure 2.14. Spectator protons spot over the proton calorimeter front face (the blue box), whose surface is (22.4×12) cm^2.

For spectators neutrons only spreading due to Fermi momentum has to be taken into account and the spot of neutrons over the front face of the ZN is 0.6×0.6 cm^2 at 1σ level (see fig. 2.15).

2.5 Nuclear fragmentation

In nucleus-nucleus collisions nuclear fragments are produced; unfortunately they have a charge to mass ratio similar to that of the beam and will therefore not be detected by the ZDC but they will remain in the beam pipes. The fragmentation of colliding nuclei will strongly affect the correlation between E_{ZDC} and b.

A study of nuclear fragment production dependence on the impact parameter at LHC energies has been carried out; here only basic hypothesis and results of this work will be presented, further details can be found in [6] (pag. 68-72). Comparing experimental data at lower energies it comes out that the cross section for fragments production depends very weekly on beam energy; it is rather related with the geometry of the collision. A simple model to evaluate fragments production at LHC energies has been developed based on this assumption.

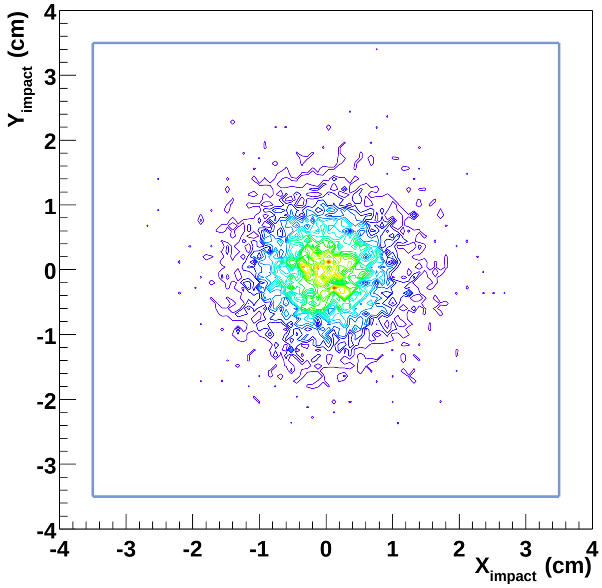

Figure 2.15. Spectator neutrons spot over the neutron ZDC front face (the blue box), whose surface is (3.5×3.5) cm^2.

The number of fragments and their charge distribution have been fitted from ALADIN experimental results [15]. They are both function of the variable Z_{bound} ($Z_{bound} = \Sigma_i Z_i$ with $Z_i \geq 2$), that can be evaluated as a function of the impact parameter. In fact, assuming that Z_{bound} is a monotonic function of the impact parameter, the following relationship holds between the two quantities:

$$\int_0^{Z_{bound}} \frac{d\sigma}{dZ^{'}_{bound}} dZ^{'}_{bound} = \int_0^b \frac{d\sigma}{db} db^{'} .$$

Therefore the number of fragments and their charge can be calculated as a function of the impact parameter. The number of fragments is found to be very small for central events, it reaches its maximum value for intermediate b values and then decreases for peripheral collisions. On the other hand the charge of produced fragments increases with centrality; therefore the production of nuclear fragments is more important for peripheral events where few fragments with an atomic number close to that of the projectile are produced.

The model used to describe fragmentation at LHC described in [6] did not consider deuteron production (since their production is not included in ALADIN results or in other emulsion experiments). The NA49 experiment measured the energy carried by all produced fragments, including deuterons, in Pb-Pb collisions at SPS energies. Their results, reported in reference [16], provide the number of spectator nucleons as a function of the impact parameter. Since our model should not depend on beam energy, we compared the number of free (not bound in fragments) spectator nucleons calculated by our model with the one measured by NA49. The found difference has been imputed to deuteron production. The ratio between the measured number of free neutrons and the calculated one has a linear behavior as a function of b and can be easily fitted (see fig. 2.16). The obtained parameterization for deuterons production has been taken into account and fragments production at ALICE energies have been evaluated. Results are reported in fig. 2.17.

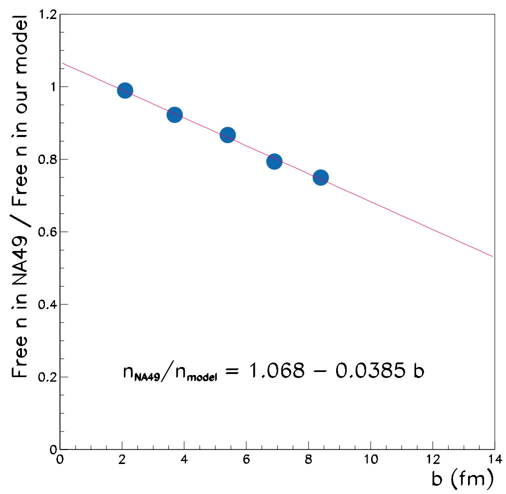

Figure 2.16. Ratio between the number of free spectator neutrons measured by the NA49 experiment [16] and the number evaluated through our fragmentation model without considering deuterons production.

The results obtained with our model have then been compared to RHIC experimental results. From PHENIX experimental data showed in fig. 2.18 we extracted the maximum number of free spectator neutrons detected by the ZDC. Correcting this number for detector acceptance (of the order of 76%), about 36 free neutrons are found in Au-Au collisions at 130 A GeV. From published NA49 results the maximum number of free nucleons is 60, that, corrected for the Z/A ratio, leads to a maximum number of free neutrons of about 38 in Pb-Pb collisions at 158 GeV per nucleon. A comparable result has been obtained with our model, as can be seen in fig. 2.17. Therefore the maximum number of free neutrons does not depend on beam energy at least from SPS to RHIC energies. Furthermore our fragmentation model, tuned on NA49 experimental data, reproduces RHIC results and therefore the assumptions made and the extrapolated parameterization are consistent.

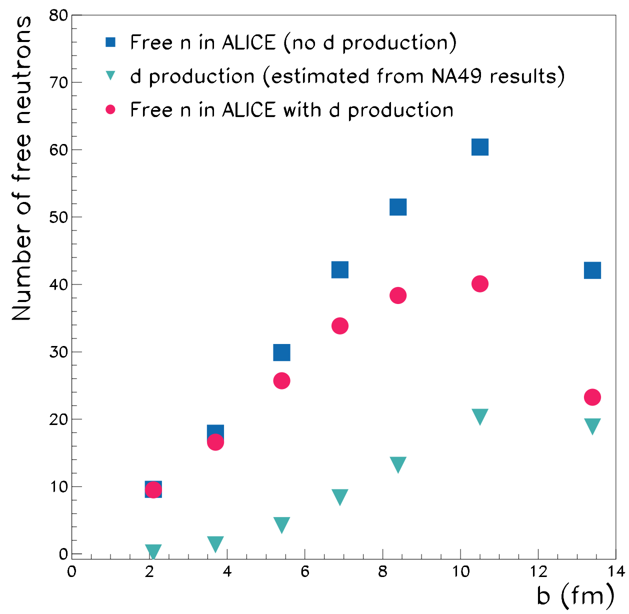

Figure 2.17. Results for fragments production at ALICE when deuteron production is taken into account.

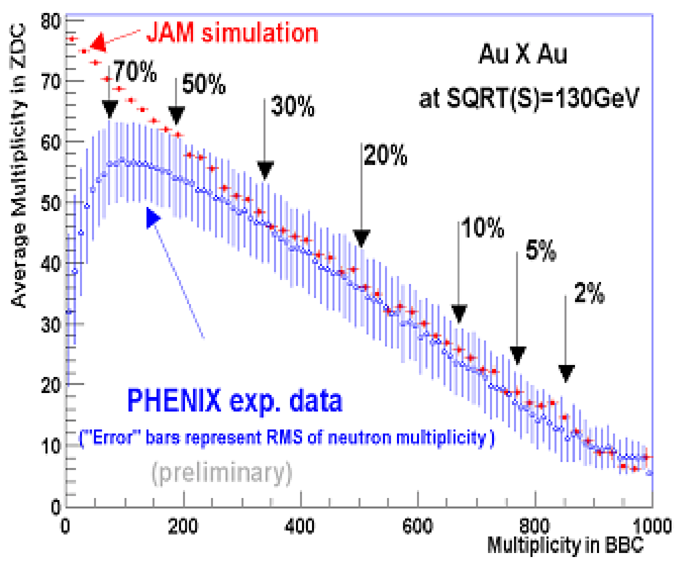

Figure 2.18. Average neutron multiplicity in ZDC as a function of particle multiplicity measured in beam beam counter at PHENIX [17].

2.5.1 Centrality determination with fragments production

The model for fragment production has been used with the HIJING event generator. From the number of spectator protons and neutrons obtained from HIJING the fragmentation algorithm calculates, as function of the impact parameter, the number of free spectators. When fragmentation is taken into account the correlation between the energy detected in ZDC and the impact parameter is no more monotonic, but the zero degrees energy is strongly lowered for peripheral collisions (see fig. 2.19).

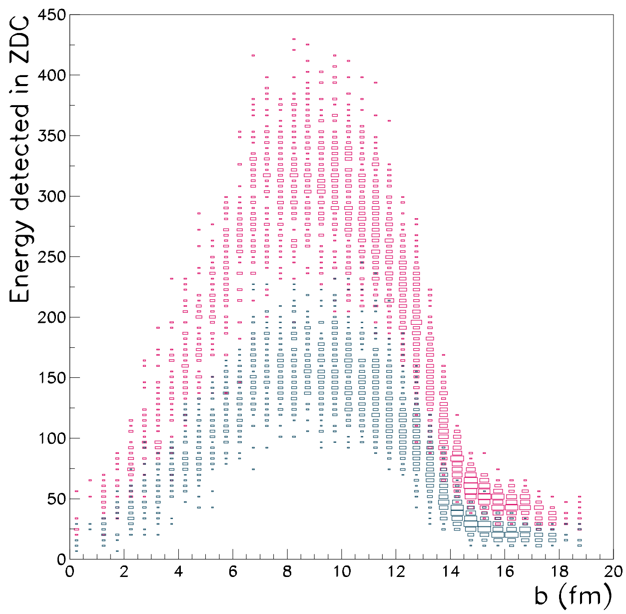

Figure 2.19. Energy detected by the ZDC as a function of the impact parameter of the collision when production of nuclear fragments is considered. In red energy is measured for both colliding nuclei, in blue only for one nucleus.

Considering fragmentation the measurement of the energy carried by spectators alone can no longer be used to unambiguously determine the impact parameter of the collision, since for a fixed E_{ZDC} value there are two possible values for the impact parameter, one corresponding to central and one to peripheral collisions.

This ambiguity can be avoided using information given by another centrality estimator such as transverse energy, forward multiplicity or participants energy. The produced multiplicity increases monotonically with the centrality of the collision; therefore, putting appropriate thresholds on the amount of multiplicity measured by (central or forward) multiplicity detectors, peripheral collision can be easily distinguished from central ones. This is the approach used by the RHIC experiments, where the energy detected in neutron ZDCs is correlated with the multiplicity measured in forward beam beam counters. The found correlation allows to define centrality classes that select a certain fraction of the total cross section, as indicated in fig. 2.18.

In ALICE the energy carried by participants and secondaries is measured by means of a forward electromagnetic calorimeter, whose design and performances will be the subject of the next chapter.

References

[1] R. J. Glauber, Lectures in Theoretical Physics, edited by W. E. Brittin. L. G. Dunham, Interscience, NY, 1959, vol. 1, p. 315.

[2] D. E. Groom *et al.*, Eur. Phys. J. C **15** (2000) 1.

[3] K. Werner, Phys. Rep. **232** (1993) 87.

[4] X. N. Wang, M. Gyulassy, Phys. Rev. D **44** (1991) 3501.

[5] ALICE Technical Proposal, CERN/LHCC/95-71.

[6] ALICE Collaboration, ZDC Technical Design Report, CERN/LHCC 99-5.

[7] P. Gorodetzky *et al.*, Proc. Fourth Int. Conf. on Calorimetry in High Energy Physics, World Scientific, Singapore (1994) 433.
G. Anzivino *et al.*, Nucl. Phys. B (Proc. Suppl.) **44** (1995) 168.
O. Ganel, R. Wigmans NIM A **365** (1995) 104.

[8] P. Gorodetzky *et al.*, Radiation Physics and Chemistry, Pergamon Press, Oxford (1992) 253.
P. Gorodetzky *et al.*, NIM A **361** (1995) 161.

[9] R. Arnaldi *et al.*, NIM A **411** (1998) 1.

[10] GEANT 3.21, CERN Program Library Long Writeup W5013.

[11] R. Arnaldi *et al.*, NIM A **456** (1998) 717.

[12] A. J. Baltz, C. Chasman, S. N. White, NIM A **417** (1998) 1.

[13] I. A. Pshenichnov *et al.*, Phys. Rev. C **64** 024903 (2001), [nucl-th/0101035].

[14] A. Shor *et al.*, Nucl. Phys. A **514** (1990) 717.

[15] ALADIN collaboration, Z. Phys. A **340** (2001) 248.

[16] NA49 Collaboration, Eur. Phys. J **A2** (1998) 383.

[17] S. White for the PHENIX collaboration, contribution to the 15th International Conference on Ultra-Relativistic Nucleus-Nucleus Collisions, QM 2001, Long Island, New York.

Chapter 3

The forward electromagnetic calorimeter

3.1 Detector characteristics and centrality determination

The ZDC project includes a forward electromagnetic calorimeter to improve the centrality trigger in ALICE. It is designed to measure, event by event, participant nucleons and secondary particles energy, essentially photons generated from π^0 decays.

The detection technique employed for the electromagnetic calorimeter is the same used for the hadronic devices described in the previous chapter. The most important difference consists in the choice of the angle of the fibres relative to incoming particles; in fact fibres are oriented at 45°, while for the hadronic devices they are at 0°. This choice has been adopted in order to maximize the detector response, since Cerenkov light production has a pronounced peak around 45° [2]. The electromagnetic calorimeter is made of lead, with quartz fibres sandwiched in layers between the absorber plates. Two consecutive planes of fibres are separated by a lead thickness of 3 mm that, due to the 45° inclination, results in a total thickness of 4.24 mm seen by incident particles. Fibre cores have a diameter of 550 μm and the active to passive volume ratio is about 1/11. The resulting calorimeter dimensions are (7×7×21) cm^3, the total absorber length corresponding to about 30 radiation lengths. This condition assures the total containment of showers generated by participants at LHC energies. As can be seen in fig. 3.1 particles detected in ZEM have energies going up to 3500 GeV, with an average value around 650 GeV.

The simulations show that the energy measured by the forward calorimeter will be anti-correlated with the impact parameter, being high for central collisions and low in peripheral ones and it has a monotonic behavior as a function of centrality.

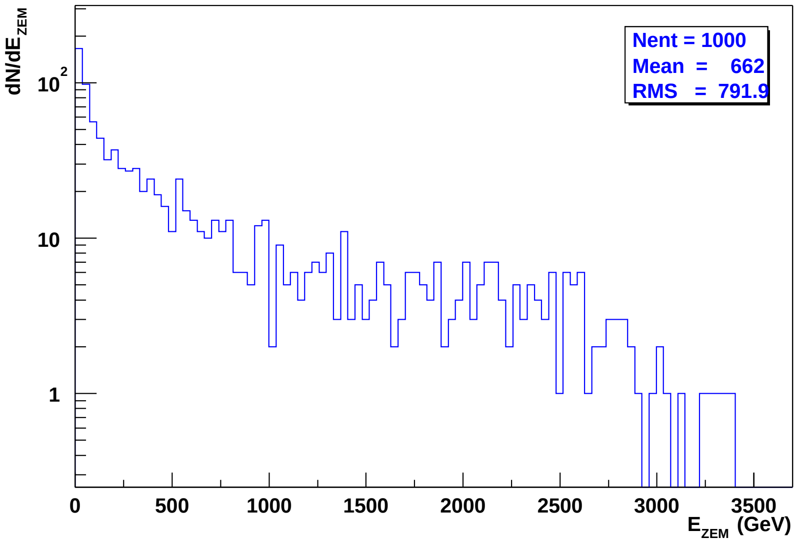

Figure 3.1. Energy detected in ZEM calorimeter obtained from a minimum bias sample of Pb-Pb collisions generated with HIJING.

Information provided by the electromagnetic calorimeter will therefore be used in order to help disentangling central from peripheral collision, assigning the correct impact parameter value to the energy measured in hadronic ZDCs.

3.1.1 Rapidity range

In ZDC Technical Design Report [1], the proposed position for the detector was at ZDC location (116 m from the IP) above the neutron calorimeter, just outside the cone of spectator neutrons. The pseudorapidity range covered by the two detectors, placed on both sides relative to IP, is between 7.8 and 9.2.

In fig. 3.2 the energy detected by the two electromagnetic detectors as a function of the impact parameter is shown. To obtain this distribution Pb-Pb collisions at LHC energies have been generated with HIJING [7], particles are tracked in the ALICE setup using the GEANT [4] code. Selecting events with an energy released in the ZDC smaller than a certain threshold, not only central but also peripheral interactions are selected, because of fragmentation (see section 2.5). Requiring the energy detected by the electromagnetic calorimeters to be higher than a certain threshold value, helps in rejecting peripheral events. Nevertheless, as can be seen in fig. 3.2, the rejection efficiency for peripheral events is not 100%.

Studying the acceptance of the detector and analyzing the correlation between electromagnetic calorimeter and ZDC energies (plotted in fig. 3.5) it has emerged that the proposed location of the electromagnetic calorimeter is far from being optimal.

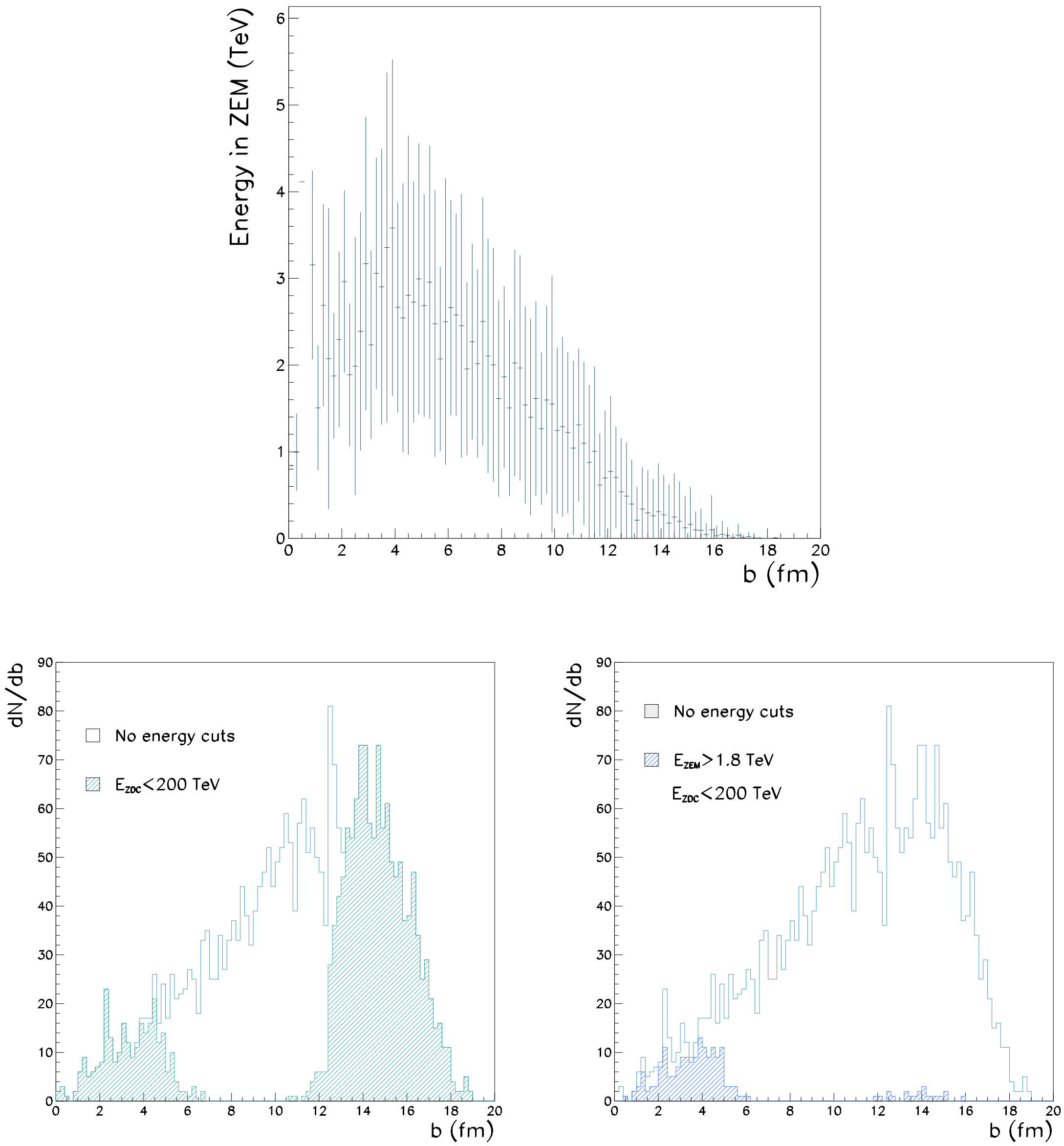

Figure 3.2. Total energy detected in electromagnetic calorimeters placed at 116 m from IP (up). Events selected requiring that the energy released in hadronic ZDCs is higher than 200 TeV (down right) and when also a threshold in energy detected by electromagnetic calorimeters is used (down left).

A way to increase detector acceptance and to obtain a narrower correlation is to move the electromagnetic calorimeters closer to the IP. In this way, shifting the detector acceptance to more central rapidities, the electromagnetic calorimeter can detect a significant number of particles produced in the interaction. In the original position the optics elements between the IP and the ZDC location drastically reduce the intercepted solid angle and therefore the number of detectable secondaries. The measurement would be substantially dominated by the high level of fluctuations in number of detected photons. The increase in detected energy obtained with the shift of detector acceptance leads to an improvement of the correlation between the measured energy and the impact parameter. Therefore the new position chosen for the calorimeters is at about 7 m from the IP, just before the coils of the first compensator dipole. Two devices will be placed on the same side relative to the IP, on the opposite side with respect to the dimuon arm. In this configuration the electromagnetic devices cover the pseudorapidity range $4.8 < \eta < 5.7$.

The correlation between energy measured by the two forward electromagnetic calorimeters (called ZEM since they belong to the ZDC project) and the impact parameter is shown in fig 3.3.

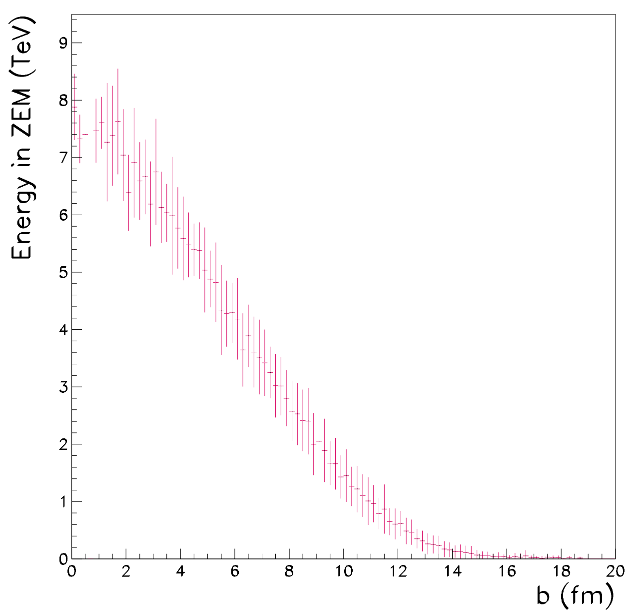

Figure 3.3. Energy detected by two zero degrees electromagnetic calorimeters as a function of the impact parameter.

In fig. 3.4 the performance of the detector in the new position is shown. It can be seen that there is no contamination due to peripheral events when both a cut on

ZDC and a threshold in ZEM energies are applied. The electromagnetic calorimeter allows to resolve the problems due to fragment production.

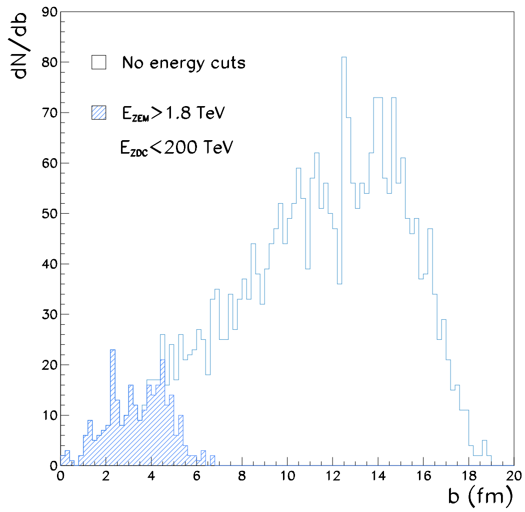

Figure 3.4. Impact parameter distribution for a minimum bias sample and, superimposed, events selected requiring that the energy detected in hadronic calorimeters is higher than 200 TeV and that electromagnetic forward energy is lower than 1.8 TeV.

The correlation between the total energy detected in the electromagnetic calorimeters in the new position and the energy measured by ZDC is shown in fig. 3.5. The improvement in the definition of the correlation is evident.

In the following, after a brief survey of the calorimeter characteristics, I will discuss the design criteria of the detector, describing in more details the studies for the optimization of its response through the use of an air light guide. Results of the beam test performed on a prototype of the ALICE electromagnetic calorimeter will be presented and compared to the simulations.

3.2 Air light guide

R&D tests performed on prototypes with fibres tilted at 45°, showed an increase of the response as a function of the vertical impact coordinate over the detector front face (see fig. 3.6). Such a strong increase in light output is due to shower leakages into the fibres outside the absorber. In fact for these prototypes fibres were directly coupled with photodetectors; therefore they exit from the absorber plates leaving a relatively long section in air. When particles hit the calorimeter near its upper edge, where fibres are in air, particles from the shower are not absorbed by lead and therefore they can cross several fibres producing an additional amount of light.

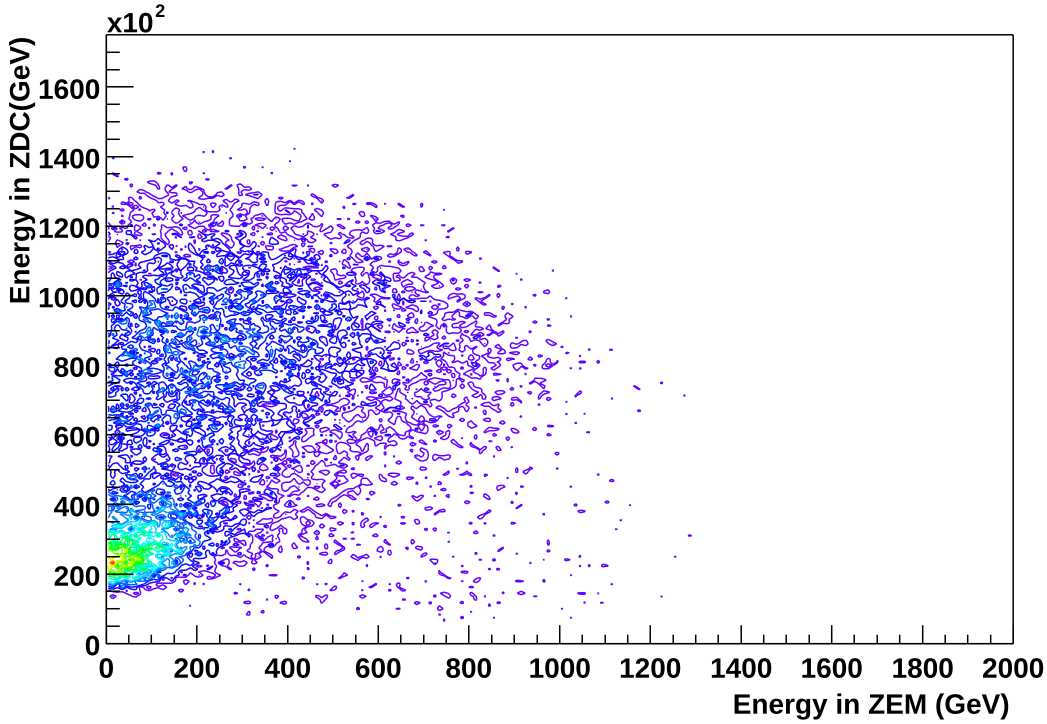

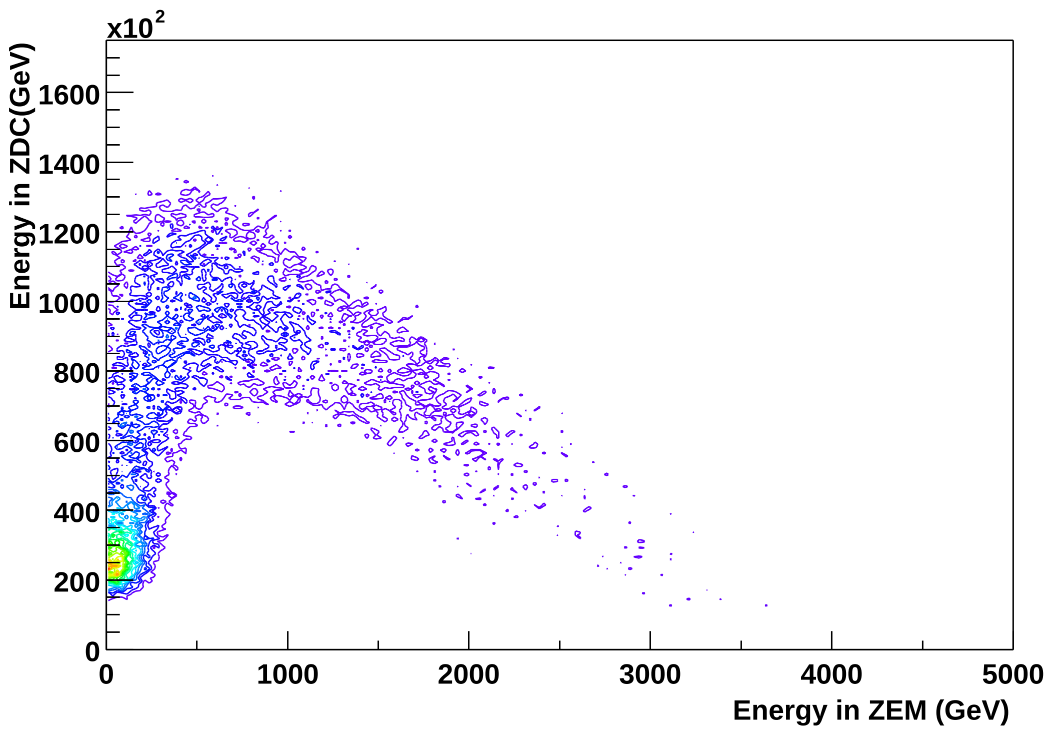

Figure 3.5. Correlation between energy measured by one ZEM and one ZDC set (up) for ZEM located at 116 m from IP and (down) for the new proposed position at 10 m from IP.

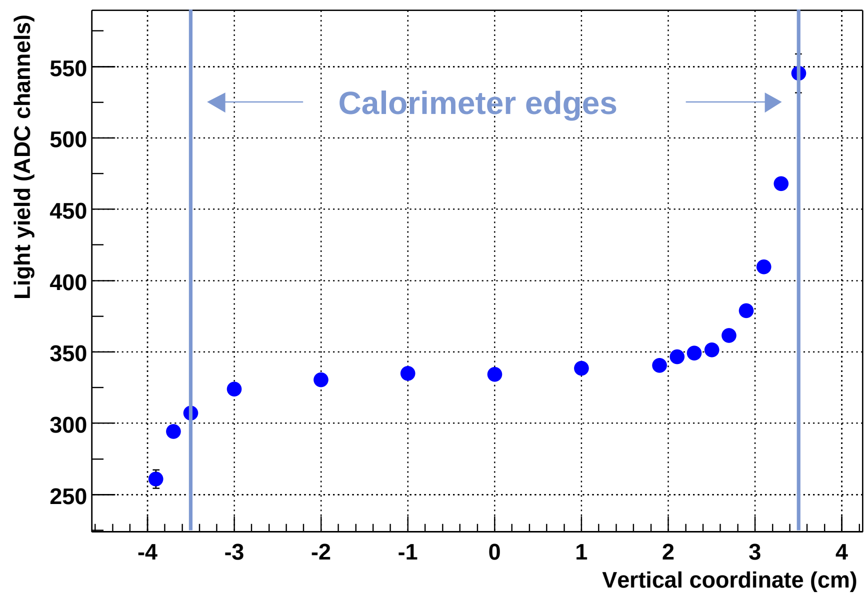

Figure 3.6. Response as a function of the vertical impact point on the front face of a prototypes with fibres tilted at 45° and directly connected to the photodetector.

The ALICE ZEM has been designed in order to limit this effect. Fibres are cut close to the upper edge of the lead plates and produced light is optically guided to the photomultiplier by means of an air light guide.

The geometry and the characteristics of the air light guide have been studied in detail in order to optimize the efficiency in light transmission and the response uniformity as a function of the point where light is produced. Concerning the uniformity of the response it is clear that, since the guide can not be symmetric along the longitudinal direction, light transmission will depend on light production point. In the following the results of the studies done for the optimization of uniformity and efficiency will be reported, then the performance obtained with a prototype of the guide in experimental tests will be discussed and compared with simulation results.

The geometry of the guide is constrained both by the dimensions of the calorimeter and by the transversal dimension of the photomultiplier. In order to maximize the response uniformity the photodetector dimension should correspond the cross section of the light guide [3]. Therefore the designed guide has a rectangular bottom face with the same dimensions of the calorimeter (21×7) cm^2 and a squared top face (2.8×2.8) cm^2 (since the diameter of the used photocatode is $\sim$3 cm). A lateral view of the guide is shown in fig. 3.7.

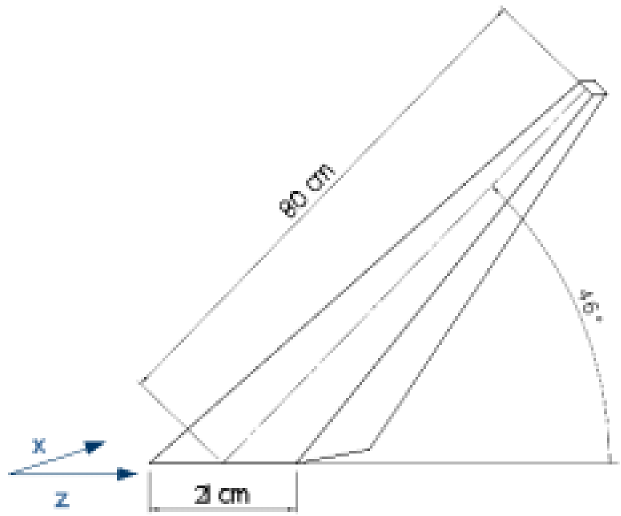

Figure 3.7. Lateral view of the air light guide.

3.2.1 Transmission efficiency and signal uniformity

Simulations

The parameters of the guide that can be studied in simulation are the guide length, the inclination angle and the treatment of the inner walls. Simulations with the GEANT package [4] have been performed and the effect of these parameters on the guide transmission efficiency and on the uniformity of the produced signal have been studied. Inclination angles going from 20° to 50° have been investigated; while the guide length has been varied between 20 and 90 cm. Two different treatments for the guide inner walls have been simulated: diffusing and reflecting surfaces. These two situations were obtained setting opportunely a GEANT parameter that defines the surface “quality”. The light output has been studied as a function of both the longitudinal (z) and the transversal (x) coordinates of the light production point (see fig. 3.7), for the different inclinations, lengths and treatment of the inner walls.

The results can be summarized as follows:

- the guide tilted at 46° shows the best signal uniformity as a function of the light production point;
- a shorter length implies a higher transmission efficiency due to the lower number of photon reflections inside the guide and thus to the lower probability of a signal loss. For longer guides the higher number of reflections reduces the transmission efficiency but the light output is more uniform;
- reflecting inner walls seems to be the more adequate choice in order to optimize light transmission efficiency.

The efficiency as a function of the light production point for two guide lengths (50 and 80 cm) and for both reflecting and diffusing inner walls are showed in fig. 3.8. Mean efficiencies values obtained from simulations are reported in table 3.1.

Inner walls	Length = 50 cm	Length = 80 cm
Reflecting	$\epsilon = (55.7 \pm 4.7)\%$	$\epsilon = (48.3 \pm 2.9)\%$
Diffusing	$\epsilon = (34.2 \pm 7.9)\%$	$\epsilon = (25.1 \pm 5.0)\%$

Table 3.1. Simulation results for mean transmission efficiency of the air light guide for different guide length and inner walls.

The degree of uniformity for the four guides has been evaluated as the maximum spread of efficiency values weighted on the mean value. In this way a factor lower than 9% has been calculated for the guides with reflecting inner walls, while for diffusing guides this ratio is around 20%. The uniformity of light output as a function of the transverse (x) coordinate is within 4% for all the guides. This could be easily predicted considering that the guide is symmetrical in that direction.

In order to test simulation reliability, three guide prototypes have been built and tested: two with inner reflecting walls, one 80 cm and the other 50 cm long, and the third with diffusing walls and a length of 50 cm. These particular lengths were chosen for two different reasons: 50 cm for the high value of efficiency in light transmission and the 80 cm length for the good uniformity as a function of the light production point. Inner walls made of Al sheets were polished for the reflecting guides and were painted in white for diffusing ones. To try further optimization of the light transmission efficiency, another guide prototype with length of 80 cm has been successively built. For this guide the reflecting inner walls have been obtained with a more sophisticated method, i.e. deposing deposited under vacuum an aluminum layer on plexiglas sheets.

Laboratory tests

The guides have then been tested in laboratory with a stable light source. The experimental setup used is quite simple and a schematic view can be seen in fig. 3.9. Light from a blue LED is directed towards two quartz fibres, of the same type of the ones that will be used for the electromagnetic calorimeter. One fibre, tilted at 45°, carries the light to the light guide. An XP2020 photomultiplier, tilted at 46° relatively to the horizontal plane and thus parallel to the guide axis is positioned on the other side of the guide. The other fibre is directly connected to another photomultiplier, whose output is stable enough to be used as reference signal to check the stability of the light source (variations of the order of 5% were observed during the whole test). The signal from the two photomultipliers has been digitized using an ADC. Dividing the mean ADC value from the guide photomultiplier by

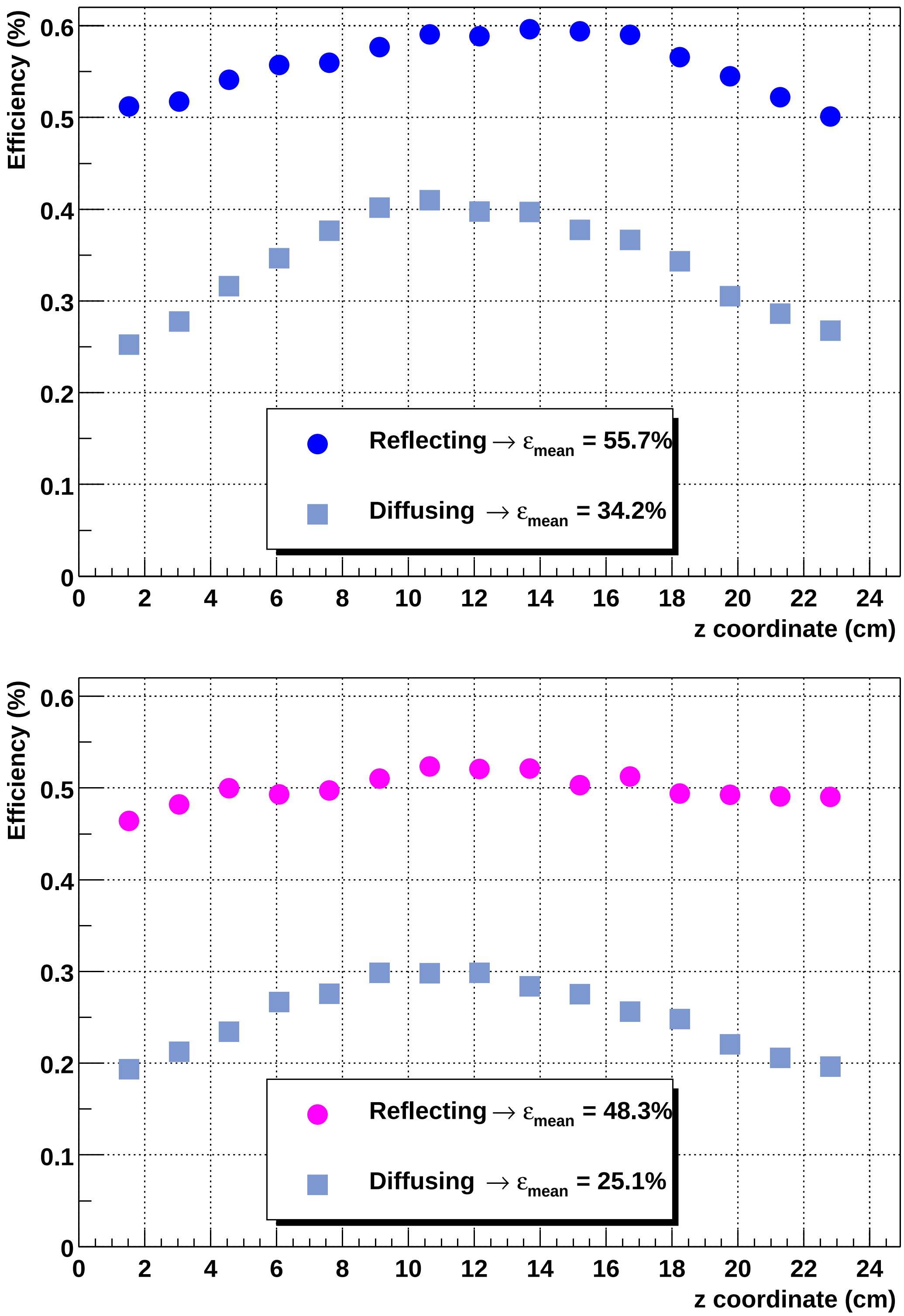

Figure 3.8. Light transmission efficiency as a function of the light production point in the longitudinal (z) direction for 50 (top) and 80 (bottom) cm long guides. Mean values for transmission efficiencies are also indicated.

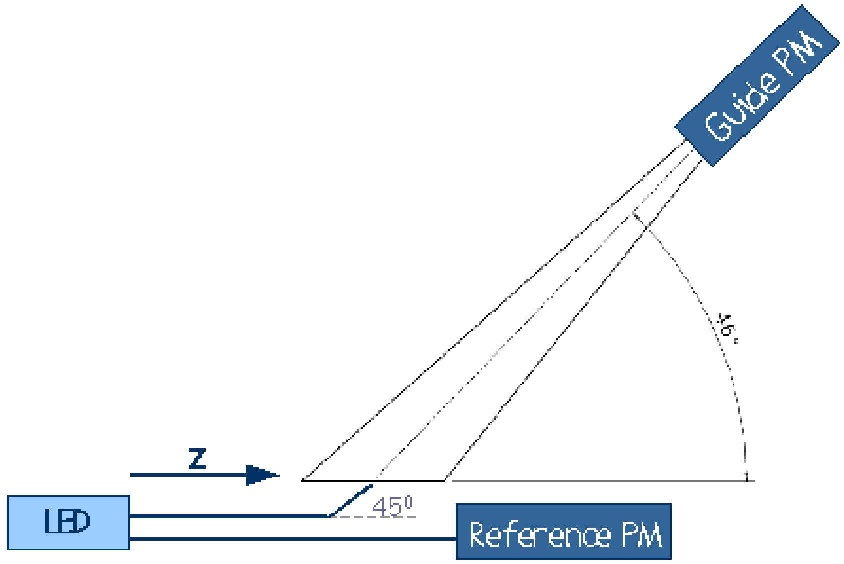

Figure 3.9. Scheme of the experimental setup for the laboratory test of the light guides.

the mean ADC value of the reference photomultiplier, comparable quantities for different guides can be obtained. The fibre position under the guide has been varied both in the longitudinal (z) and in the transverse (x) direction using a little trolley. In this way a study of the dependence of the transmission efficiency on the light production point can be done and the results can be compared with the ones obtained in simulations.

The main results on transmission efficiency as a function of the light production point are the following:

- as found in simulation, transmission efficiency practically does not depend on the transverse (x) coordinate;
- the efficiency as a function of the z coordinate shows a slightly different behavior when compared to simulations: while in simulations a flat behavior was found, in the laboratory test rather a linear dependence has been observed (see fig. 3.8 and fig. 3.10).

The uniformity of the response as a function of the z coordinate, again evaluated as the ratio between the maximum spread of measured values and the mean value, is 27% for the 50 cm long guide and 25% for the 80 cm long guide.

In order to investigate the influence of the guide inclination on signal uniformity, the angle of the guide with respect to horizontal plane has been varied between 46° and 52°. The results are reported in fig. 3.10 (for sake of clarity only results for the most significant angles are plotted). The plateau behavior found in simulations is reproduced by a higher inclination angle of the guide. The best signal uniformity has been obtained at 51°.

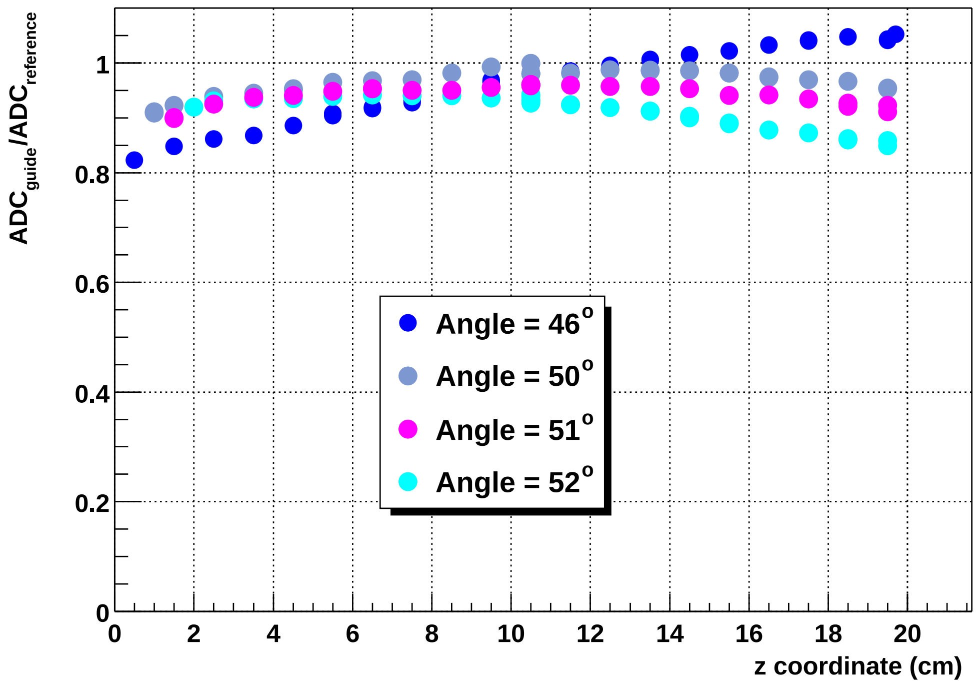

Figure 3.10. Comparison of transmission efficiencies as a function of light production point for different guide inclination angles.

The laboratory test has also allowed the determination of the absolute transmission efficiency, a quantity that is not accessible in other ways. Once the light yield with the fibre in central position with respect to the guide has been measured, the light yield with the fiber directly connected to the XP2020 photomultiplier (namely without the guide) is measured. The ratio between these two values (each one still compared to the reference value) gives the absolute value of light transmission efficiency for photons generated in the center of the bottom face of the guide. This measurement was performed on two prototypes: the 50 cm long guide with reflecting walls transmits 19% of the generated photons, while the 80 cm long guide with the aluminum deposit has a higher transmission efficiency, equal to 31%. In tab. 3.2 the results for transmission efficiency measured in laboratory test are reported.

Length = 50 cm	Length = 80 cm
$\epsilon = (19.0 \pm 5.1)\%$	$\epsilon = (31.0 \pm 7.8)\%$

Table 3.2. Transmission efficiencies measured in laboratory for two guide lengths. Reflecting inner walls are polished for the 50 cm long guide and are obtained with the Al deposition for the longer one.

Beam test

The guides have also been tested using positron beams at the CERN SPS accelerator. The experimental setup used was conceptually similar to the laboratory one: a set of 4 fibre layers has been put between some lead plates and could be moved under the guide. The output of the photomultiplier due to propagation of Cerenkov light produced in the fibres by the electromagnetic shower has been studied for different fibres positions. The results for the dependence of the light yield on the photon entrance point in the guide are showed in fig. 3.11, respectively for transverse and longitudinal coordinates. The observed differences for different x positions are again within 4%, also signal behavior as a function of the x coordinate is very similar to the one measured in laboratory. In the z direction the maximum spread weighted on the mean value gives a factor of about 18% for both guides, that is lower than the 25% found in laboratory test. The linear behavior as a function of z observed in laboratory is confirmed by test beam results.

The beam test has also demonstrated that diffusing walls are not very much efficient for light transmission (see fig. 3.11). It has to be reminded that the results reported in fig. 3.11 compare diffusing with the polished inner walls; with the aluminum deposit a higher efficiency is obtained. Such guide was unfortunately still not available when beam tests have been performed.

3.2.2 Conclusions on the light guide

Simulations, laboratory and beam test results for the two reflecting guides with polished inner walls are compared in fig. 3.12. From these comparison we can conclude that laboratory and beam test results are in a very good agreement. The choice of the light guide for the ALICE electromagnetic calorimeter can be safely done on the basis of these results.

The conclusions resulting from the studies performed are the following:

- inner walls need to be reflecting in order to maximize the transmission efficiency and the Al deposition under vacuum has demonstrated to be the best choice;

- a guide length of 80 cm has given a transmission efficiency comparable to the one obtained with the 50 cm long guide, but a considerably better uniformity;

- laboratory tests has indicated that the optimal inclination of the guide is 51° since it assures the best uniformity as a function of the photon generation point.

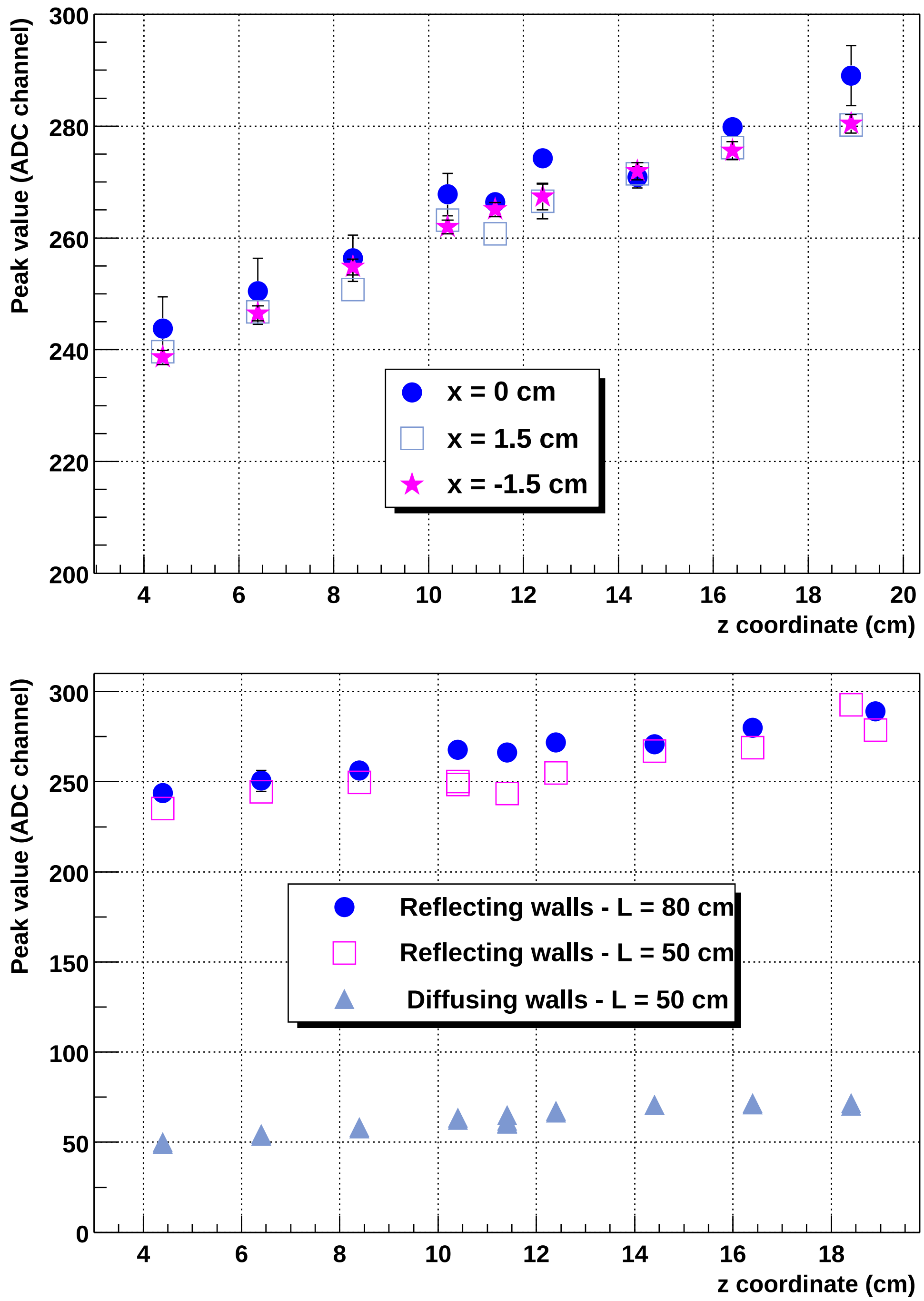

Figure 3.11. Beam test results for light yields as a function of the light production point. Top: for the transverse (x) coordinate; bottom: for the longitudinal (z) one.

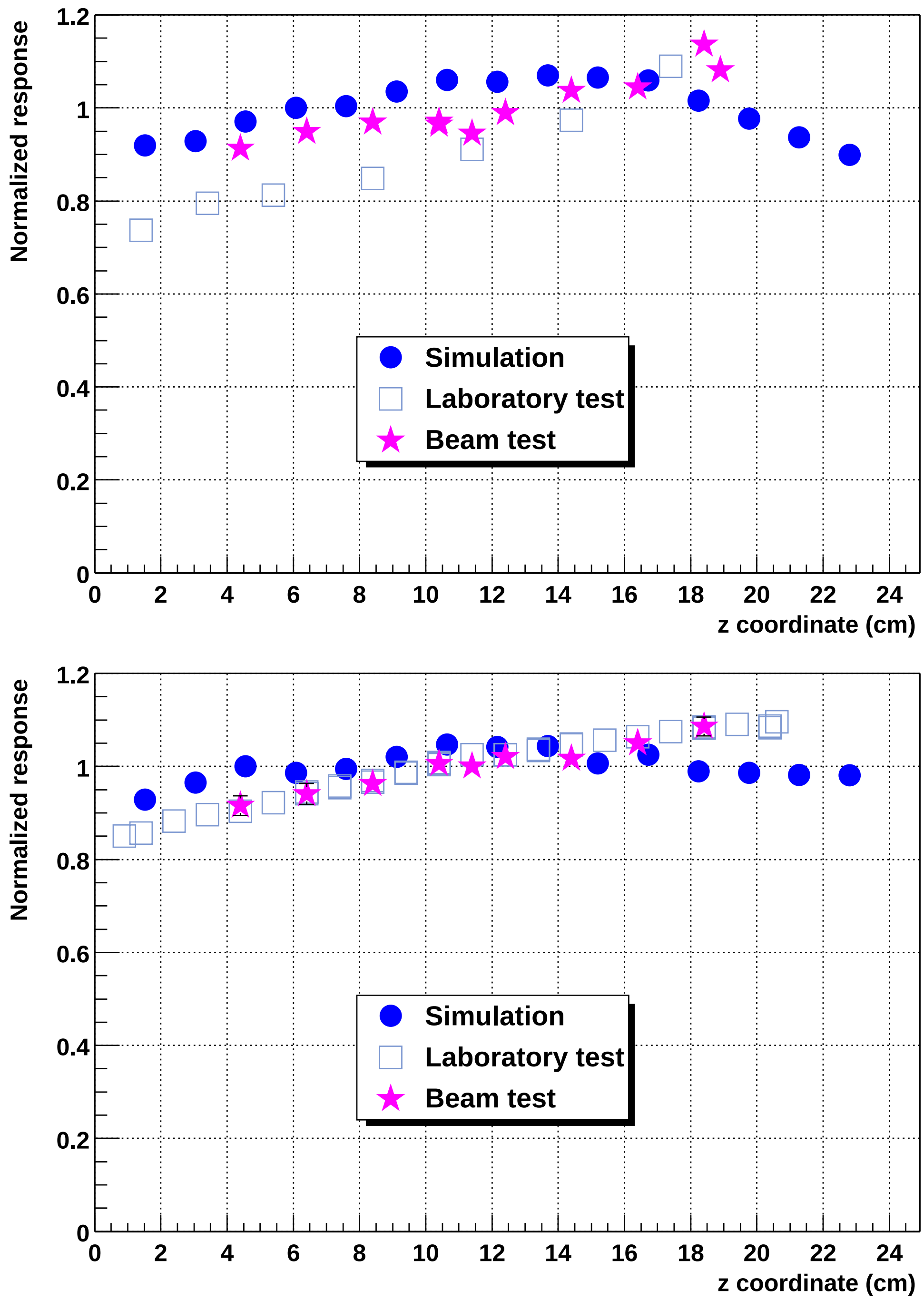

Figure 3.12. Simulations, laboratory and beam test results for the guides with polished inner walls. Top: guide length 50 cm; bottom: guide length 80 cm..

3.3 Prototype beam test

In year 2000 a prototype of the ALICE zero degree electromagnetic calorimeter has been built and tested with positron beams of various energies at the CERN SPS accelerator. It was equipped with the 80 cm long air light guide with Al deposited inner walls. The aim of the test was to study the detector response and the energy resolution as a function of the incident energy. The available beam energy went from 10 to 150 GeV. In fig. 3.13 the linear behavior of the calorimeter response and its energy resolution as a function of beam energy are shown, together with simulation results.

The Monte Carlo simulations of the detector response have been performed with GEANT 3.21 [4]. The effect of the light guide has been included: the Cerenkov light output obtained with GEANT has been folded with the transmission efficiency measured in laboratory.

Comparison with simulations

The signal measured in test beam can be compared to the one obtained in simulations, converting the ADC channels to photoelectron signal. The conversion factor can be obtained measuring with a stable light source the ADC peak value for a single photoelectron. The single photoelectron spectrum is obtained inserting a series of filters between the light source and the photodetector. When the "single photoelectron condition" is reached, increasing further the filter density will only decrease the number of event under the peak but the peak value remains constant. Once the ADC channel corresponding to one photoelectron is known for a certain photomultiplier gain, the experimental spectra can be converted to photoelectron yields with a suitable rescaling of the photomultiplier gain to the value used in test beam. The conversion factor for the photomultiplier used in the test beam has found to be 0.65 photoelectrons per ADC channel. In this way test beam results have been converted in photoelectron yields and compared to simulations. As can be seen in fig. 3.13 results are in fair agreement.

The linear fit of the detector response as a function of beam energy gives a light yield of 1.7 photoelectrons per GeV in simulation and 1.9 in test beam. The experimental trend begins to saturate for the highest beam energies. The slightly higher light yield measured in test beam could indicate that probably the light guide efficiency was slightly underestimated in simulations.

The energy resolution is fitted with the quadratic sum of two independent terms [5]:

$$\frac{\sigma}{E} = \frac{a}{\sqrt{E}} \oplus b.$$

the first one being due to statistical fluctuations while the second can be imputed to instrumental factors such as calibration errors or non compensating response. For

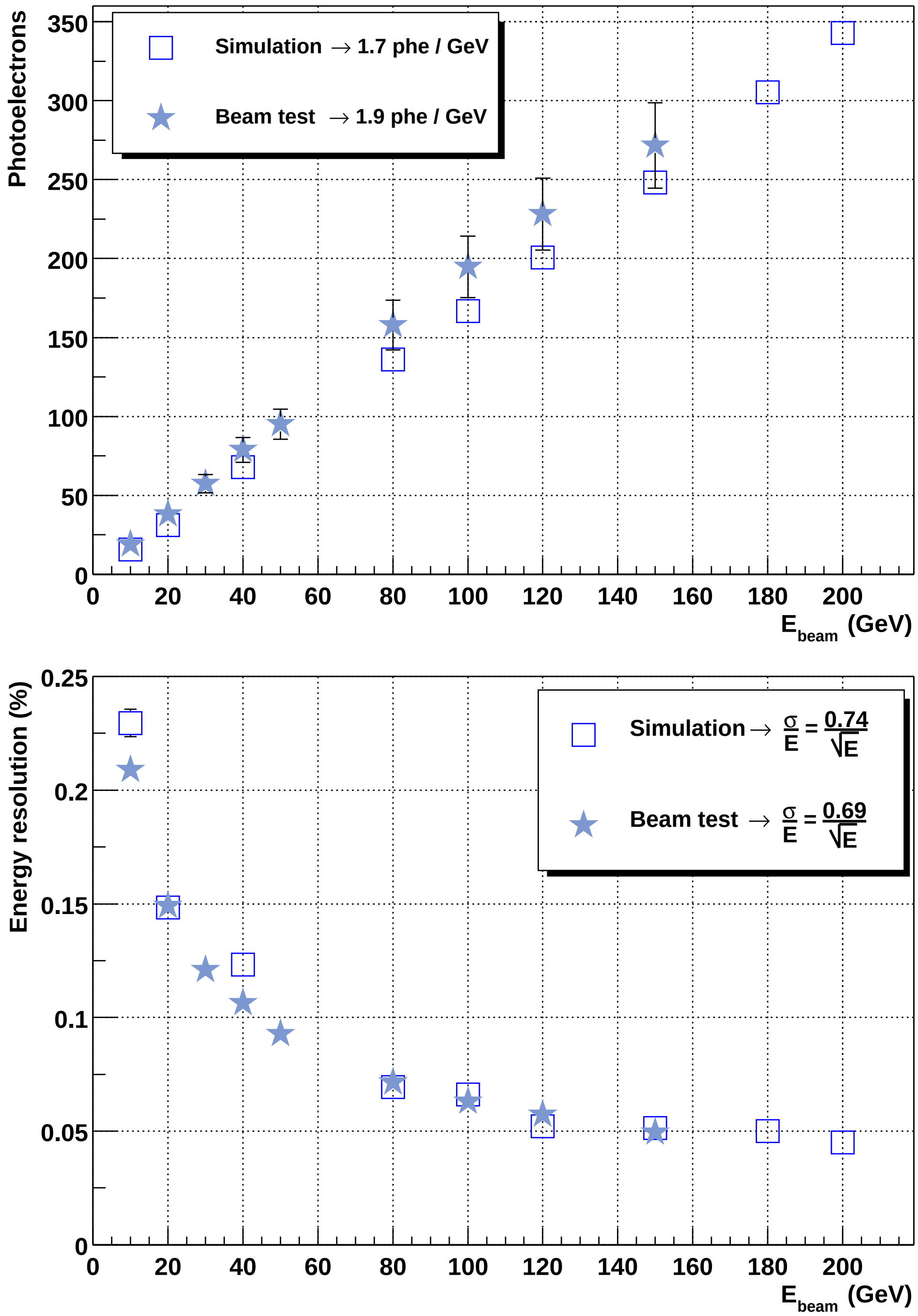

Figure 3.13. Beam test results for the ZEM prototype linearity and resolution as a function of the incident energy compared to simulation.

the ZEM prototype the fit of the experimental resolution as a function of incident energy gives b∼0, while a = 0.737 in simulations and a = 0.694 in test beam. A better resolution is found in beam tests where the light yield was slightly higher; however for energies higher than 80 GeV simulation and beam test resolutions are in complete agreement.

Detector response as a function of particles impact point

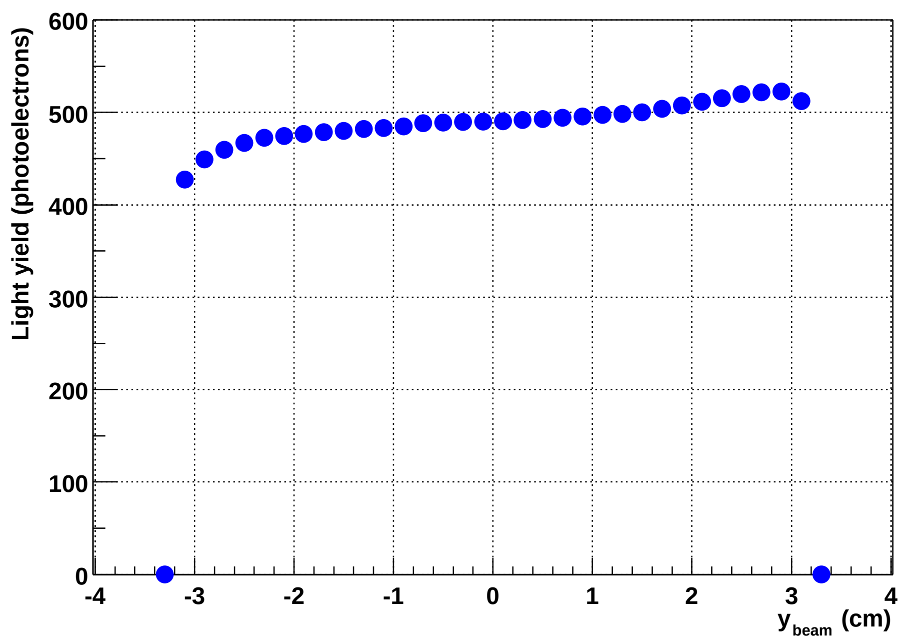

Figure 3.14. Detector response as a function of particle impact point on its front face (3.5 × 3.5) cm^2 wide.

The air guide light solves the problem of signal increasing observed when fibres are directly connected to the photodetector (see fig. 3.6). Using the air light guide a limited increase is observed as can be seen in fig. 3.14. The maximum spread in the response is of about 15% and a slight increase in signal when particles hit the calorimeter upper edge is still observable. Reasons for this behavior should be further investigated. It could be due to light being transported by fibre cladding that, when produced at the end of the fibre, is not much attenuated. Unfortunately we do not know anything about light transmission in cladding material but it would be very important to investigate this aspect in detail. To avoid this effect fibres of the RHIC zero degree calorimeters have been painted in black in the section that comes out from the absorber plates [6].

3.3.1 Detector resolution at ALICE energies

To estimate the energy resolution that can be achieved with the electromagnetic forward calorimeter for the typical ALICE range of energies in the rapidity domain 4.8< η <5.7, simulations have been performed with HIJING generator and GEANT package. Energy distribution of particles detected by the forward calorimeter is shown in fig. 3.1. According to fig. 3.3, in central collisions (b < 2 fm) the total incident energy on the two electromagnetic calorimeter is about 6 TeV, while in more peripheral interactions (b $\sim$ 10 fm) it is of the order of 1.5 TeV. Considering the resolution experimentally measured:

$$\frac{\sigma}{E} = \frac{0.69}{\sqrt{E[GeV]}},$$

a resolution $< 1\%$ for central collisions is obtained and it increases up to 1.8% in the most peripheral ones. This result assures that the designed detector described in this chapter can be successfully adopted at ALICE for the measurement of secondaries at forward rapidity.

References

[1] ALICE Collaboration, ZDC Technical Design Report, CERN/LHCC 99-5.

[2] P. Gorodetzky *et al.*, NIM A **361** (1995) 161.

[3] E. C. Dukes and J. White, Proc. of the First International Conference on Calorimetry in High Energy Physics, FNAL, Batavia, Illinois, 29 Oct. - 1 Nov. 1990, ed. by World Scientific.

[4] GEANT 3.21, CERN Program Library Long Writeup W5013.

[5] M. Lundin *et al.*, NIM A **372** (1996) 359.

[6] C. Adler *et al.*, NIM A **470** (2001) 488, [nucl-ex/0008005].

[7] X. N. Wang, M. Gyulassy, Phys. Rev. D **44** (1991) 3501.

Chapter 4

Development of an object oriented code for ZDC simulations

4.1 Introduction

The response of the ZDC calorimeters to test beam particles has been first studied through simulations using GEANT 3.21 [1] for particle tracking. The results of these simulations were used to help defining detector design parameters. In particular the response and the energy resolution of the calorimeters as a function of beam energy have been analyzed in order to choose the absorber materials and the fibre orientation that assure a good resolution at LHC energies. Moreover, detector responses as a function of particle impact point on their front faces have been studied to determine a fiber to absorber volume ratio value that would not dump the electromagnetic component of the hadronic shower. Finally, as has been shown in chapter 3, the simulation has also been used to optimize the geometry of the air light guide for the electromagnetic calorimeter. Beam tests of the prototypes have allowed a comparison between simulations and experimental results. It has emerged that the simulation systematically overestimates the energy resolution for hadronic beams, while for electron (or positron) beams the simulated values are in good agreement with the experimental ones (see section 3.3 and fig. 3.13).

Extrapolating the results of the simulations to ALICE energies, the parameters of the ZDCs have been fixed in order to obtain an energy resolution of the order of 10% at that energy. Such an energy resolution is suitable to detect spectator nucleons in hadronic calorimeters.

It is clear that in order to extract the physics performances of the ZDC it is necessary to study the detector responses in the frame of the ALICE experimental setup; therefore simulations with the complete detector geometry are needed. This allows to study various details and especially the background contribution and the detector acceptances taking into account the other detectors and the beam line elements.

Furthermore the analysis of detector response in the overall ALICE environment can also give indications on the accuracy that can be reached in determining the physical observables that will be studied by the ZDCs.

4.2 The simulation framework: AliRoot

The ALICE offline framework, AliRoot [2], for simulation, reconstruction and analysis makes use of Object-Oriented (OO) programming techniques and C++ as the implementation language. It is based on the ROOT framework [3], providing as main components persistency, container classes, histogramming, data analysis and graphical user interfaces. GEANT is used as the tracking engine; it provides particle transport through the geometry and simulates the interaction between particles and the materials of detectors and structural elements. The information from tracking are stored in objects called "hits". Then the detector response is simulated and the obtained information is recorded in objects called "digits". Between the various advantages of the OO technique there is the opportunity of reuse of code, thanks to the C++ inheritance property. This characteristic allows the development of base classes which contain virtual common methods and derived classes in which these methods can be implemented according to class requirements and more specific functions can be declared, preserving code modularity.

Simulation and transport code

The run manager class is `AliRun`. A global object of type `AliRun` called `gAlice` is instantiated by the main program, aliroot. The `gAlice` object owns pointers to the list of detectors, to the array of particles and to the Monte Carlo object. It also has pointers to the trees that will be filled during simulation: the hits tree (filled at the end of each primary track), the kinematic and digit trees (filled once per event) and the event tree (filled once per event) that contains the general information relative to each event. Furthermore the `AliRun` class supports geometry and event displaying. When the `gAlice` object is instantiated, the `AliRun` constructor initializes all its data members; then it sets the random seeds generator and initializes the particle stack.

Configuration

Initialization values for `AliRun` data members are set at run time by means of a configuration file. In this file the Monte Carlo object is initialized. Monte Carlo interface class `AliMC` is a generalization of GEANT and therefore provides functions for geometry description and visualization, for the definition of physics processes and for access tracking during transportation. Transport can be provided by either

GEANT3 or GEANT4, since `AliMC` gives the possibility to choose the transport code within the same user simulation code. At the moment AliRoot makes use of GEANT3 and therefore the `AliMC` object is initialized to be of type `TGeant3`. GEANT parameters are defined in the configuration file: processes are switched on according to simulation requirements and energy cuts, beyond which particles are no more followed, are defined. Furthermore the configuration file sets the data file from which magnetic fields are read, it initializes the primary particle generator and the various detector that are switched on during simulation.

Detectors

Each ALICE detector has to implement a detector simulation class deriving from `AliDetector`, which derives from `AliModule`. Therefore, for each detector code, common methods that are purely virtual in the base classes are implemented. Detector classes should also contain the geometry description, together with materials and tracking media definition. They also have to provide a `StepManager` to be processed at each transport step, methods for hits and digits generation and an algorithm for reconstruction. During the run the global `gAlice` object checks which detectors are switched on and calls their methods to process the event and to add hits, digits and reconstructed quantities for these detectors to the global list.

4.3 Primary particle generation

Primary particle generation is managed by the virtual base class `AliGenerator`. This class contains methods to generate primaries and to put them on the GEANT stack for transport, it has functions to set the kinematic region allowed for produced particles and to define vertex position. In addiction `AliGenerator` owns two purely virtual methods, `Init` and `Generate`, that need to be implemented in derived classes respectively to initialize the generator and to start the generation mechanism.

Many kinds of particle generators have been implemented in AliRoot:

- simple generators to be used as tools to test detector responses;
- generators that read from external files events containing Monte Carlo data (`AliGenExtFile`);
- on the flight generation with external Monte Carlo generators such as HIJING or PYTHIA (`AliGenHijing` and `AliPythia` classes);
- generators that use parameterized transverse momentum and rapidity distributions stored in libraries (`AliGenParam`).

The generator to be used in simulations is created and configured at run time. Being `AliRun` a client of the `AliGenerator` class, the global object `gAlice` owns a pointer to the created `AliGenerator` object and the relationship between the two is used during the run. `AliGenerator` constructor uses the `SetGenerator` method of `AliRun` to let the run manager know about the generator and the `Generate` method of `AliGenerator` calls the `SetTrack` method of `AliRun` to put generated particles in the stack.

4.3.1 C++ interface to Hijing generator

A primary particle generator that uses p_T and η parameterizations deduced from HIJING is implemented in AliRoot. This parameterization is valid for particles with $\eta < 8$ and therefore it does not work to describe the forward rapidity range covered by the ZDCs. Therefore the generation of full HIJING events is needed for the ZDCs. For this reason we introduced in AliRoot the `THijing` class that provides a C++ interface for the HIJING generator, whose code is written in Fortran language.

`THijing` derives from `TGenerator`, the ROOT abstract base class that defines the ROOT interface for various event generators. The `ImportParticles` method of `TGenerator` dumps the result from the event generator into a `TClonesArray` of `TParticle` objects. `THijing` provides access to HIJING common blocks through its member functions that have been defined in order to correctly match the Fortran structure. Data members of this class are the energy value, the system reference frame (laboratory or center of mass), the colliding systems (proton or nucleus), the atomic and mass number of projectiles and the impact parameter range for the generation. An object of type `THijing` can also be constructed without specifying values for these data members, in this case HIJING is initialized to the default ALICE values provided by the constructor, that correspond to Pb-Pb collisions at 2.76 TeV per nucleon. The main member functions of the class are: `Initialize`, `GenerateEvent` and `ImportParticles`. The first two methods call the corresponding Fortran routines for initialization and event generation, with either the default parameters or the ones set by the user. The purpose of the `ImportParticles` method is to store generated particles in the `TClonesArray` of `TParticle` defined by `TGenerator`. The default action is to store all generated particles, but the user can choose to store only stable particles.

The `AliGenHijing` class inherits from `AliGenerator` and makes use of `THijing` to provide the full Hijing generation. Its data members and methods set initialization values for HIJING generator, configure physics processes to be considered for the generation and fix the kinematic cuts for generated particles to be put in the stack.

4.4 ZDC classes

In fig. 4.1 the implemented classes for the ZDC detectors are shown.

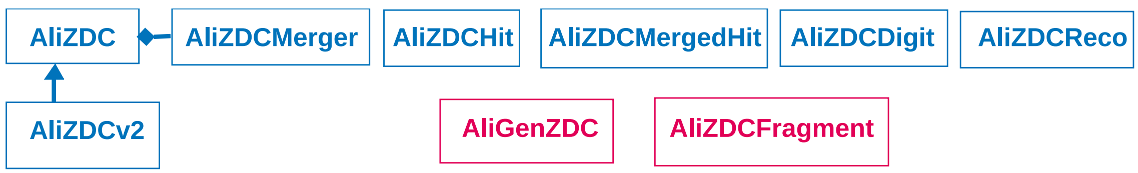

Figure 4.1. Scheme of the implemented classes for the ZDC detector in the AliRoot framework.

`AliZDC` and `AliZDCv2` describe detector geometry and provide their response. `AliZDCHit` and `AliZDCDigit` define objects to store respectively hits and digits. `AliZDCMerger` builds the full event starting from separate background and signal files and store special hits defined by `AliZDCMergedHit` class. `AliZDCReco` defines the reconstructed variables. Two special classes, `AliGenZDC` and `AliZDCFragment`, provide respectively a test particle generator and a class to compute fragments production.

4.4.1 Classes for detector geometry and response

Base class for ZDC: AliZDC

`AliZDC` is the base class for ZDC detectors; it inherits from `AliDetector` and provides basic functions for the ZDC, while geometry definition and specific functions are implemented in the derived classes. `AliZDC` data members are reported below:

```
Int_t         fNoShower;    // Flag to switch off the shower
AliZDCMerger *fMerger;      // !  Pointer to merger object
Int_t         fNMergedhits; // Number of Merged hits for background
TClonesArray *fMergedHits;  // TClonesArray for "merged" hits
TTree        *fTreeSD;      // TreeS for merging
TTree        *fTreeMD;      // TreeD for merging
Int_t         fNRecPoints;  // Number of RecPoints
TClonesArray *fRecPoints;   // List of RecPoints
```

Some of them are needed for the event merging, that is the procedure used to add signal to background obtaining a full ALICE event for the ZDC (and that will be described in section 4.5). The other data members are used to store reconstructed quantities (reconstruction will be discussed in section 4.6). Finally the data member `fNoShower` is a flag to switch off shower development in the ZDCs. This possibility is very useful to study, for example, detector acceptances or particle impact points over the detector front faces and in all the cases where the shower development, which is very time consuming, is not necessary. The default value for this data member in the constructor is zero, that corresponds to the ordinary condition of full shower development. When the ZDC constructor is invoked in the configuration file, the `NoShower` method can be called to switch off the shower development.

The implemented member functions in the `AliZDC` class are:

```
virtual void AddHit(Int_t track, Int_t *volume, Float_t *hits);
virtual void AddDigit(Int_t *volume, Int_t digit);
virtual void MakeBranch(Option_t* opt, const char *file=0);
virtual void MakeBranchInTreeSD(TTree *treeS, const char *file=0);
virtual void MakeBranchInTreeD(TTree *treeD, const char *file=0);
virtual void Hits2SDigits();
virtual void SDigits2Digits();
virtual void Hits2Digits();
virtual void Digits2Reco();
```

As said before, the virtual methods of the `AliModule` class are implemented in each detector code: the `AddHit` method adds a hit for ZDC to the global hit list and `AddDigit` does the same for ZDC digits. The function `MakeBranch` has the aim to create the ZDC branch inside the trees produced during simulation; in addition specific member functions to add the ZDC branch in a particular tree have been implemented (`MakeBranchInTreeD` and `MakeBranchInTreeR`). `Hits2SDigits` creates summable digits from simulated hits, while `Sdigits2Digits` runs the digitization procedure and `Digits2Reco` performs reconstruction for the ZDC.

Derived class containing geometry: AliZDCv2

There are two classes that derive from `AliZDC`: the first one (`AliZDCv1`) contains the geometry corresponding to the TDR design, while in the second one (`AliZDCv2`) the geometry is updated to the (up to now) final version. This latter geometry foresees only one hadronic ZDC system, even if the experiment will have two of them. This is due to the fact that the definition of both systems would imply a mother volume more than 200 m long and this would considerably slow down AliRoot simulations. The hadronic ZDCs are placed on the same side of the dimuon arm relative to IP. On the contrary both the electromagnetic calorimeters are included in `AliZDCv2` geometry. They are both placed on the same side relative to IP, on the opposite side with respect to the hadronic ones.

`AliZDCv2` class has many data members, used to define the parameters for calorimeter geometries, sensitive tracking media and the arrays for Cerenkov light production in fibres. They are reported below:

```
// Sensitive media
Int_t   fMedSensF1;          // Fibres sensitive medium
Int_t   fMedSensF2;          // Fibres sensitive medium
Int_t   fMedSensZP;          // ZP absorber sensitive medium
Int_t   fMedSensZN;          // ZN absorber sensitive medium
Int_t   fMedSensZEM;         // ZEM absorber sensitive medium
Int_t   fMedSensGR;          // Air in absorber grooves

// Parameters for light tables
Int_t   fNalfan;             // Number of steps in α (n)
Int_t   fNalfap;             // Number of steps in α (p)
Int_t   fNben;               // Number of steps in radius (n)
Int_t   fNbep;               // Number of steps in radius (p)
Float_t fTablen[4][90][18]; // Light table for neutrons
Float_t fTablep[4][90][28]; // Light table for protons

// Parameters for calorimeters geometry
Float_t fDimZN[3];           // ZN dimensions
Float_t fDimZP[3];           // ZP dimensions
Float_t fPosZN[3];           // ZN position
Float_t fPosZP[3];           // ZP position
Float_t fFibZN[3];           // ZN fibres dimensions
Float_t fFibZP[3];           // ZP fibres dimensions
Float_t fPosZEM[3];          // Position of EM detector
Float_t fZEMLength;          // EM calorimeter length
```

Data members for detector geometries are initialized in `AliZDCv2` constructor. The constructor also checks that beam pipe, muon absorber, beam shielding and magnetic dipole are switched on, otherwise ZDC is not built. In fact these modules are needed for ZDC simulations since their geometry and the magnetic fields affect proton trajectories and consequently detector acceptances.

The member functions for this class are:

```
virtual void CreateGeometry() {}
virtual void CreateBeamLine() {}
virtual void CreateZDC() {}
virtual void CreateMaterials() {}
virtual void Init();
virtual void InitTables();
virtual void StepManager() {}
```

The method `CreateGeometry` calls first `CreateBeamLine` to define beam line geometry from the end of the dimuon arm till the hadronic ZDCs and then `CreateZDC` to create the calorimeter geometries. In `CreateBeamLine` a vacuum mother volume for ZDC is defined. Inside this volume the beam pipe and the magnet elements are placed, starting from the end of the second compensator dipole, 20 m far from the IP, to the second bending dipole D2, 121.5 m from the IP (see fig. 2.3 for a sketch of the beam line).

`CreateZDC` creates calorimeter geometries. Neutron and proton calorimeters are box volumes, each one divided in four towers to simulate the experimental signal readout. In fact the optical readout for each hadronic calorimeter will be made with five photomultipliers: four receive signal from half of the fibres of each tower ("tower" photomultipliers) and the fifth reads the output from half of the fibres uniformly distributed in the calorimeter ("common" photomultiplier). Adjacent fibres in each tower are connected alternatively to the tower and to common photomultipliers, as can be seen in fig. 4.2. To easily assign produced light to the relative photomultiplier, fibres are defined with two different tracking media corresponding to the same material. ZN volume is placed at 116.5 m from the IP and is 1 m long, while the proton one is placed at 116 m and is 1.5 m long. Their position relative to beam pipes is shown in fig. 4.3 where also the division in towers can be seen. Each electromagnetic calorimeters will be read with a single photodetector, therefore the main volume has not been subdivided. They are placed at 7.35 m from the IP, just before the compensator magnet. In fig. 4.4 a side view of the detector is shown: the 45° geometry and the structure made by one Pb slice and one fibre plane can be noticed. In fig. 4.5 a front view of the two detectors is plotted to show their position relative to the beam pipe.

The definition of materials and tracking media for beam pipe, magnetic elements and calorimeters is done in the `CreateMaterial` method. As can be seen in the data member list reported before, sensitive media are absorber materials, air for absorber grooves and quartz for fibres. `CreateMaterial` also defines standard GEANT cut values for sensitive media. The `Init` member function is used to call the `InitTables` method that initializes data members for light production in fibres, reading data for photon production from external files. These data members provide photoelectron yields at the photocatode of the photomultiplier (taking into account the photocatode wave length sensibility and its quantum efficiency) as a function of the velocity β of the particle which crosses the fibre, of the track inclination α with respect to fibre axis and of its distance from the fibre axis. Light yields also depend on fibre diameters, therefore different data members are defined for ZN and ZP (ZEM fibres are the same used for ZP).

The ZDC `StepManager` is called by `AliRun` every time a particle is inside a ZDC sensitive volume, namely every time a particle is inside one of the calorimeters. The aim of the `StepManager` is to evaluate energy losses and light yields and then to call the `AddHit` method to create the ZDC hits, that contain such information.

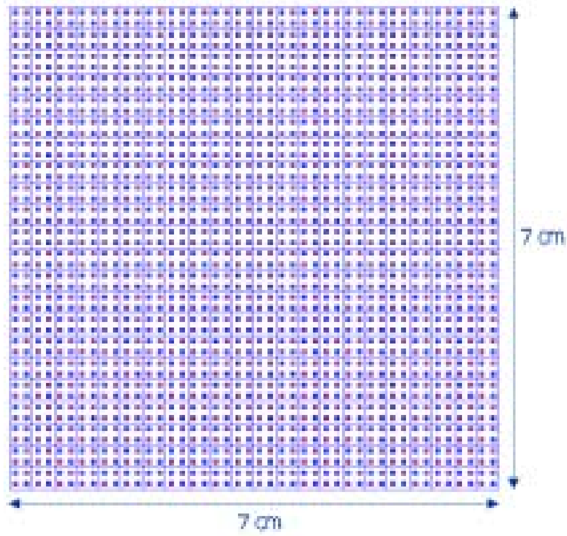

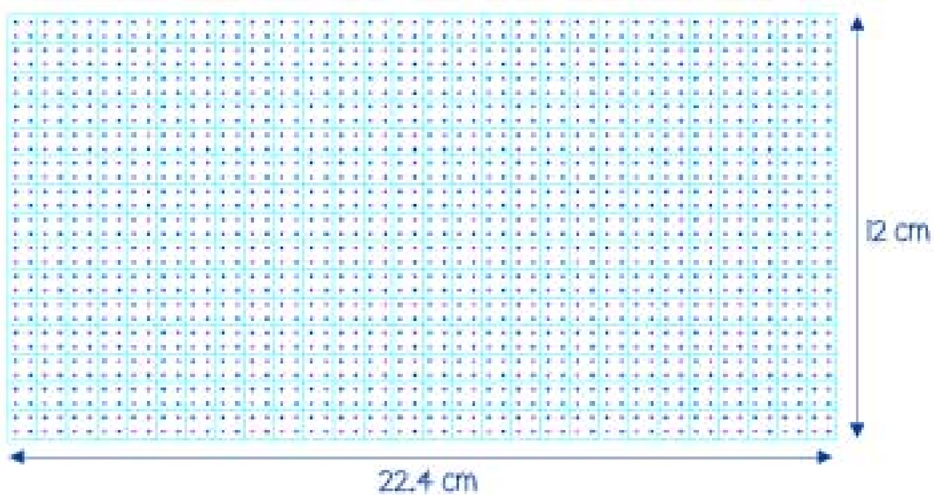

Figure 4.2. Geometry layout of the two hadronic calorimeters (not to scale). Fibres in blue are connected to the tower photomultiplier while fibres in red are connected to the common one.

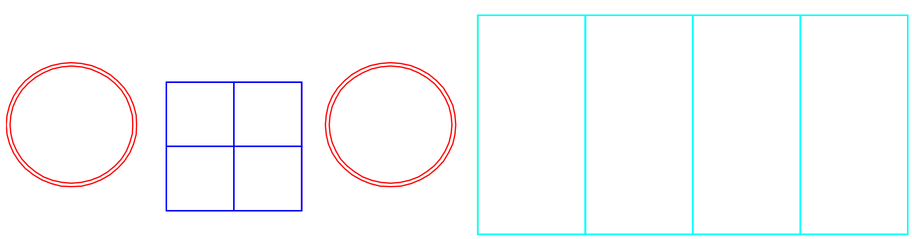

Figure 4.3. Front view of hadronic ZDCs at z = 116.5 m from IP. The division in four towers can be seen for both detectors. Red circles represent beam pipes.

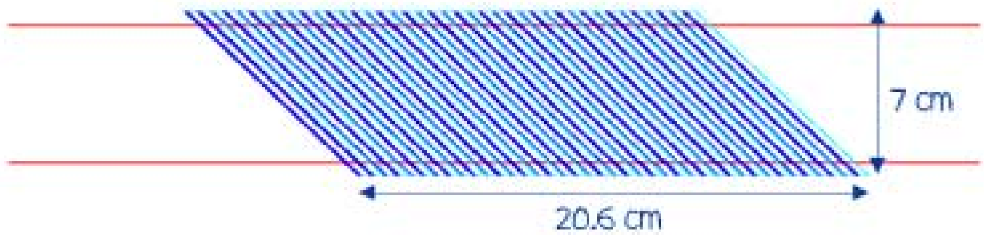

Figure 4.4. Side view of the electromagnetic calorimeter created with AliZDCv2 class. The red volume is the beam pipe.

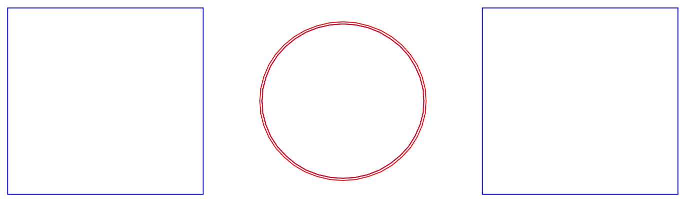

Figure 4.5. Front view of the electromagnetic calorimeters placed on both sides of the beam pipe. The centers of the two detectors are 8 cm distant from the LHC axis.

4.4.2 Spectator nucleons generator

A particle generator for spectator nucleons, `AliGenZDC`, has been implemented in the ZDC code. Spectator momenta are generated taking into account Fermi motion, beam divergence and beam crossing angle, since these phenomena could in principle affect nucleon momentum distributions.

Data members for this class are the code of particles to be generated, the director cosines (or the pseudorapidity) of the track, the Fermi momentum flag, the beam divergence and crossing angles, the crossing plane and two arrays containing nucleon Fermi momenta distributions.

```
Int_t    fIpart;           // Particle code
Float_t  fCosx;            // Director cos of the track
Float_t  fCosy;            // Director cos of the track
Float_t  fCosz;            // Director cos of the track
Float_t  fPseudoRapidity;  // Pseudorapidity flag
Int_t    fFermiflag;       // Fermi momentum flag
Float_t  fBeamDiv;         // Beam divergence (angle in rad)
Float_t  fBeamCrossAngle;  // Beam crossing angle (angle in rad)
Int_t    fBeamCrossPlane;  // Beam crossing plane
Double_t fProbintp[201];   // p momentum distribution due to Fermi
Double_t fProbintn[201];   // n momentum distribution due to Fermi
Double_t fPp[201];         // Nucleon momentum due to Fermi
```

Being a class derived from `AliGenerator`, `AliGenZDC` has a method for initialization (`Init`) and one for generation (`Generate`), in which `SetTrack` method of `AliRun` is called to put generated particles in the stack. Specific methods of `AliGenZDC` are listed and described below:

```
void Init();
void Generate();

// Setters for spectators generation
void SetParticle(Int_t ipart) {fIpart=ipart;};
void SetMomentum(Float_t ptot) {fPMin=ptot; fPMax=ptot;};
void SetDirection(Float_t eta, Float_t cosx, Float_t cosy,
     Float_t cosz) {fPseudoRapidity=eta; fCosx=cosx; fCosy=cosy;
     fCosz=cosz;};
void SetFermi(Int_t Fflag) fFermiflag=Fflag;;
void SetDiv(Float_t div, Float_t cro, Int_t ipl)
     {fBeamDiv=div; fBeamCrossAngle=cro; fBeamCrossPlane=ipl;};

// Fermi smearing, beam divergence and crossing angle
void FermiTwoGaussian(Float_t A, Float_t Z, Double_t *pp,
     Double_t *probintp, Double_t *probintn);
void ExtractFermi(Int_t id, Double_t *pp, Double_t *probintp,
     Double_t *probintn, Double_t *pFermi);
void BeamDivCross(Int_t icross, Float_t divergence,
     Float_t crossangle,Int_t crossplane, Double_t *pLab);
```

Particle code and momentum are set respectively by the `SetParticle` and `SetMomentum` member functions that assign a value to the relative `AliGenerator` data members. The `SetDirection` member function allows to give the director cosines of the track or its pseudorapidity: if the pseudorapidity flag is equal to zero the director cosines of the track are given by the following three values. Otherwise the flag itself corresponds to particle pseudorapidity. `SetFermi` is used to set the Fermi flag value, Fermi motion is applied to the generated particles if this flag is equal to 1. Arguments for the `SetDiv` functions are respectively the angles due to beam divergence and crossing angle (in radians) and the crossing plane; this latter should be set equal to 2 for vertical and to 1 for horizontal crossing plane. All these setters can be called by the user during initialization to configure the generator. Default values for data members in the constructor initialize the `AliGenZDC` object for the generation of one neutron with momentum equal to 2.76 TeV directed along the LHC axis; Fermi motion is considered, divergence angle is equal to $3.2\ 10^{-5}$ rad, crossing angle is 10^{-4} rad and the crossing plane is vertical.

During `AliGenZDC` initialization, the `FermiTwoGaussian` method is called to initialize momentum distributions for neutrons and protons due to Fermi motion. These distributions are calculated according to a double gaussian distribution (as described in reference [4]). In the `Generate` method the initial components of nucleon momentum are calculated and passed to `BeamDivCross` method that applies beam divergence and crossing angle and then computes the components of nucleon quadrimomentum. After that, if Fermi motion has been selected, the `ExtractFermi` function extracts nucleon Fermi momentum from the previously initialized distributions. Finally Fermi momentum is Lorentz boosted with nucleon momentum and the generated particle is put in the stack with the obtained momentum.

In fig. 4.6 the three components of the generated nucleon momentum are shown. The distributions refer to 10^4 nucleons of 2.7 TeV generated along the beam direction, taking into account Fermi motion, beam divergence and crossing angles. In fig. 4.7 only the smearing due to Fermi motion is considered. The spread of momentum component along the beam direction is of the order of 500 GeV/c and, as already discussed in section 2.4, it becomes crucial for spectator protons tracking.

4.4.3 A class for nuclear fragmentation

Usual events generators do not consider nuclear fragment production; however, as it has been shown in section 2.5, this process has very important consequences in experiments at colliders. It is particularly crucial for ZDC since it affects spectators detection.

For this reason a class, called `AliZDCFragment`, for the evaluation of nuclear fragments production has been included in the ZDC code. Starting from the number of spectators given by an event generator, the number of spectators that remains bound in fragments is calculated by `AliZDCFragment`, that acts as an "afterburner" for spectators generation. Being a class used only for ZDC simulations it does not need to inherit from any other AliRoot class and therefore it is derived from the base ROOT class `TNamed`. The aim of the `AliZDCFragment` class is to provide the number of nuclear fragments as a function of the impact parameter. It is based on the parameterization of lower energies experimental results (as described in section 2.5).

Data members of the class (reported below) are the impact parameter, the mean value of the Z_{bound} variable, the number of Intermediate Mass Fragments (IMF), the maximum charge and the exponent τ of the charge distribution of produced fragments ($dN/dZ = k\ Z^{-\tau}$), the arrays containing respectively fragment atomic numbers and number of neutrons, the number of α particles and the number of spectator protons and neutrons bound to form fragments.

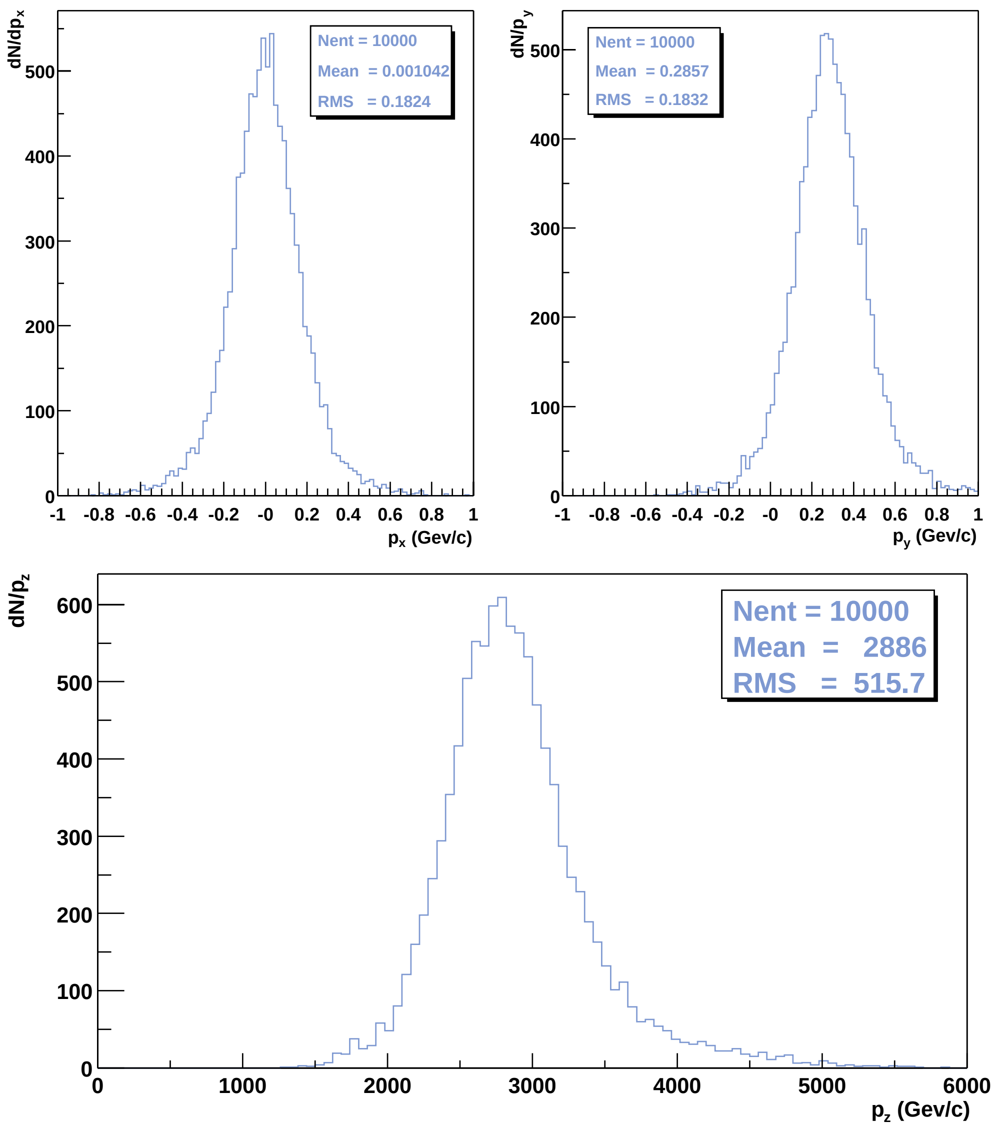

Figure 4.6. Components of nucleon momentum generated by AliGenZDC taking into account Fermi motion, beam divergence and crossing angles.

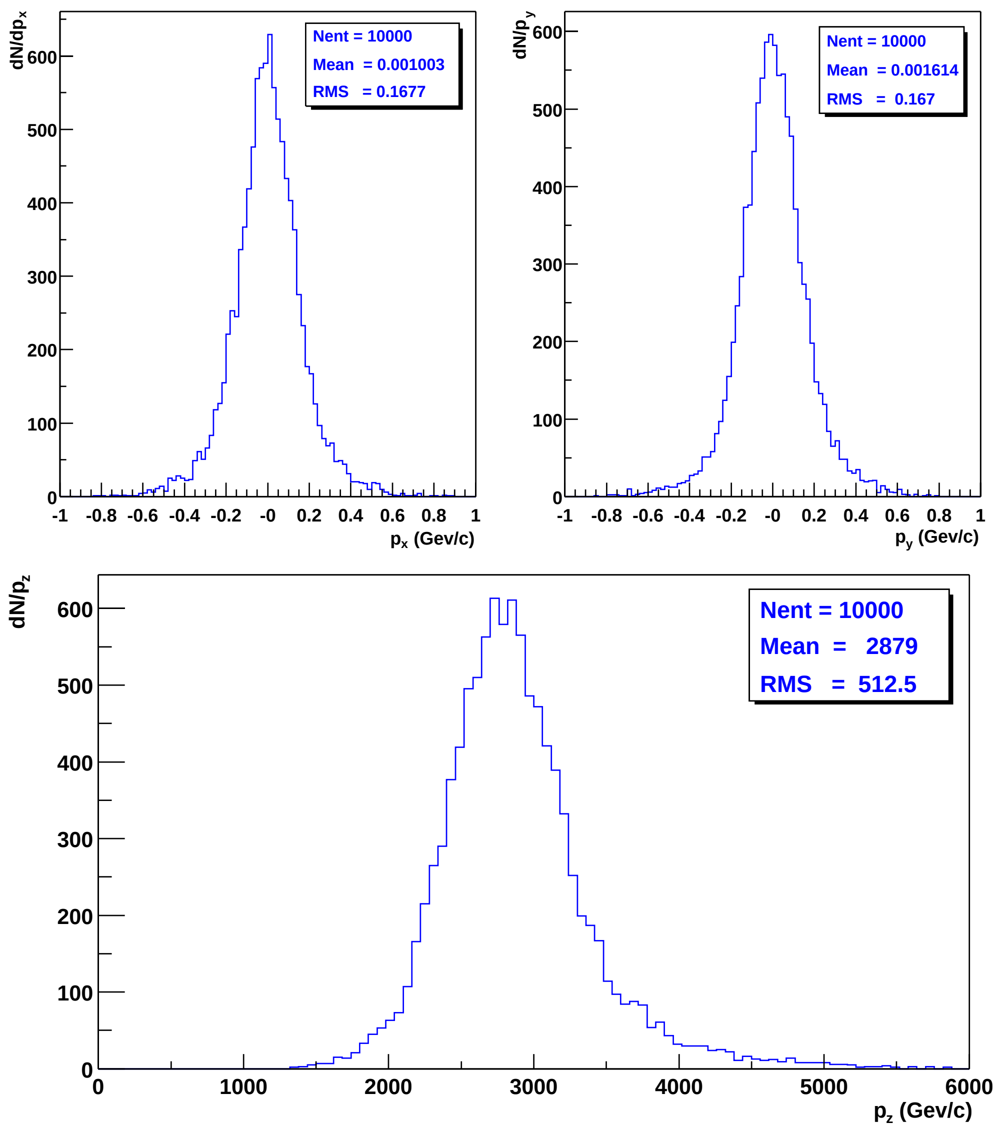

Figure 4.7. Components of nucleon momentum computed by AliGenZDC when only Fermi motion is considered.

```
Float_t fB;          // Impact parameter
Float_t fZbAverage; // Mean value of Z bound
Int_t   fNimf;       // Number of IMF
Float_t fZmax;       // Mean value of maximum Z of fragment
Float_t fTau;        // Exponent of charge distribution
Int_t   fZZ[100];    // Array of atomic numbers of fragments
Int_t   fNN[100];    // Array of number of neutrons of fragments
Int_t   fNalpha;     // Number of alpha particles
Int_t   fZtot;       // Total number of bound protons
Int_t   fNtot;       // Total number of bound neutrons
```

The impact parameter is the only data member that can be set from the user through the apposite member function `SetImpactParameter`. The constructor must be called with the impact parameter value as unique argument. Member functions provided by the class are:

```
void GenerateIMF(Int_t* fZZ, Int_t &fNalpha);
void AttachNeutrons(Int_t* fZZ, Int_t* fNN, Int_t &Ztot,
     Int_t &Ntot);
// Setters
void SetImpactParameter(Float_t b) {fB=b;};
// Getters
Int_t GetFragmentNum() {return fNimf;};
```

The method `GenerateIMF` calculates the number of intermediate mass fragments as a function of b; it computes the atomic number of produced fragments and the number of α particles emitted for the impact parameter value set in the constructor. For that purpose Z_{bound} is calculated from the impact parameter, then the average number of IMF, the maximum charge and the value of the τ exponential, together with their fluctuations, are evaluated from fits of ALADIN experimental distributions [5]. Finally the charge of produced fragments is extracted by sampling the distribution obtained with `GenerateIMF` (since ALADIN distributions are referred to fragment charge). A second method, `AttachNeutron`, is then used to compute the fragment mass number starting from their charge Z. The number of bound neutrons is calculated attaching as many neutrons are needed to get, for that Z, a nucleus which lies in the stability valley. Finally deuteron production is estimated and the method returns the total number of protons and neutrons that are bound in fragments. The class has also one getter, `GetFragmentNum`, that returns the number of generated fragments.

Once the event has been generated (for example with `AliGenHijing`), the impact parameter and the number of spectator protons and neutrons can be read from the event header. Then the number of free spectators can be evaluated by means of `AliZDCFragment`. A simple example is provided in the following code lines:

```
// Initializing AliZDCFragment object
AliZDCFragment *frag = new AliZDCFragment(b);

// Initializing needed variables
Int_t j, zz[100], nn[100], nAlpha, Ztot, Ntot;
for(j=0; j<=99; j++){
zz[j] =0;
nn[j] =0;
}

// Fragments generation
frag->GenerateIMF(zz, nAlpha);
// Neutrons ``attachment''
frag->AttachNeutrons(zz, nn, Ztot, Ntot);

// Calculating number of FREE spectators
Int_t FreeSpecNeutrons = GenSpecNeutrons - Ntot - 2*nAlpha;
Int_t FreeSpecProtons  = GenSpecProtons  - Ztot - 2*nAlpha;
```

In fig. 4.8 spectator nucleons produced in a minimum bias HIJING generation are plotted as a function of the impact parameter before and after applying fragmentation. It can be seen that, when the production of nuclear fragments is considered, the maximum number of free spectators nucleons for each colliding nucleus is about 20 for protons and 40 for neutrons.

4.4.4 Hits

AliZDCHit class

`AliZDCHit` is the class that defines hits object for ZDC detectors. This class is derived from `AliHit` whose constructor has two arguments: shunt and track. If shunt is equal to 1, hits are all referred to the primary particle that has generated the track, otherwise the memory of every track is preserved in hits structure. For the ZDC the first case is always used due to the large amount of secondaries generated in the shower development. `AliHit` has four data member: the track number and the overall coordinates (x, y, z) in the ALICE setup of the track that generates the hit. These coordinate values have to be set in the classes derived from `AliHit`.

`AliZDCHit` data members are reported below. The first one is an array of two elements used to define the detector and the tower the hit refers to. The value of

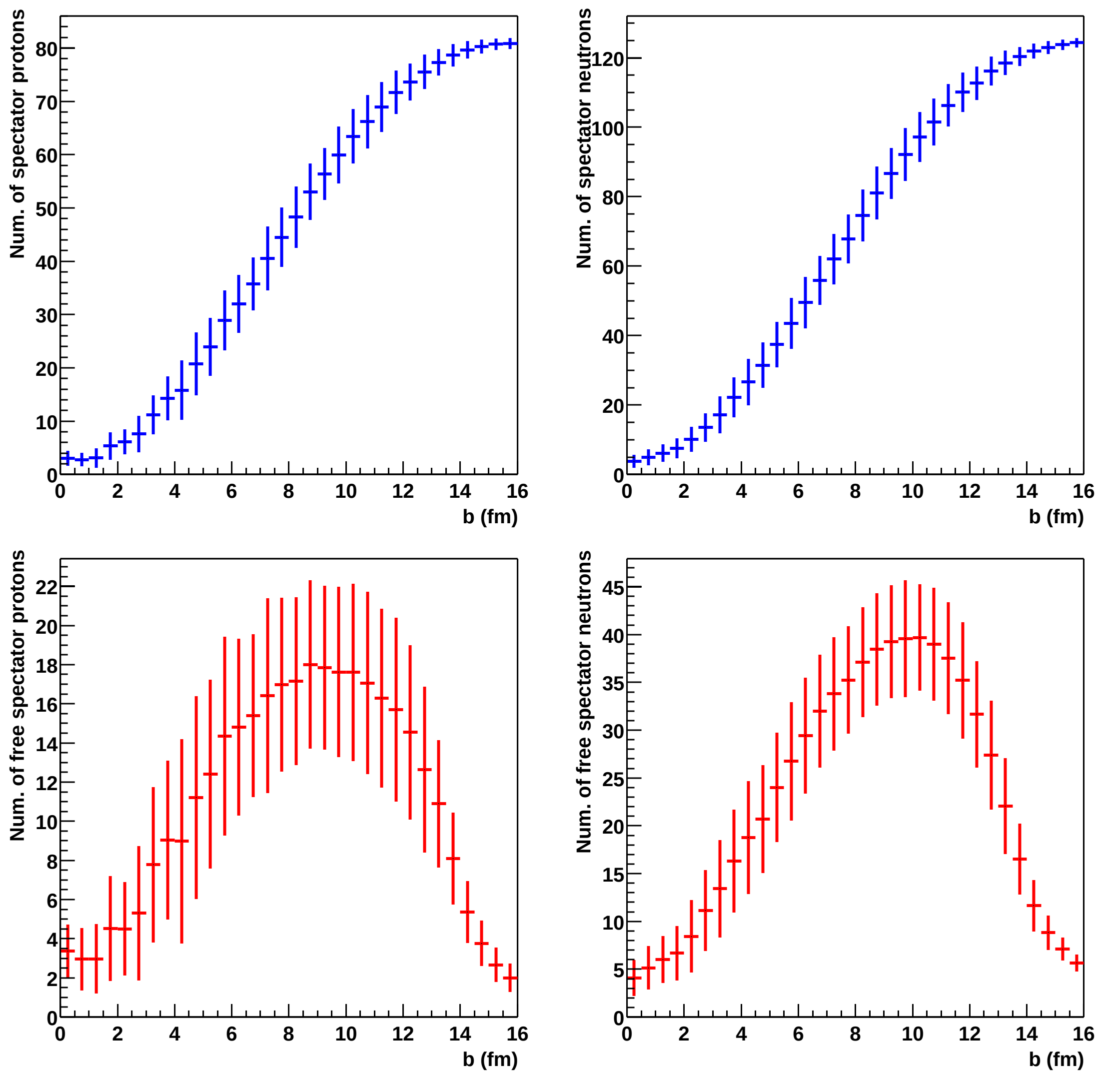

Figure 4.8. Number of spectator nucleons generated with HIJING (up) and after considering nuclear fragment production (down).

the first element indicates the detector (1 for ZN, 2 for ZP, 3 for ZEM), the second element of the array indicates the tower of the hadronic calorimeters (it is always set to 1 for the electromagnetic ones). An `AliZDCHit` is constructed assigning values to kinetic energy of the incident primary, storing coordinates of particle impact point over the detector front face, setting the flag used to distinguish primaries from secondaries and giving the values of the three physical quantities that characterize calorimeter responses: the light produced in tower and in common photomultipliers and the energy loss in the detector.

```
Int_t   fVolume[2]; // Array of volumes
Float_t fPrimKinEn; // Primary particle energy
Float_t fXImpact;   // Impact point x-coordinate over the ZDC
Float_t fYImpact;   // Impact point y-coordinate over the ZDC
Float_t fSFlag;     // Secondary flag
Float_t fLightPMQ;  // Cerenkov light produced in each tower
Float_t fLightPMC;  // Cerenkov light seen by the common PM
Float_t fEnergy;    // Total energy deposited in eV
```

`AliZDCHit` constructor is called with four arguments: shunt and track (that derive from `AliHit` constructor), a pointer to the array of volumes and a pointer to the array that contains the values of all the other data members. Member functions to get the values of the data members are provided. In `AliZDCHit` the operators sum and equality between two objects of the class are defined: two ZDC hits are defined equal if they refer to the same track in the same sub-volume and the sum between two such objects consists in the sum of the three data members that contain the light yields and the energy loss.

As said before, the `AddHit` method of `AliZDC` adds a ZDC hit to the global list. It is called by the `StepManager` in two different cases: if a new track is entering a ZDC volume and when there is Cerenkov light production or an energy loss. In both cases AddHit perform a scan over the already stored hit, if a hit equal to the current one is found, the two are summed; otherwise a new hit is created. Values for data members that are not updated (primary kinetic energy, impact point coordinates and secondary flag) are stored for the first hit of each primary particle and are copied for following hits. Hits are reset by `AliRun` at the end of each primary.

Summable digits

The structure for ZDC summable digits is very simple and not very different from the hits since they have no particular meaning for our detectors. Therefore, apart from the overall coordinates in the ALICE setup, which are not included, they are simply a copy of the ZDC hits. Summable digits play anyway a different role in case of event merging, as will be clarified in the following section.

4.5 Event merging and digits production

4.5.1 Merging aim and procedure: AliZDCMerger class

The signal for hadronic ZDCs is given by spectator nucleons; the background is due to participants and secondary particles which fall in the ZDC acceptance. The HIJING generator in principle can provide both signal and background for the hadronic ZDCs. Then GEANT transport for nucleons of 2.76 TeV requires a relatively long time, mostly spent to follow shower development. For this reason a procedure to merge background and signal has been studied, which allows to generate only once a large number of spectator events and then merge them with the background.

To implement this scheme, two samples (one for spectator neutrons and one for spectator protons) of 10^4 events each have been generated with `AliGenHijing` generator and tracked through the ALICE setup, storing spectator hits. Then in `AliGenHijing` an option that allows generation without putting spectators in the stack has been introduced. In this way it is possible to generate only background for the hadronic ZDCs, without tracking spectators event by event. The appropriate number of spectator signal events is then extracted from the stored distributions and merged with the background. In this way the full event is obtained saving a lot of computing time. This merging procedure is needed only for hadronic ZDCs, since for the electromagnetic ones it is not possible to define a signal and a background.

The class designed for event merging is `AliZDCMerger`. This class has two different applications: it can simply produce digits or it can first merge background and signal and then digitize the full event, depending on the value of its data member `fMerge`. Event merging is performed if this data member is equal to 1, while if it is equal to zero only digits are produced. The other data members are listed below:

```
MergeMode_t  fMerge;     // Merging type (kDigitize or kMerge)

// Background event
char         *fFnBgr;    // Background file name
TFile        *fBgrFile;  // Pointer to background file
Int_t        fNEvBgr;    // Number of events in background file
TTree        *fTrHBgr;   // Hits tree for background event
TClonesArray *fHitsBgr;  // TClonesArray of background hits
TTree        *fTrSDBgr;  // SDigits tree for background event
TTree        *fTrDBgr;   // Digits tree for background event
Float_t      fImpPar;    // Impact Parameter of the collision
Int_t        fSpecn;     // Number of spectator n
Int_t        fSpecp;     // Number of spectator p
```

```
// Signal events
Int_t        fFreeSpn;   // Signal event number x spectator n
Int_t        fFreeSpp;   // Signal event number x spectator p
char         *fFnSpecn;  // Spectator n file name
TFile        *fSpecnFile;// Pointer to signal file -> spectator n
char         *fFnSpecp;  // Spectator p file name
TFile        *fSpecpFile;// Pointer to signal file -> spectator p
Int_t        fNMhits;    // Number of Merged hits for background
TClonesArray *fMHits;    // TClonesArray for "merged" hits
```

An object of type `AliZDCMerger` must be initialized by setting the merger mode, the background file name and the number of the event to be processed. The `AliZDC` class owns a pointer to the `AliZDCMerger` object and a member function, `SetMerger`, to set the pointer to the initialized merger object.

`AliZDCMerger` member functions are:

```
void         InitMerging();
void         Background(Float_t &b, Int_t &nspecn, Int_t &nspecp);
void         Fragmentation(Float_t b, Int_t nspecn, Int_t nspecp,
             Int_t &nfreespn, Int_t &nfreespp);
void         Mixing();
void         ExtractSignal(Int_t SpecType);
void         Digitize(Int_t NMhits, TClonesArray *MHits);
Int_t        Phe2ADCch(Int_t Detector, Int_t Tower, Int_t Light);
Int_t        AddPedestal();
// Inline functions
TClonesArray *MergedHits() const {return fMHits;}
Int_t        GetNMhits() const {return fNMhits;}
TFile        *BgrFile() const {return fBgrFile;}
Int_t        EvNum() const {return fNEvBgr;}
// Setters
void         SetMode(MergeMode_t mode) {fMerge = mode;}
void         SetBackgroundFileName(char* file) {fFnBgr = file;}
void         SetBackgroundEventNum(Int_t nev) {fNEvBgr = nev;}
```

If the `AliZDCMerger` object is constructed with the merging option selected, its `InitMerging` method is invoked by `Hits2SDigits` function of `AliZDC`. `InitMerging` calls the `Background` method to open background file and read from the event header the impact parameter and the number of generated spectator protons and neutrons. These three values are passed to the `Fragmentation` method that, using functions of `AliZDCFragment` class, calculates the number of produced fragments. The number of signal events to be merged with the background is given by the number of free spectator nucleons. Background and signal hits are summed by the `Mixing` method. Background hits are directly read from the opened file; while hits for signal events are randomly extracted from the stored distribution using the `ExtractSignal` method.

4.5.2 AliZDCMergedHit class

Summed hits are used to define new objects of type `AliZDCMergedHit`. This class is very similar to `AliZDCHit` for what concerns data members and member functions. The main difference is that `AliZDCMergerHit` derives directly from `TObject` and is therefore not known by `AliRun`. This allows to write the `TClonesArray` of `AliZDCMergedHit` objects at merging time, when information about the primary track that has generated the hit (needed by `AliHit` constructor) are no more accessible. Two `AliZDCMergedHit` objects are defined equal when they refer to the same sub-volume in the same detector and the sum between two of these objects consists in the sum of produced light and deposited energy, as it is for two ordinary ZDC hits.

In `InitMerging` a new `AliZDCMergedHit` object is created by copying each hit of the background event; then hits for signal are appended to the list. The `TClonesArray` of merged hits is then passed to `Hits2SDigits` method to be written in the summable digits tree. Therefore when merging is performed, summable digits correspond to the hits of the full event, while the hit trees contain the generated hits for the background. If `AliZDCMerger` is initialized without the merging option, `AliZDCMergedHit` are simply a copy of the simulated hits. This is done in order to fill the summable digits tree with the same type of objects in both cases.

4.5.3 Digits production

The digit tree is filled event by event by the method `SDigits2Digits`, called by `AliRun`. The digitization procedure for the ZDC is implemented in `Digitize` method of `AliZDCMerger`. `Digitize` uses the information stored in the summable digits tree to calculate the total light collected by each photomultiplier; this gives 12 values since there are 5 photomultipliers for each hadronic ZDC and 2 for the electromagnetic ones. Then photoelectron yields are converted in ADC channels by means of `Phe2ADCch` method, simply multiplying the photoelectron yield by photodetector gain and dividing it by the ADC resolution. The used values are 10^5 for the gain and 2.5 pC/channel for ADC resolution (corresponding to the Le Croy 2242 ADC), but they can be set through appropriate member functions provided by `AliZDCMerger`.

A pedestal value is then extracted randomly from a gaussian distribution, whose mean value and width are defined on the basis of beam test results. Pedestals are added to the calculated ADC value by means of the `AddPedestal` function. Finally the ADC values are added to the list of ZDC digits calling the `AddDigit` method of `AliZDC`. `AddDigit` creates a new object of type `AliZDCDigit` and writes it into the apposite `TClonesArray` that, at the end of each event, is written into the ZDC branch of digits tree by the `SDigits2Digits` function.

AliZDCDigit class

The class for ZDC digits inherits from `AliDigitNew` and has only two data members: an array of two elements that specify detector and sub-volume and the ADC value. An `AliZDCDigit` object is therefore constructed specifying values for these data members.

In the following figures hits, summable digits and digits for the ZDC, obtained with the described classes, are shown.

In fig. 4.9 hits corresponding to the energy deposited in hadronic calorimeters respectively for background particles, for spectator neutrons and protons are shown. Background hits are obtained with 1100 minimum bias events generated with HIJING 1.36. Hits for signal are given by 10^4 spectator neutrons and 10^4 spectator protons generated with `AliGenZDC`.

In fig. 4.10 summable digits and digits for the merged events are plotted. The effect of nuclear fragments production is reflected in both spectra. In fact there are two distinct classes of events: one with a lower number of spectators, corresponding to very central (where a few spectators are produced) and to very peripheral collisions (where fragmentation is more important) and the second one with a higher number of free spectators corresponding to intermediate impact parameters (see also fig. 4.8).

4.6 Reconstruction

Reconstructed quantities: AliZDCReco class

The reconstruction is the phase of data analysis in which the physics quantities are extracted from detector response, given either by the simulation or by raw data from the experiment.

Concerning the ZDC, aim of the reconstruction is to provide an estimate of the number of participants and of the impact parameter of the collision. Some of the reconstructed quantities are directly calculated (like energy detected in each detector and the number of detected spectators), while others are evaluated in a more indirect way (like the number of participants and the impact parameter). The class that defines the reconstructed objects for ZDC is `AliZDCReco`. Like `AliZDCMergedHit`, `AliZDCReco` is a very simple class that inherits from `TObject`.

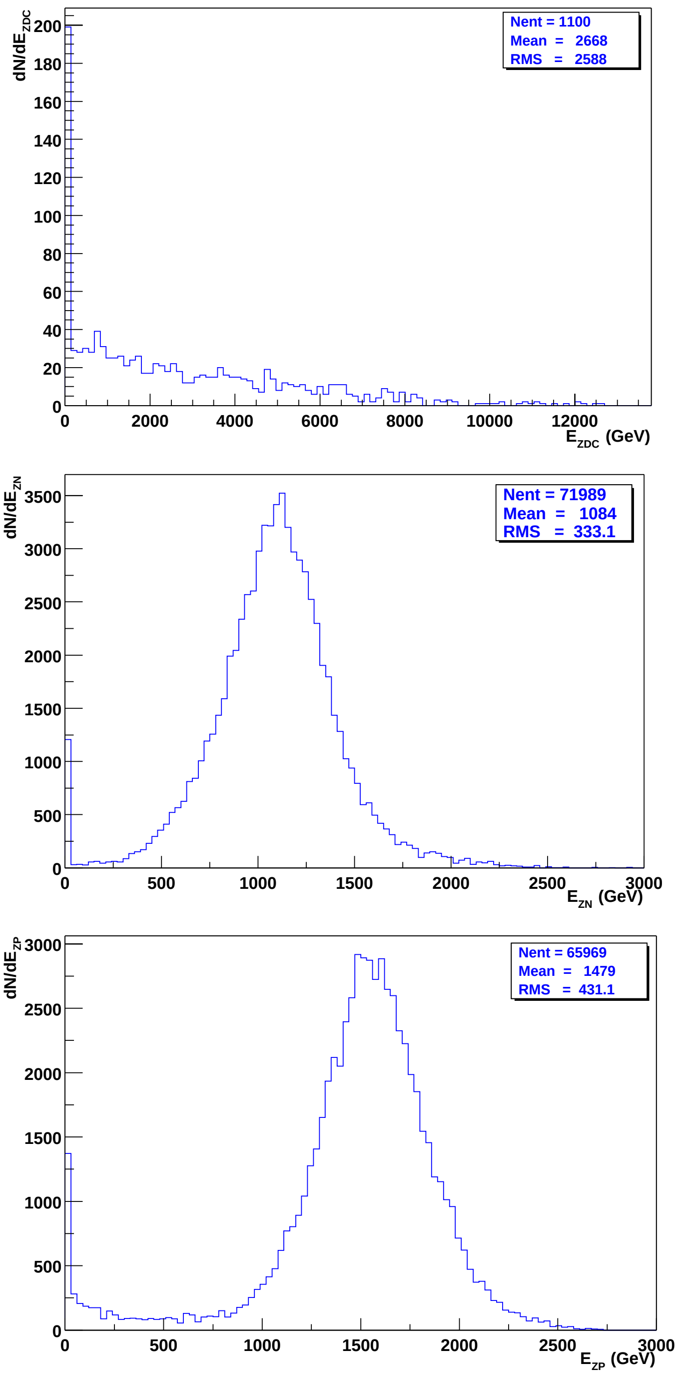

Figure 4.9. Up: energy measured in the hadronic calorimeters due to background. Middle: energy detected in neutron calorimeter for 10^4 spectator neutrons. Down: energy deposited in proton calorimeter by 10^4 spectator protons.

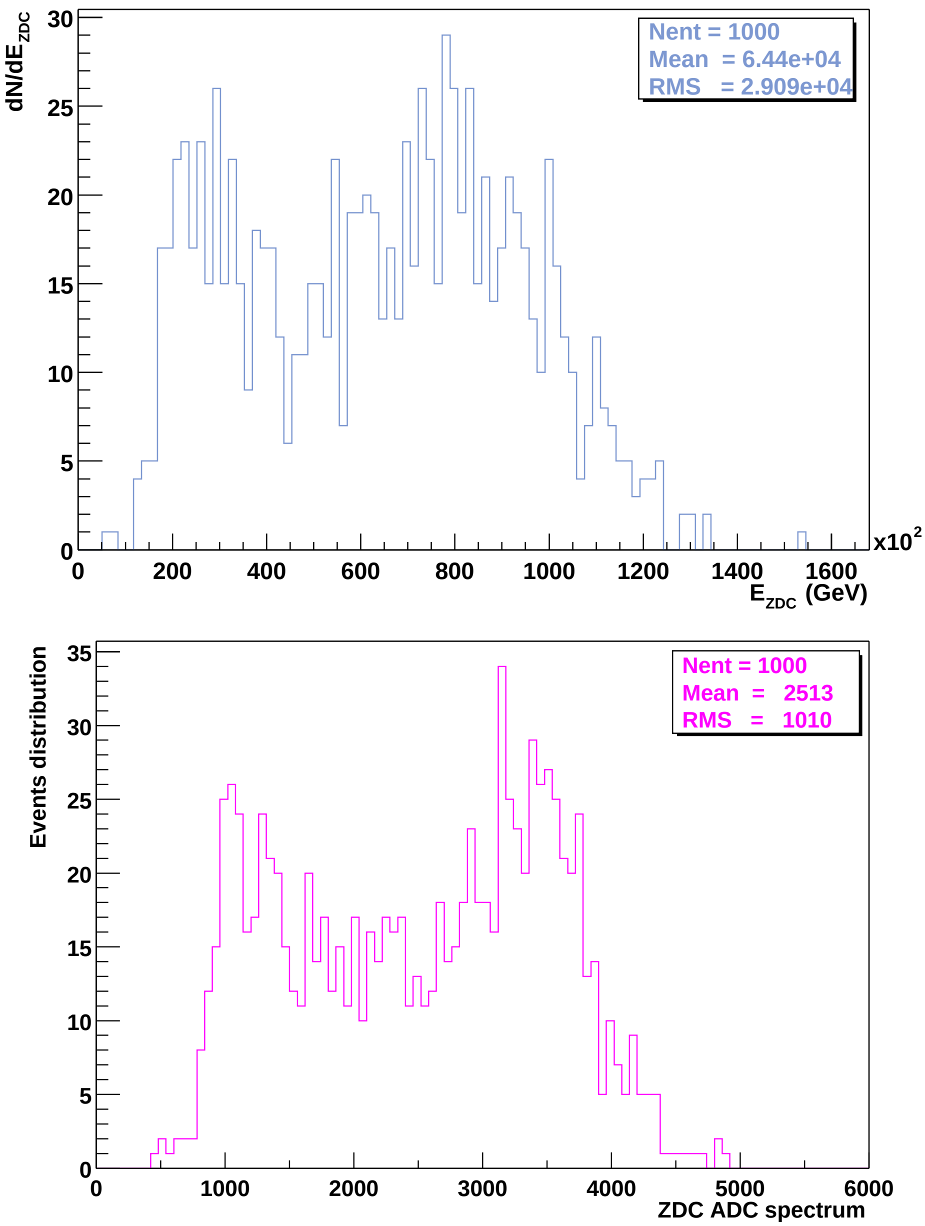

Figure 4.10. Summable digits (up) and digits (down) for 1000 minimum bias Pb-Pb interactions at 2.7 TeV generated with HIJING 1.36 and merged with signal.

The class is characterized by the following data members:

```
Float_t fZNenergy;  // Energy detected in neutron ZDC
Float_t fZPenergy;  // Energy detected in proton ZDC
Float_t fZDCenergy; // Total energy detected in hadronic ZDCs
Float_t fZEMenergy; // Energy detected in EM ZDC
Int_t   fNDetSpecN; // Number of detected spectator neutrons
Int_t   fNDetSpecP; // Number of detected spectator protons
Int_t   fNRecSpecN; // Number of true spectator neutrons
Int_t   fNRecSpecP; // Number of true spectator protons
Int_t   fNRecSpec;  // Number of true spectators
Int_t   fNPart;     // Number of participants
Float_t fImpPar;    // Estimated impact parameter value
```

Reconstruction method

Reconstruction is performed event by event in `Digits2Reco` method of `AliZDC`. Digits are read from their trees and are summed to obtain three ADC values respectively for neutron, proton and electromagnetic calorimeters. ADC signals are then corrected with pedestal subtraction and converted in photoelectrons yields. The procedure adopted is specular to the one followed for digitization; the only difference is due to the fact that the subtracted pedestal values are in this case the mean values (since the fluctuation on ADC pedestals is not known a posteriori).

Photoelectron yields should then be converted to energies. For this purpose calibration factors for the three detectors have been deduced from simulations. The hadronic calorimeters will be experimentally calibrated with the single neutron emitted in the process of mutual electromagnetic dissociation. Therefore conversion factors have been obtained fitting light distributions for an incident spectator of 2.76 TeV and dividing the mean value of the fit by the known incident energy value. For neutron ZDC such a calibration leads to 0.329 produced photoelectrons per GeV of incident energy, for the proton detector the factor is equal to 0.369 (fig. 4.11). For the electromagnetic calorimeters the conversion should be experimentally done using the measured response as a function of incident energy; in fact the energy of incident particles is distributed over a rather broad range (as shown in fig. 3.1). Therefore energy losses in ZEM have been evaluated as a function of light yields (see fig. 4.11) and the conversion is given by the following calibrating function:

$$E_{ZEM}\,[GeV] = 0.322 \cdot < phe > + 0.994.$$

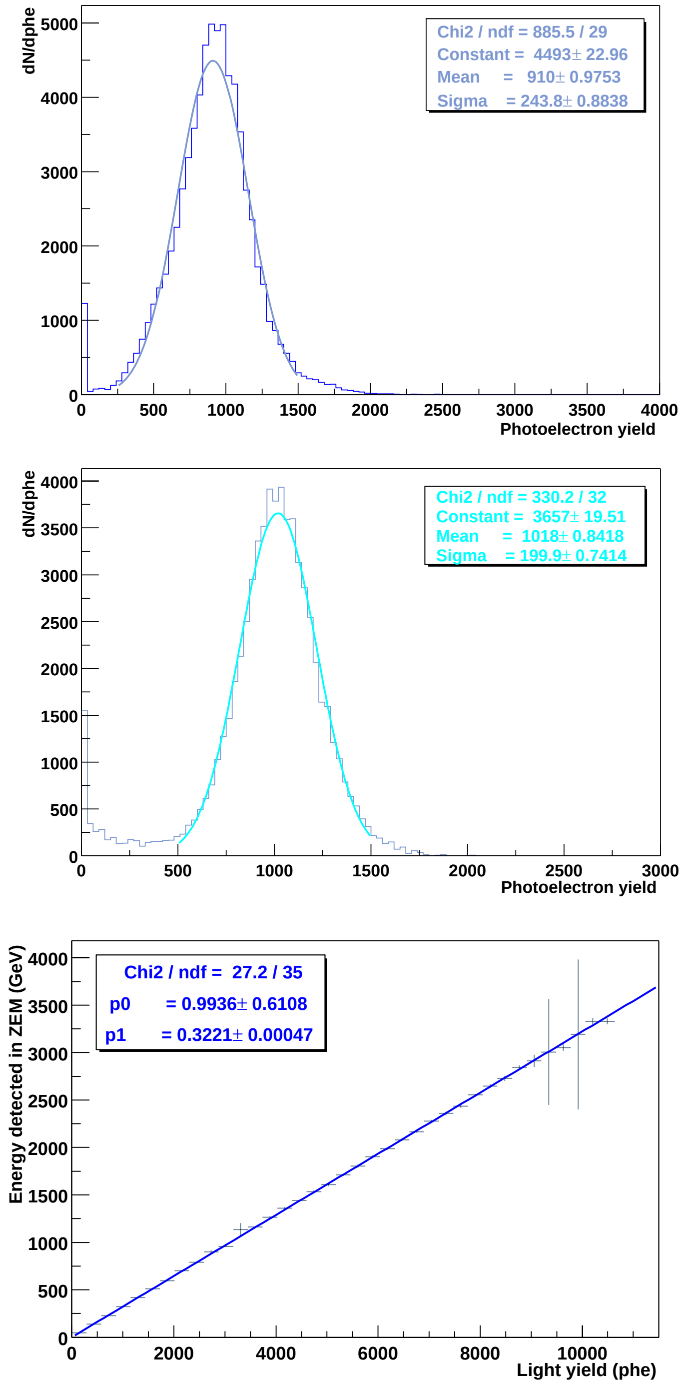

Figure 4.11. Fits for the determination of conversion factors from light yield to incident energy (see text for details).

The estimate of the number of incident spectator neutrons and protons can be given by simply dividing the total incident energy by the energy of each nucleon. The tree containing reconstructed quantities is filled event by event by the `Digits2Reco` method called by `AliRun`. The procedure adopted to reconstruct the global variables of the collision such as the impact parameter and the number of participants is more complicated and will be discussed in detail in the following chapter.

Results

The reconstructed energy spectrum for hadronic calorimeters is plotted in fig. 4.12. Comparing this distribution with the one obtained for summable digits (reported in fig. 4.10), a different energy scale can be noticed. This is due to the fact that summable digits refer to energy loss as calculated by GEANT, while the calibration made during reconstruction gives the incident energy.

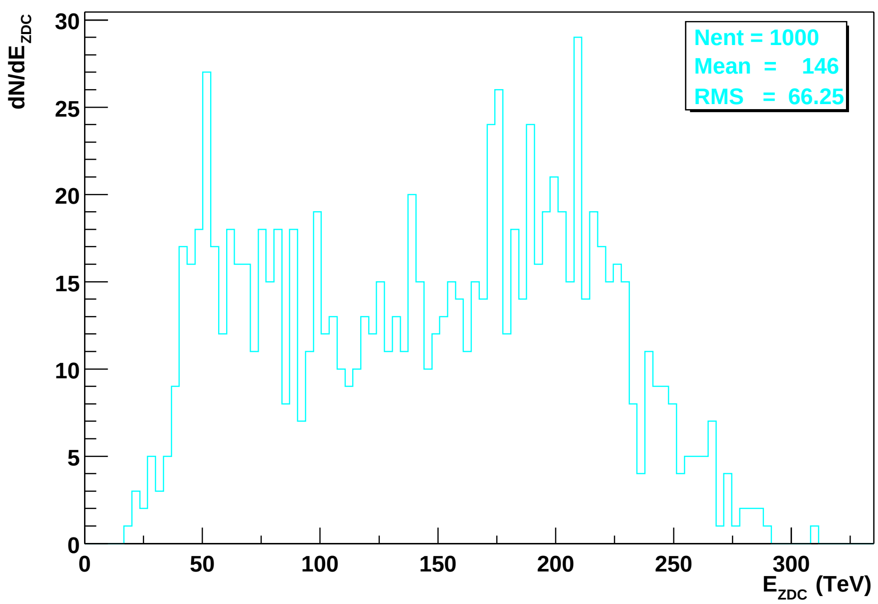

Figure 4.12. Reconstructed energy spectrum in ZDC for 1000 minimum bias events generated with HIJING 1.36.

In fig. 4.13 the simulated and the reconstructed energy spectra are compared for hadronic and electromagnetic detectors and it can be seen that the reconstruction procedure reproduce quite well simulation results. In fig. 4.14 the energy detected by the calorimeters as a function of the generated impact parameter is shown. Finally, in fig. 4.15 the reconstructed correlations between energy detected in hadronic calorimeters and that in the electromagnetic ones are plotted. As will be discussed in next chapter, such correlations can be used for reconstruction of number of participants and impact parameter.

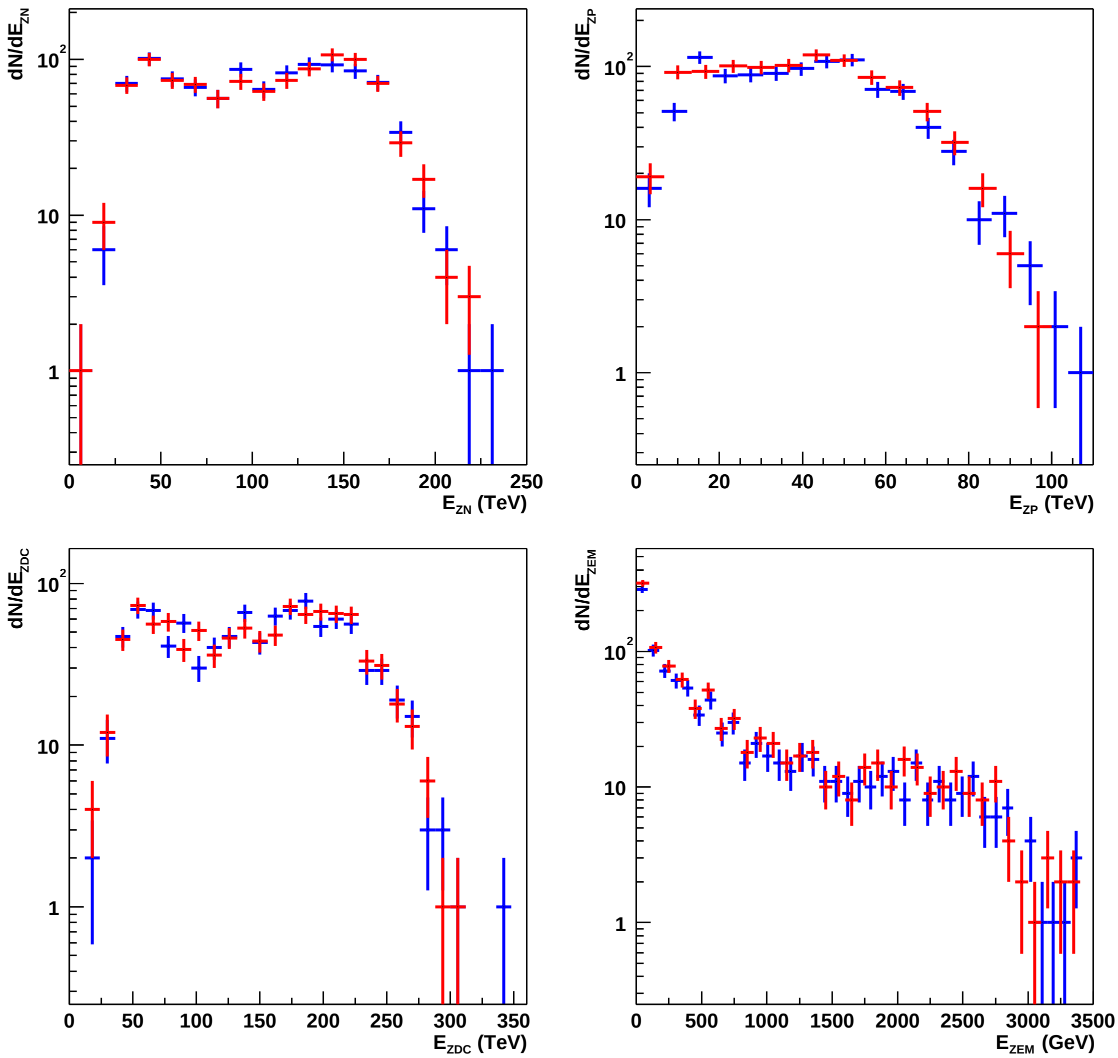

Figure 4.13. Comparison of reconstructed (red) and simulated (blue) energy spectra for ZN (up left), ZP (up right), for both hadronic calorimeters (down left) and for the electromagnetic ones (down right).

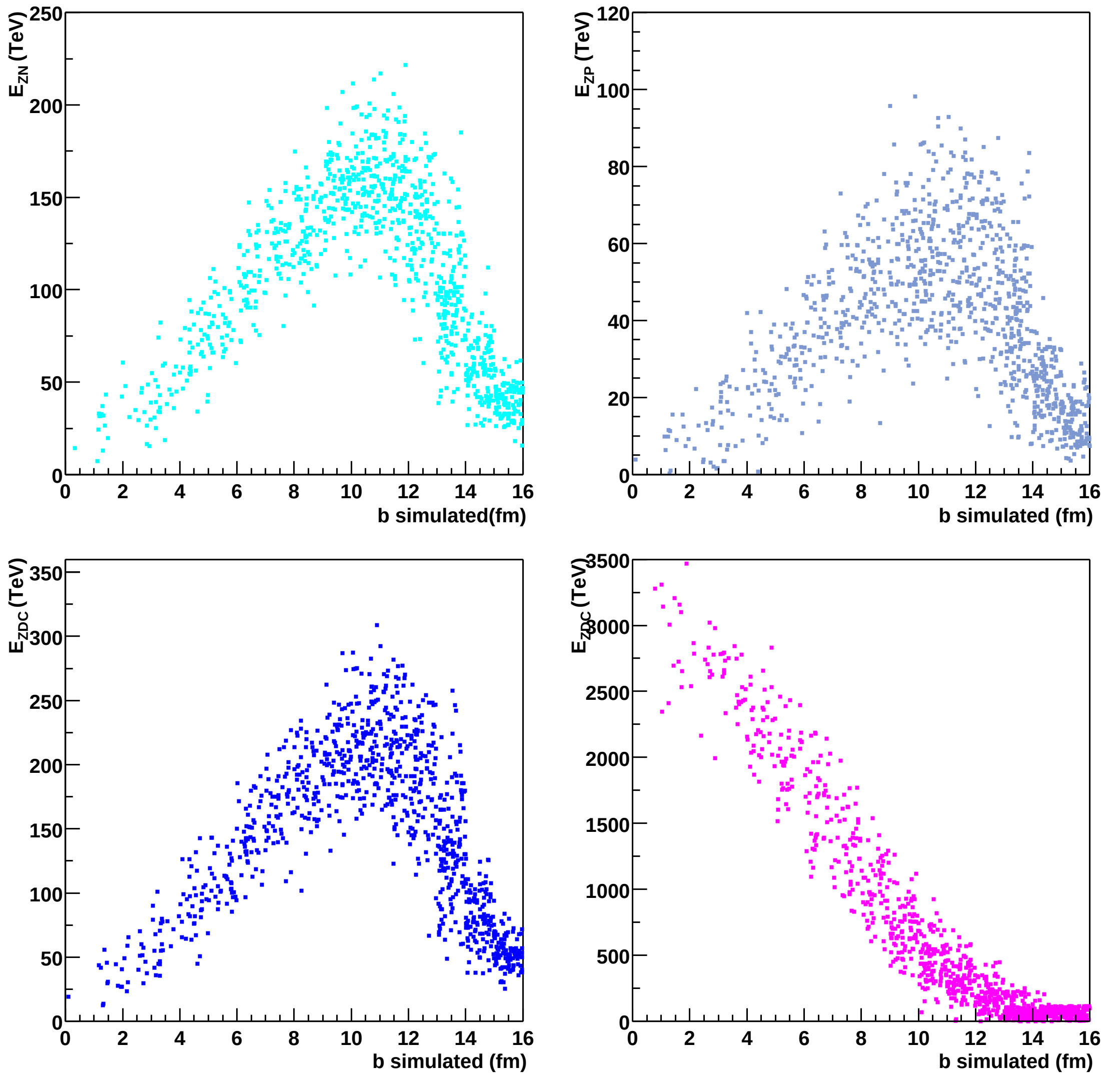

Figure 4.14. Reconstructed energies as a function of impact parameter for ZN (up left), ZP (up right), both hadronic ZDC (down left) and ZEM (down right).

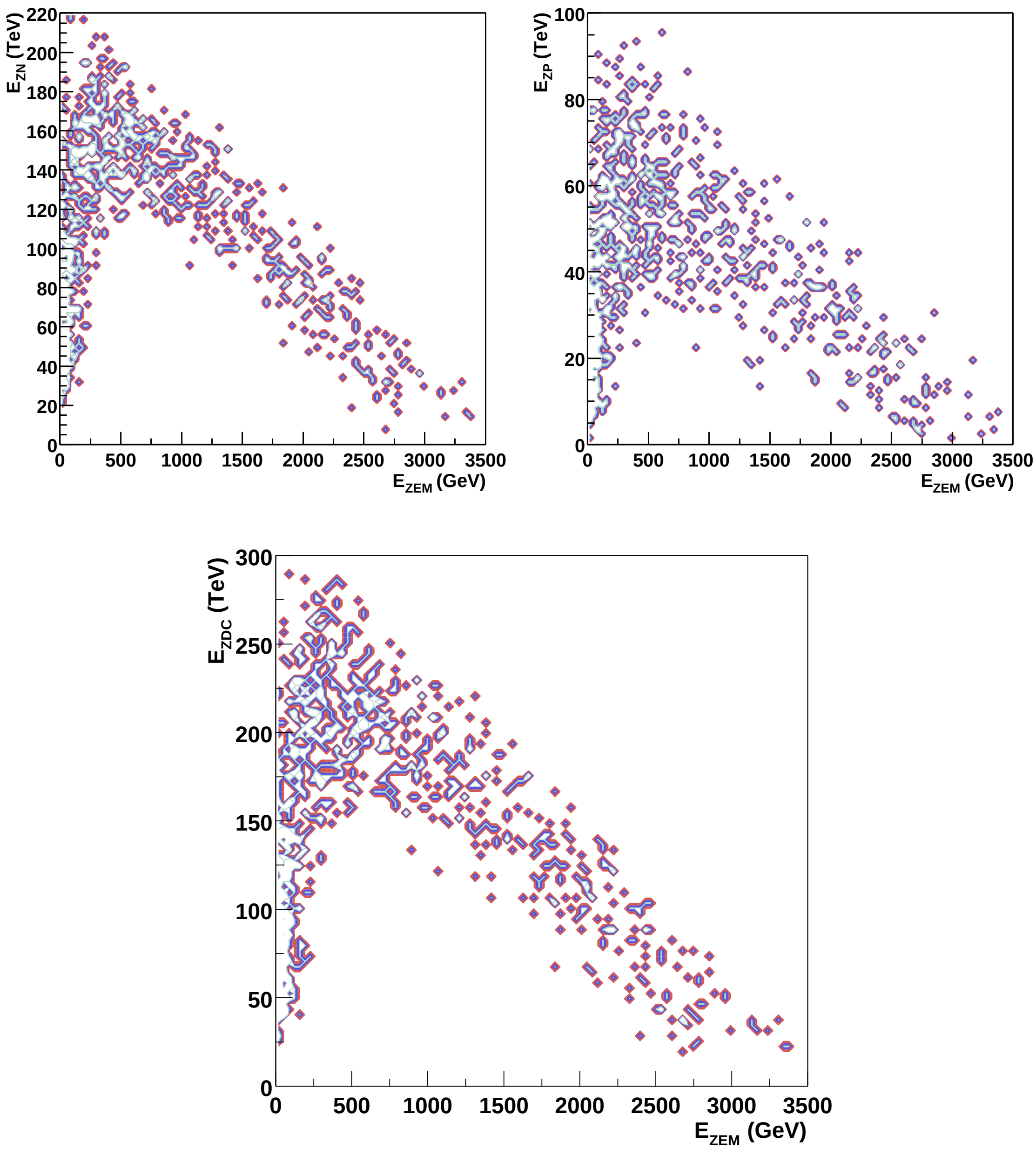

Figure 4.15. Reconstructed correlations between energy detected in hadronic calorimeters (ZN up left, ZP up right, both ZDCs down) and in ZEM.

References

[1] GEANT 3.21, CERN Program Library Long Writeup W5013.

[2] http://alisoft.cern.ch/offline

[3] http://root.cern.ch

[4] A. Shor *et al.*, Nucl. Phys. A **514** (1990) 717.

[5] A. Schuttauf *et al.*, Nucl.Phys. A **607** (1996) 457.

Chapter 5

Centrality measurement at ALICE: simulation results

In this chapter I will discuss two different methods that can be used to provide an estimate of the impact parameter and of the number of participants from the zero degree energy measurement. For such a study 1000 minimum bias events have been generated with HIJING 1.36, in the impact parameter range 0<b<16 fm. For these events, as explained in the previous chapter, only the background due to secondaries and participants is generated. Then the spectator signal is merged using two samples of 10^4 events each, for spectator protons and neutrons respectively. In fig. 5.1 the impact parameter distribution of the generated events is plotted. As expected, for geometrical reasons, the event distribution grows linearly with b.

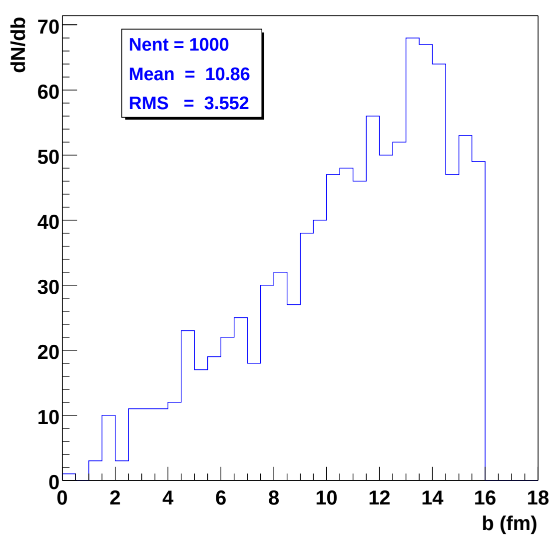

Figure 5.1. Impact parameter distribution for 1000 minimum bias events generated with HIJING 1.36.

5.1 Event by event reconstruction

The first method applied for the reconstruction of the centrality of the collision starts from the fits to simulated correlations between reconstructed energy and global variables (namely the number of participants and the impact parameter) and provides an event by event estimate of the number of participants and of the impact parameter. For this purpose the correlations between the number of spectators and the energy reconstructed in ZN and ZP and between the impact parameter and the total energy measured in all the hadronic calorimeters E_{ZDC} are fitted. The information provided by the electromagnetic calorimeters is used in order to avoid the ambiguity caused by fragmentation (see section 3.1).

To estimate the number of participants the following procedure is adopted: first each of the correlation E_{ZN} versus $N_{spec,n}$, E_{ZP} versus $N_{spec,p}$ and E_{ZDC} versus $N_{spec,tot}$ is fitted with two polynomial functions, imposing the condition that the two functions assume the same value for the abscissa corresponding to the maximum of the correlations (the results can be seen in fig. 5.2). After that, the functions are inverted so that each of them describes one of the two branches of the correlations between detected energies and the number of generated spectators. The resulting functions are plotted in fig. 5.3 on top of the corresponding correlations. The value of spectators where the functions are linked is indicated in figure; it corresponds to 97 spectator neutrons in ZN and 73 spectator protons in ZP. The relative energy values are 158.5 TeV for ZN and 58.91 TeV for ZP.

The correlation between the number of spectators and the energy detected in the electromagnetic calorimeters is then fitted with a parabolic function (see fig. 5.4). The energy value corresponding to the number of spectators for which the two branches of the previous correlations are linked is ~360 GeV. This value is considered as the ZEM energy threshold that allows to distinguish between peripheral and central branch in the above mentioned correlations. In practice, if the energy detected in ZEM is higher than this threshold value, the number of spectators is evaluated from the branch corresponding to central events. On the contrary if ZEM energy is below the threshold, the functions which fit the peripheral branches are rather chosen to calculate the number of spectators.

However, as can be seen in fig. 5.3, there are some events with energy values higher than the maximum value reached by the fitting functions. These events correspond to about 14.6% of the total numbers of events for ZN, to 19.1% for ZP and to 13.7% for both ZDCs. For such events the number of spectators is directly evaluated from the correlation with ZEM energy.

To estimate the impact parameter, the correlation between b and the sum of the energies detected in hadronic calorimeters is fitted. In this case the two branches corresponding to central and peripheral events have been fitted separately, the first one with a third order polynomial function and the second with a parabolic function.

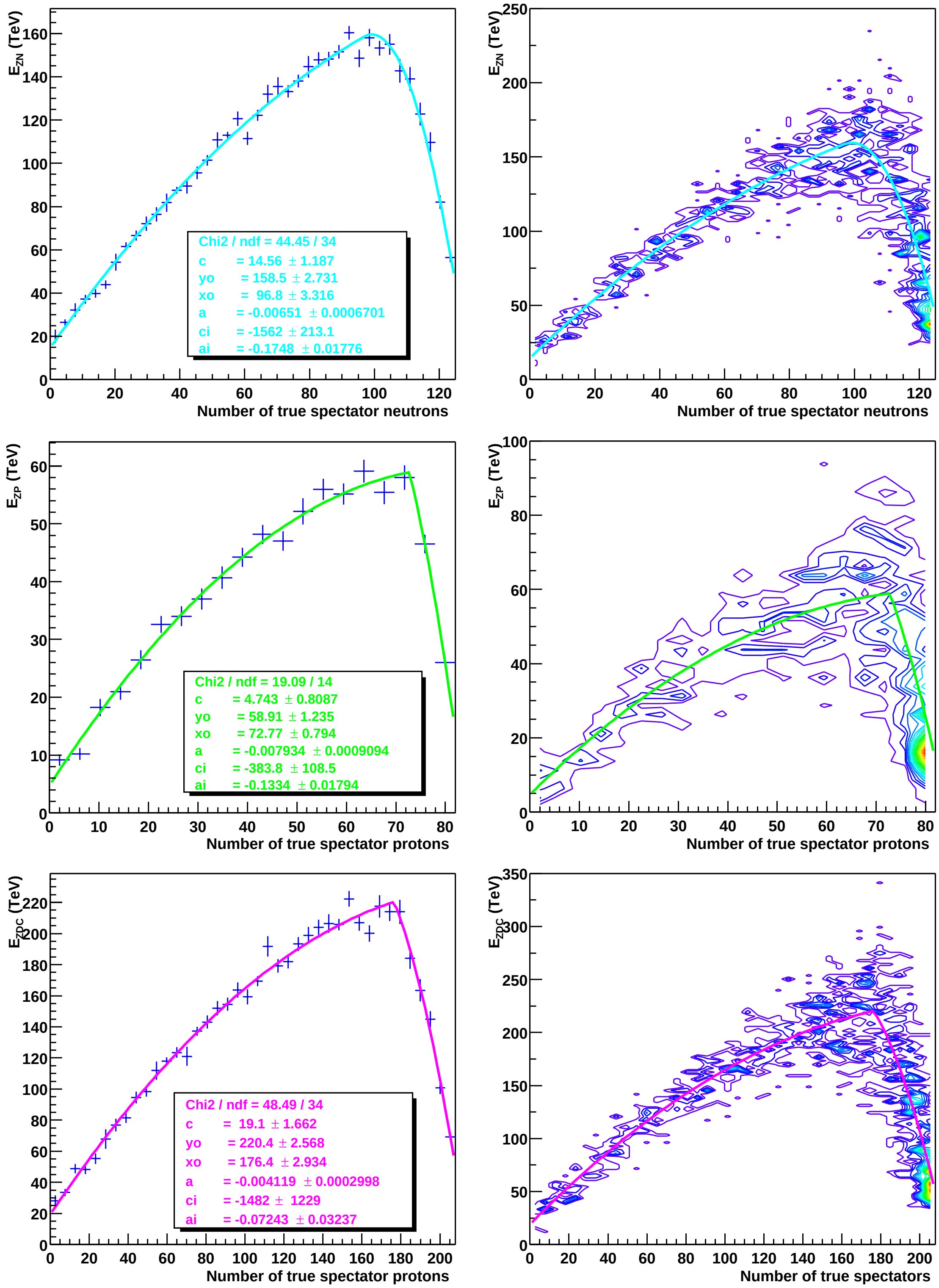

Figure 5.2. Fit of the correlations between the number of generated spectators and energy detected respectively in ZN (up) and in ZP (middle) and in both ZDCs (down). On the left the fits are shown and on the right they are superimposed on the corresponding correlations.

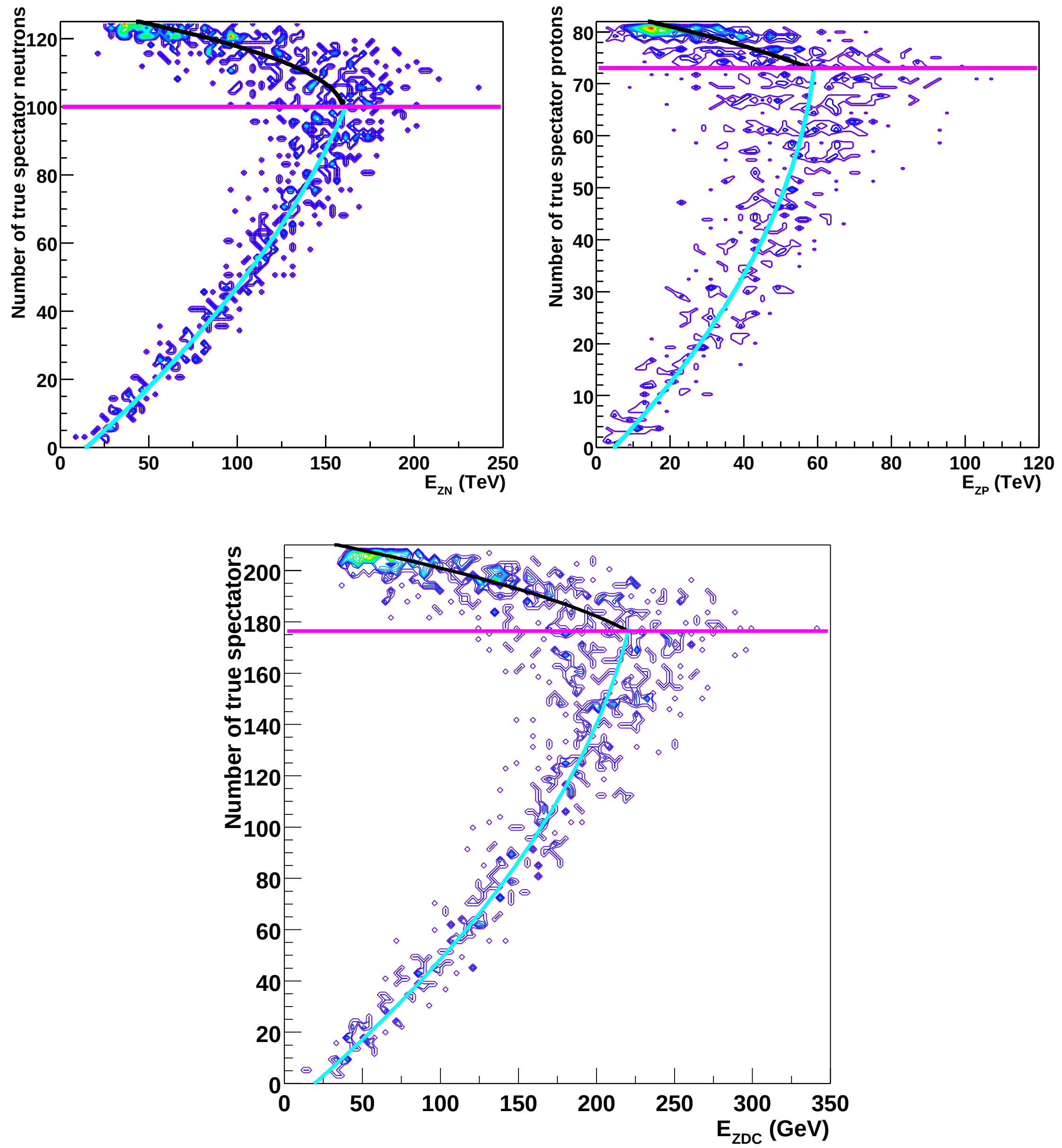

Figure 5.3. Correlations between incident energy and the number of generated spectators in ZN (up left), in ZP (up right) and in both hadronic ZDCs (down). Magenta lines represent spectator values in which the two functions are linked (see text for the values).

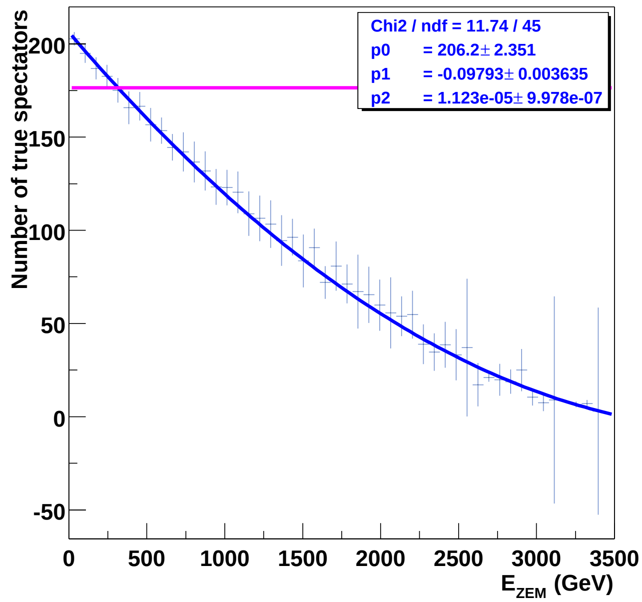

Figure 5.4. Correlation between the number of generated spectators and the energy detected in ZEM. The horizontal line corresponds to the number of spectators for which the correlation E_{ZDC} vs. N_{spec} has a maximum. The corresponding E_{ZEM} value is $\sim$ 360 GeV.

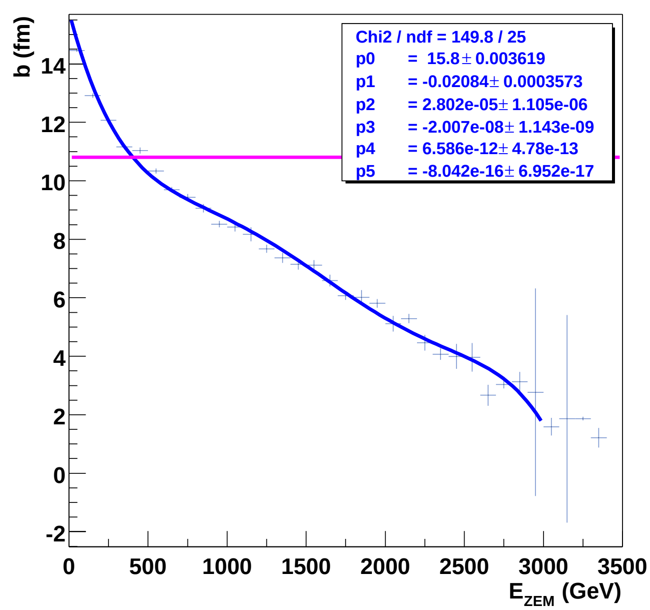

Figure 5.5. Fit of the correlation between b and energy measured in electromagnetic calorimeters. The magenta line corresponds to the impact parameter value in which the correlation E_{ZDC} vs. b reaches its maximum (b$\sim$ 11.1 fm).

The two functions are connected as explained before; the results are shown in fig. 5.6.

To choose the branch an event belongs to, the same threshold value in ZEM energy evaluated before has been considered. When the energy detected by the hadronic calorimeters is higher than the maximum value reached by the fitting functions, the impact parameter is directly evaluated from E_{ZEM} versus b correlation (this happens in the 11.6% of the cases). The correlation between the impact parameter and the energy detected in ZEM has been fitted with a fifth order polynomial function (as can be seen in fig. 5.5).

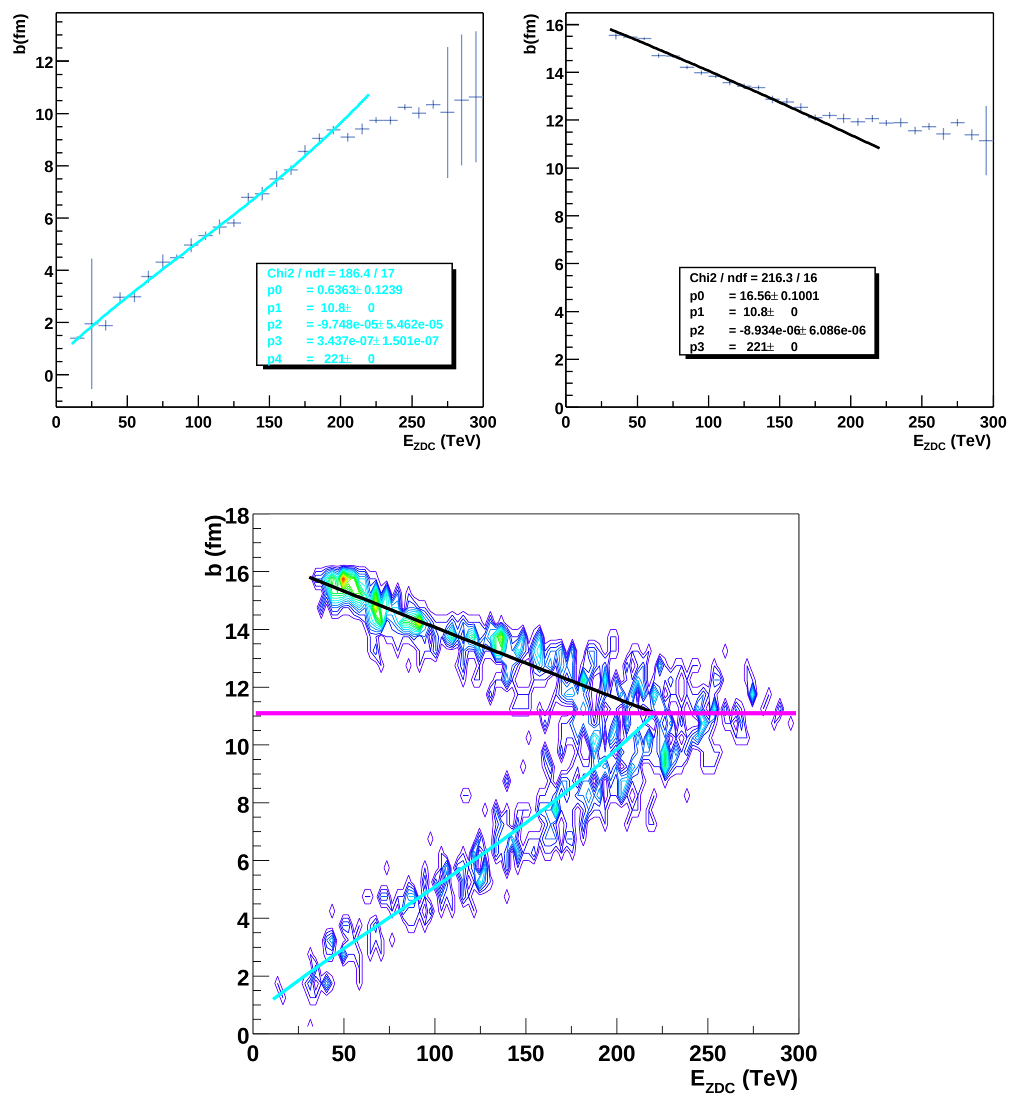

Figure 5.6. b vs. E_{ZDC} correlation: fit of the branch corresponding to central (up left) and to peripheral events (up right). Resulting is superimposed on the simulated correlation (down left).

Using the described method, the number of spectators can be evaluated from the energy reconstructed in ZN and in ZP and the impact parameter can be estimated from the total hadronic energy. The number of participants is simply obtained by subtraction, once the number of spectators has been determined. The energy measured by ZEM calorimeters is used to select the correct branch in the correlations; in 15% of the events it is used to determine directly the number of spectators or the impact parameter.

5.1.1 Results on global variables reconstruction

The results obtained with the described reconstruction procedure have to be compared to the corresponding generated values to test the reliability of the method. In fig. 5.7 the reconstructed number of spectators is compared to the simulated one.

The number of spectator neutrons is well reconstructed over all its range; it is only slightly underestimated in the region around $N_{spec,n} \sim 97$ where the two fitting functions are linked. This effect is more important for spectator protons, for which the distribution has a larger spread (as can be better seen in the lego plots of fig. 5.7). The root mean square of the distribution of reconstructed spectators for a given number of generated spectators is about 8 for both neutrons and protons, as can be inferred from fig. 5.8, where the distribution of the difference between reconstructed and simulated values is plotted.

Being derived from the number of spectators, the reconstructed number of participants is slightly overestimated in the region where the two branches of the correlations are connected. The error made in the determination of the number of participants is about 30 (fig. 5.9). The resolution on this variable as a function of centrality goes from more than 75% for very peripheral events, corresponding to about 20 participants, down to a few percent for central collisions, with $N_{part} \gtrsim 350$. The resolution is below 10% for $N_{part} \gtrsim 250$, corresponding, according to the Glauber model, to $b \lesssim 6$ fm.

Concerning the estimation of the impact parameter, the reconstructed values are different from the generated ones for very central collisions (see fig. 5.10), where the fit of the correlation b vs. E_{ZDC} is most sensitive to the initial values of the parameters essentially because of the low number of generated events. The distribution resolution on the reconstructed values of b, for a certain generated impact parameter, is of the order of 1 fm over the whole centrality range. It's important to note that the method used to reconstruct impact parameter does not give a significant bias since the mean value of this distribution is close to zero. The resolution on b as a function of centrality is around 55% for $b \sim 1$ fm, then it drops under 20% for $b \sim 3$ fm and remains under 10% for $b \gtrsim 9$ fm.

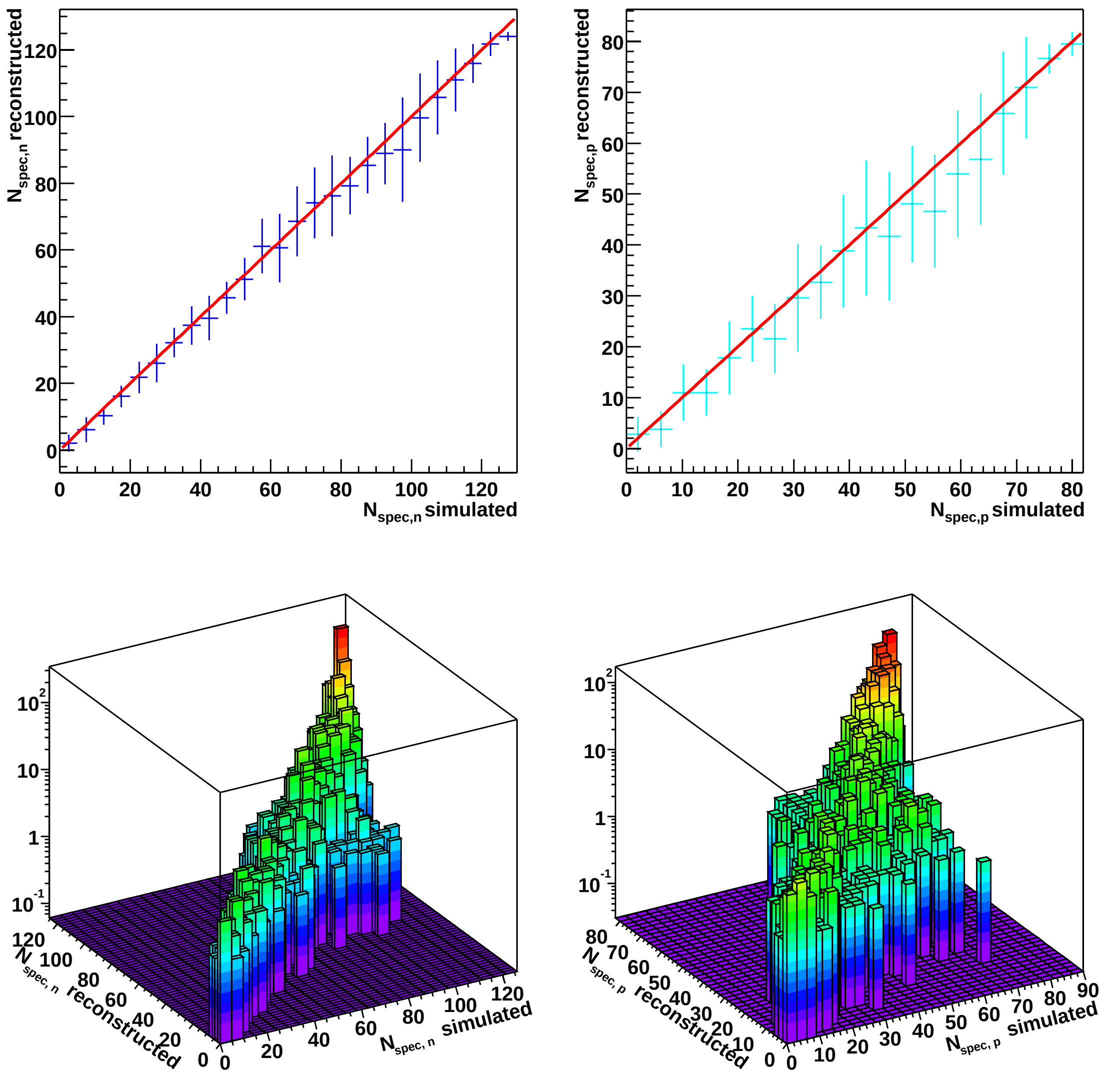

Figure 5.7. Reconstructed number of spectator neutrons (left) and protons (right) as a function of the simulated one (the diagonal are indicated by the red lines).

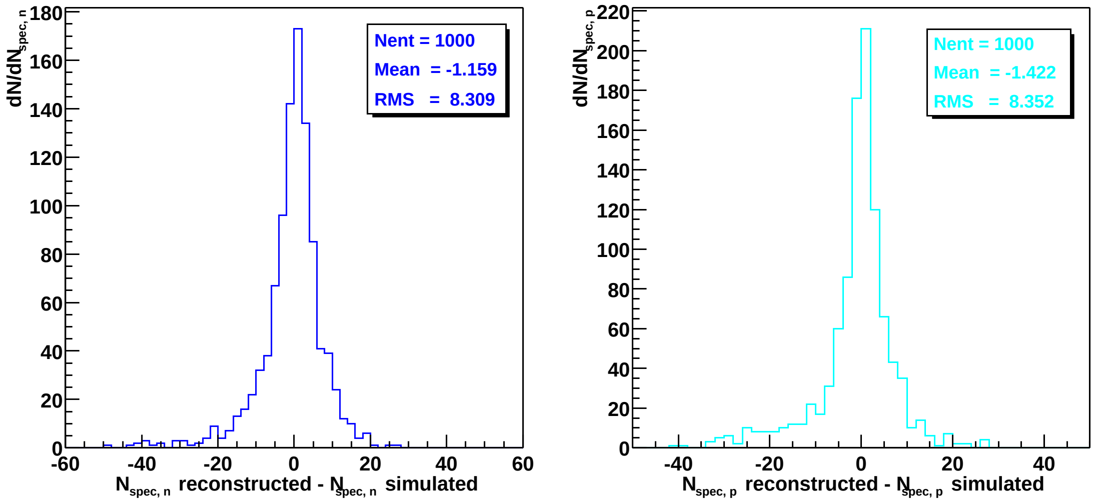

Figure 5.8. Distributions of the difference between the reconstructed and the simulated number of spectator neutrons (left) and protons (right).

5.1.2 Centrality classes in the event by event method

The simulated b sample has been divided in 5 centrality classes using the following ranges in generated impact parameter:

- class 1: 0<b<3 fm
- class 2: 3<b<6 fm
- class 3: 6<b<9 fm
- class 4: 9<b<12 fm
- class 5: 12<b<16 fm

From the reconstructed distributions we can extract the mean value and the width for each class and compare them with the simulated ones. Event distributions for both simulated and reconstructed classes are shown in fig. 5.11, while the mean value of the reconstructed impact parameter and its error, calculated for each class, are reported in table 5.1.

The width of each distribution is smaller than the separation between consecutive classes, therefore five centrality bins can be safely defined. The event by event estimation of the impact parameter provides a good b reconstruction since the simulated and reconstructed values differ by 0.5 fm at most. The degree of contamination in each class, due to the tails of adjacent distributions, is 28% for the most central events, 18% for the second class, 35% for the third one, 32% for the fourth and 16% for the last one.

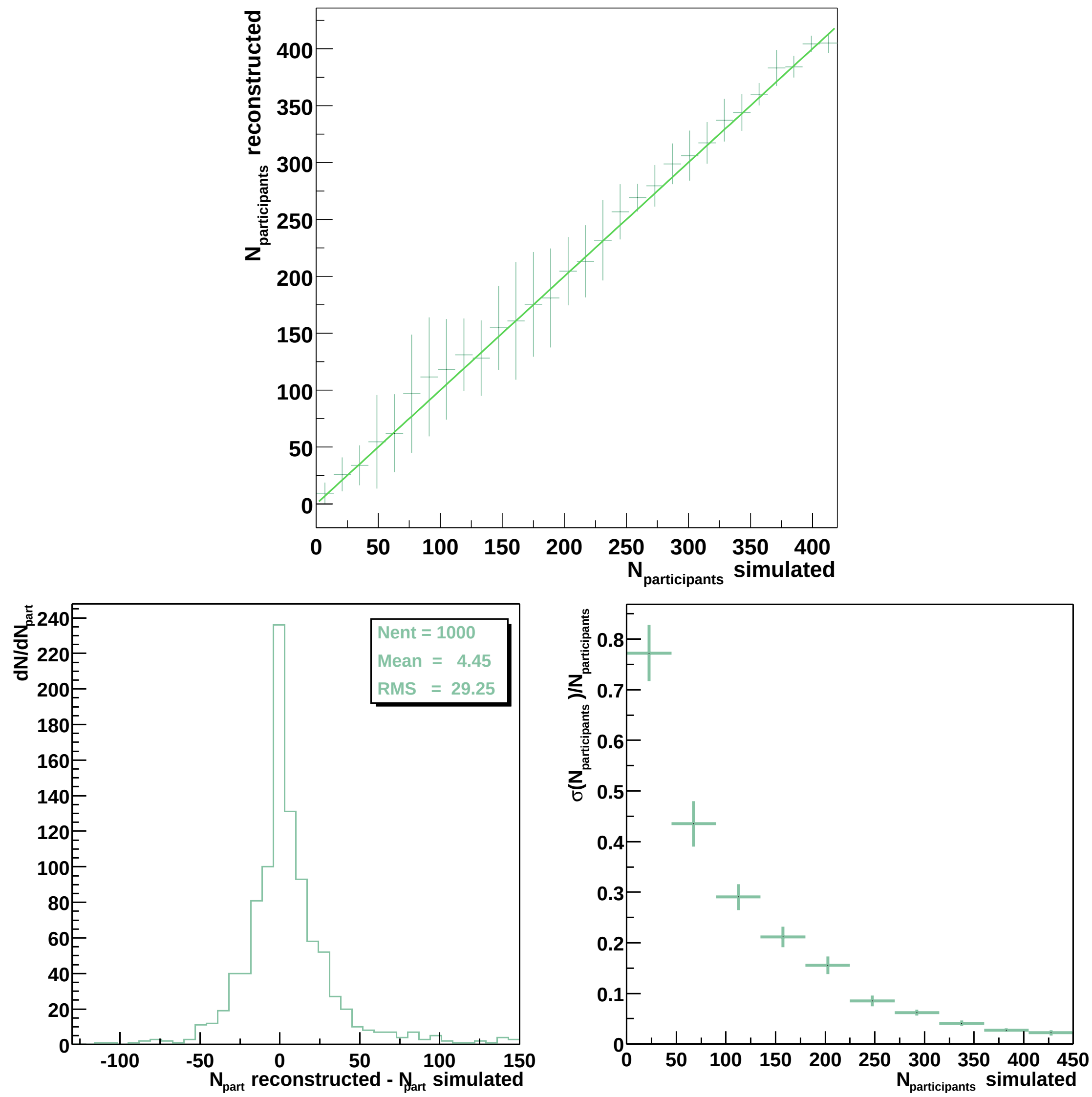

Figure 5.9. Reconstructed number of participants as a function of the generated one (up), distribution of the difference between reconstructed and simulated values (down left) and relative error as a function of the generated number of participants (down right).

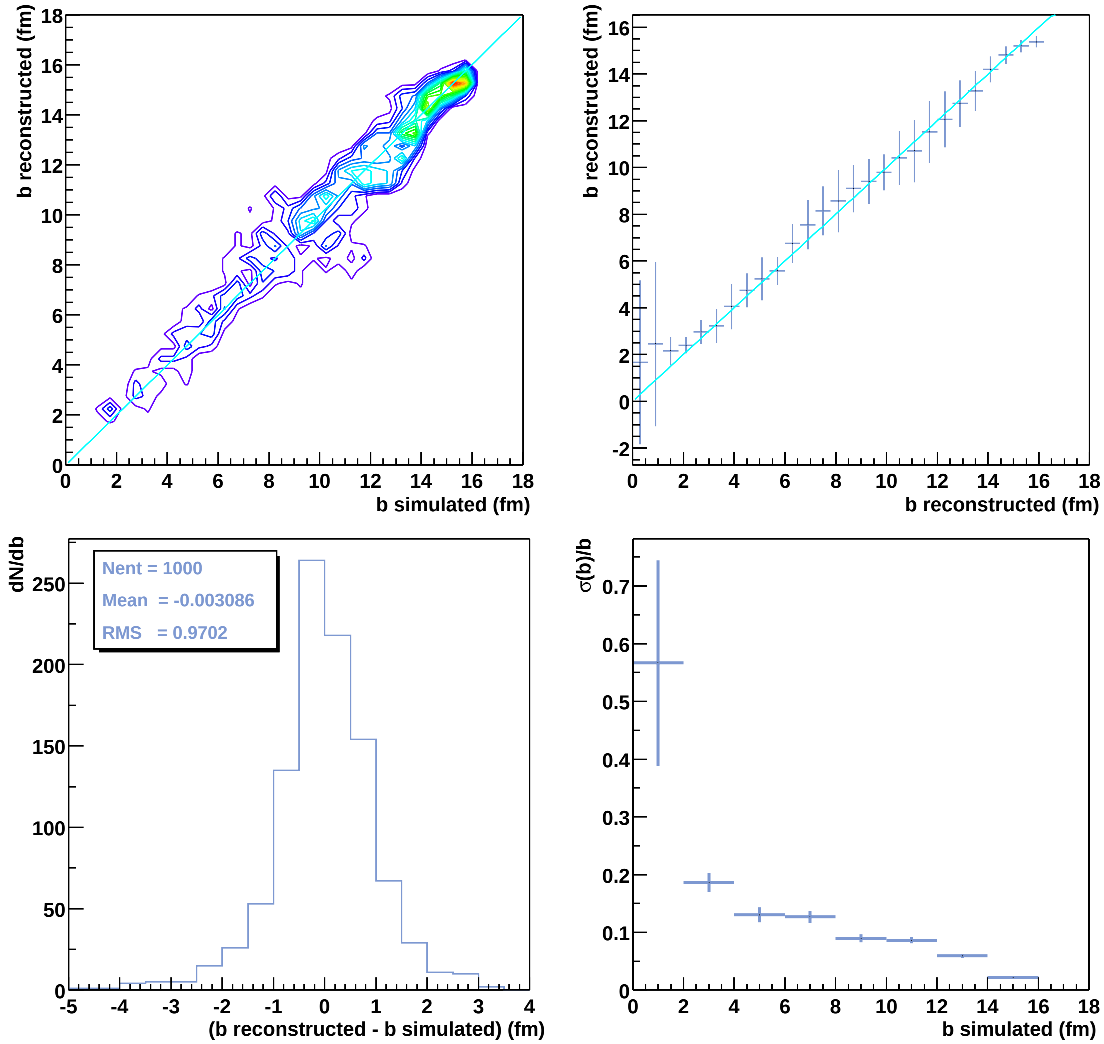

Figure 5.10. Impact parameter reconstruction: correlation with simulated b (up), distribution of the difference between reconstructed and simulated values (down left) and relative error (down right) as a function of generated impact parameter.

b range	$< b_{simulated} >$ (fm)	$< b_{reconstructed} >$ (fm)
0-3 fm	2.1 ± 0.6	2.6 ± 0.6
3-6 fm	4.7 ± 0.8	4.8 ± 1.1
6-9 fm	7.6 ± 0.8	8.1 ± 1.3
9-12 fm	10.6 ± 0.9	10.4 ± 1.4
12-16 fm	14.0 ± 1.1	13.8 ± 1.4

Table 5.1. Mean value and width of simulated and reconstructed impact parameter in five centrality classes.

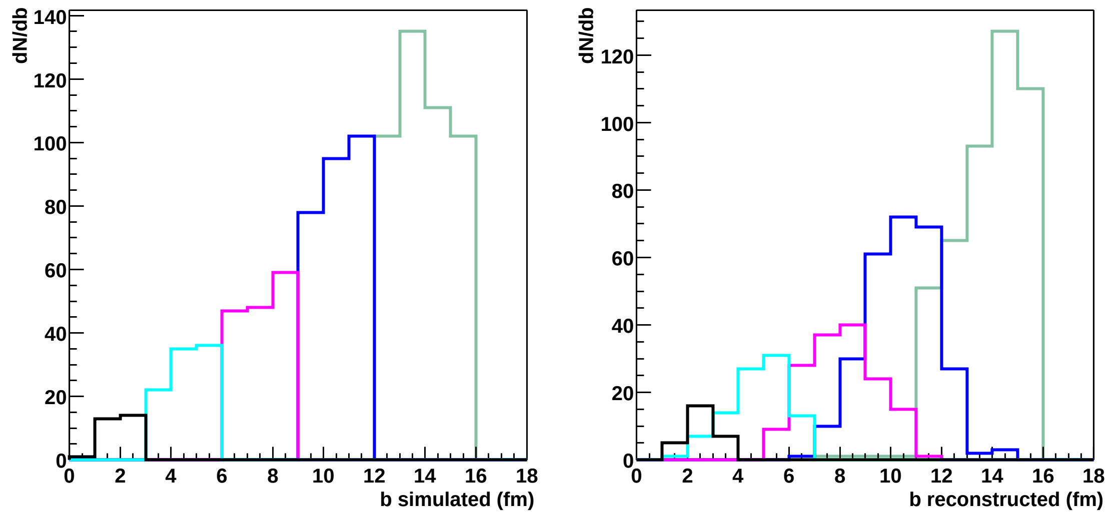

Figure 5.11. Left: centrality classes defined on simulated sample. Right: the same centrality classes as obtained with event by event reconstruction.

Similarly the simulated distribution in number of participants has been divided in five bins corresponding to the following N_{part} ranges.

- class 1: $375 < N_{part} < 414$
- class 2: $276 < N_{part} < 375$
- class 3: $152 < N_{part} < 276$
- class 4: $54 < N_{part} < 152$
- class 5: $0 < N_{part} < 54$

These intervals have been chosen in order to select the same fraction of the total hadronic cross section used in the definition of b classes. The obtained classes are plotted for simulated and reconstructed events in fig. 5.12 and the corresponding results concerning the determination of the number of participants are in table 5.2.

Also in this case, five centrality classes can be defined since their width is smaller than their separation. A discrepancy of about 17% between simulated and reconstructed mean values is found for the most peripheral class ($N_{part} < 54$), it becomes 10% for the class corresponding to the range $54 < N_{part} < 152$. For the other classes this difference is of the order of 1%. The contamination of events from other centrality classes amounts to 17% for the most central class, 28% for the one with $276 < N_{part} < 375$, 40% for $152 < N_{part} < 276$, 22% for $54 < N_{part} < 152$ and 6% for the most peripheral bin.

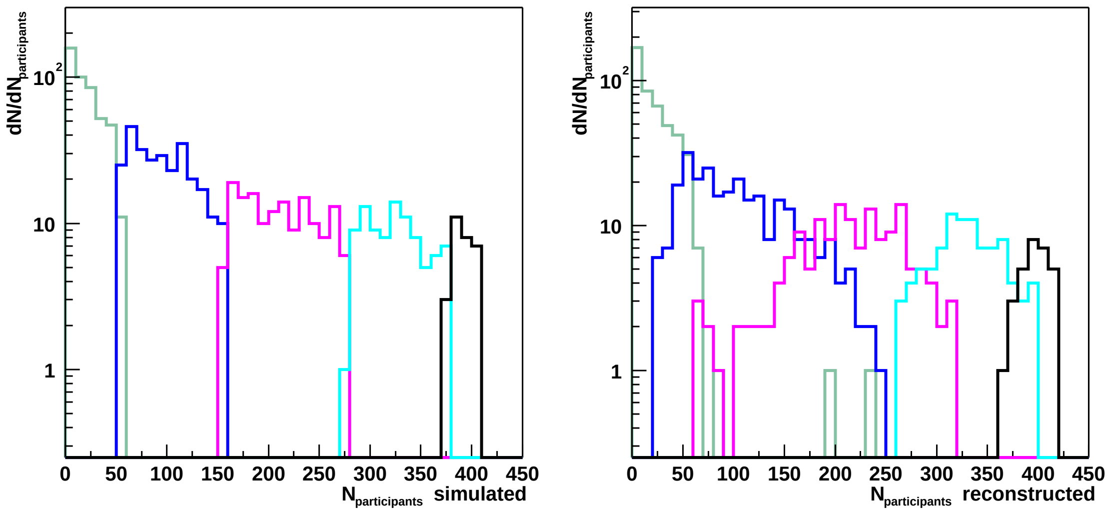

Figure 5.12. Simulated (left) and reconstructed (right) centrality classes in N_{part} variable.

$N_{participants}$ range	$<N^{simulated}_{participants}>$	$<N^{reconstructed}_{participants}>$
375-414	391 ± 10	395 ± 14
276-375	323 ± 28	329 ± 33
152-276	210 ± 35	211 ± 54
54-152	94 ± 28	104 ± 51
0-54	18 ± 14	21 ± 22

Table 5.2. Mean value and width of simulated and reconstructed number of participants in the five centrality classes defined.

5.1.3 Model dependence of the event by event method

The advantage of the described method is that it allows an event by event estimation of impact parameter and number of participants. On the other hand, being based on the parameterization of simulated correlations it is in principle sensitive to the event generator used for the simulation. Therefore we tried to estimate to what degree the reconstruction depends on the assumed model. For this purpose we made a very simple test, varying the HIJING background contribution and comparing the results obtained with the same reconstruction procedure used for "true" HIJING events (i.e., without fitting again the correlations). The background contribution due to participants and secondaries has been doubled and halved. The background contamination to the ZDC signal is obviously more important for central events, where the number of participants and secondaries emitted within ZDC pseudorapidity acceptance is higher and the number of spectators is low. In fig. 5.13 the background over signal ratio is plotted as a function of the impact parameter for the three simulated situations.

The reconstructed values of impact parameter and number of participants are significantly affected by background contamination only for very central events. A small disagreement can be seen in the case corresponding to the higher background, where the impact parameter is overestimated for b $\lesssim$8 fm and the number of participants is underestimated for $N_{part} \gtrsim$200. The results are summarized in fig. 5.14, that has to be compared to fig. 5.10 and 5.9 for ordinary HIJING background.

The mean values of the impact parameter and of the number of participants in the five centrality bins defined above are reported in tables 5.3 and 5.4. It can be verified that in both cases the average values of b and N_{part} for centrality classes do not change significantly, indicating that the model used to describe the background can introduce only a small bias. Moreover the resolution on global variables is not worsened, as can be seen for the impact parameter in table 5.5. Therefore we conclude that the event by event method for centrality reconstruction depends on the model used for simulation, but it can be safely used to provide a "first order" evaluation of centrality.

$b_{simulated}$ range (fm)	$<b_{sim}>$ (fm)	$<b_{reco}>$ (fm) HIJING	$<b_{reco}>$ (fm) $0.5 \cdot$ HIJING	$<b_{reco}>$ (fm) $2 \cdot$ HIJING
0-3	2.1 ± 0.6	2.6 ± 0.6	2.2 ± 0.6	3.2 ± 0.7
3-6	4.7 ± 0.8	4.8 ± 1.1	4.4 ± 1.1	5.3 ± 1.2
6-9	7.6 ± 0.9	8.1 ± 1.3	7.8 ± 1.4	8.5 ± 1.2
9-12	10.6 ± 0.9	10.4 ± 1.4	10.7 ± 1.5	10.5 ± 1.2
12-16	14.0 ± 1.1	13.8 ± 1.4	13.9 ± 1.3	13.8 ± 1.3

Table 5.3. Mean values of the reconstructed impact parameter for the three different background evaluations.

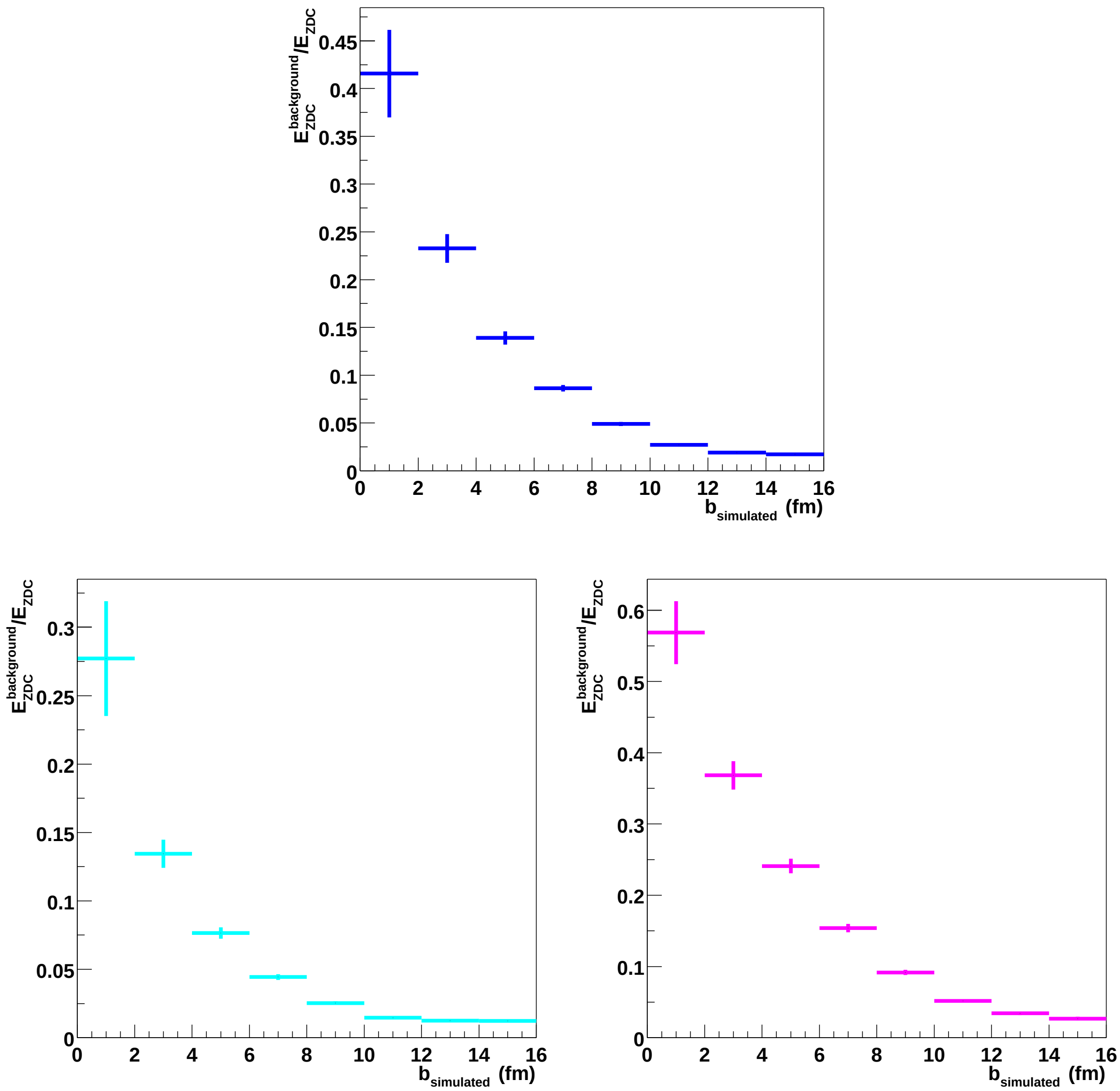

Figure 5.13. Background over signal ratio in the ZDCs as a function of centrality for the "normal" HIJING simulation (up) and when background contribution is respectively halved (down left) and doubled (down right).

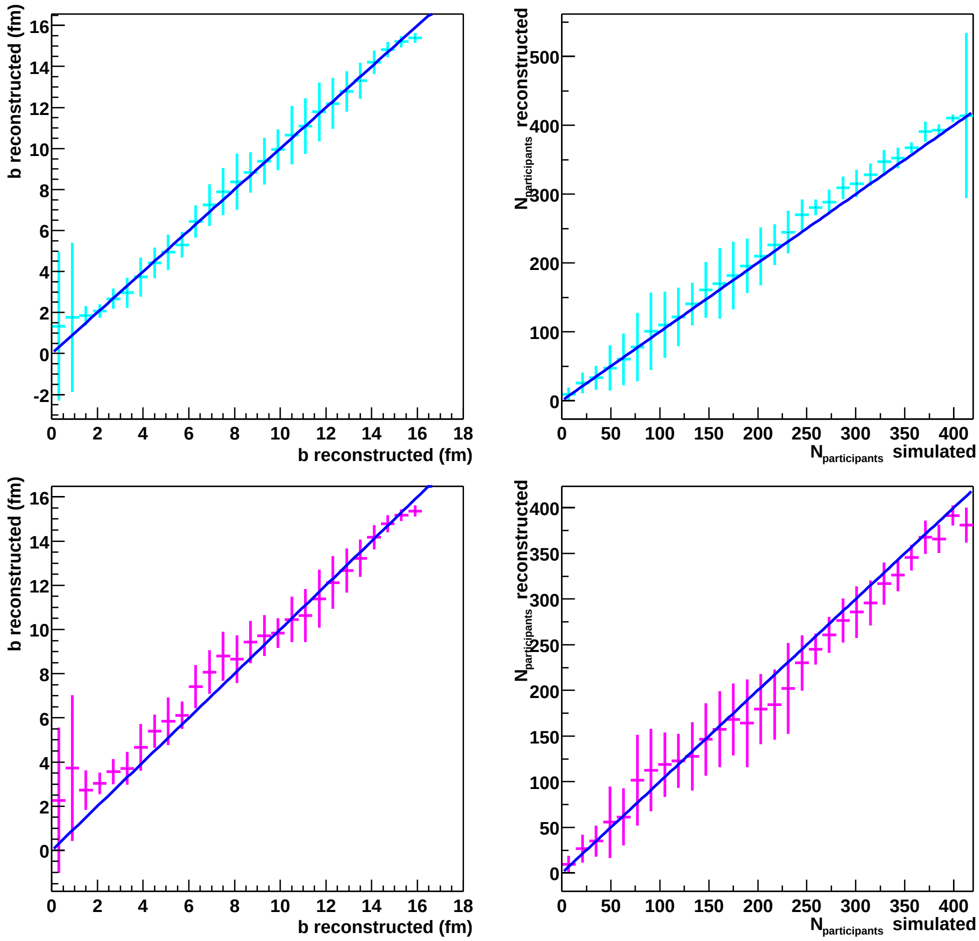

Figure 5.14. Global variable reconstruction for HIJING generated background contribution divided (up) and multiplied (down) by a factor 2.

N_{part}^{sim} range	$<N_{part}^{sim}>$	$<N_{part}^{reco}>$ HIJING	$<N_{part}^{reco}>$ $0.5 \cdot$ HIJING	$<N_{part}^{reco}>$ $2 \cdot$ HIJING
375-414	391 ± 10	395 ± 14	402 ± 12	379 ± 19
276-375	323 ± 28	329 ± 33	338 ± 32	309 ± 37
152-276	210 ± 35	211 ± 54	221 ± 56	192 ± 52
54-152	94 ± 28	104 ± 51	97 ± 55	103 ± 47
0-54	18 ± 14	21 ± 22	20 ± 20	22 ± 22

Table 5.4. Mean values of the reconstructed impact parameter for the three different simulated background.

$b_{simulated}$ range	σ(b)/b HIJING	σ(b)/b $0.5 \cdot$ HIJING	σ(b)/b $2 \cdot$ HIJING
0-3 fm	0.23	0.27	0.22
3-6 fm	0.23	0.25	0.23
6-9 fm	0.15	0.18	0.14
9-12 fm	0.13	0.14	0.11
12-16 fm	0.10	0.09	0.09

Table 5.5. Impact parameter resolution for different background contribution.

5.2 Reconstruction from the measured correlation E_{ZDC} versus E_{ZEM}

A second method to estimate global variables makes use of the correlation between the reconstructed E_{ZDC} and E_{ZEM} values. Events with increasing centrality can be selected by means of appropriate cuts on the correlation. In practice, by selecting centrality classes perpendicularly to the E_{ZDC} versus E_{ZEM} correlation, events with increasing b can be selected. Defining cuts in the space E_{ZDC} versus E_{ZEM}, allows the determination of centrality classes corresponding to well defined percentiles of the total hadronic cross section:

$$\int_{E_{ZEM,i}} \int_{E_{ZDC,i}} \frac{d^2\sigma}{dE_{ZEM} dE_{ZDC}} = \int_{b_{min}}^{b_{max}} db \frac{d\sigma}{db} = x_i \cdot \sigma_{tot},$$

where i is the index referring to the selected region, corresponding to an impact parameter range $b_{min} < b < b_{max}$ and x_i is the selected fraction of the total cross section. The corresponding number of participants, N_{part}^{min} and N_{part}^{max}, can be calculated using the Glauber model or from the HIJING event generator.

To directly compare the two methods, five classes have been defined selecting the same fraction of the total cross section defined for the event by event method. In fig. 5.15 the E_{ZDC} versus E_{ZEM} correlation is shown with the cuts used to select the five centrality classes.

The impact parameter and the number of participants distributions obtained for the five classes are plotted in fig. 5.16. In table 5.6 the reconstructed mean values are compared to the simulated ones. The reconstructed mean values reproduce quite well the simulated ones in each class. The widths of the distributions are comparable with those calculated with the event by event method, therefore the resolutions achieved by the two methods are comparable (see table 5.7).

This method is particularly useful since, being based on experimental quantities, does not depend on the model used for the simulation and is not sensitive to the exact level of background contamination.

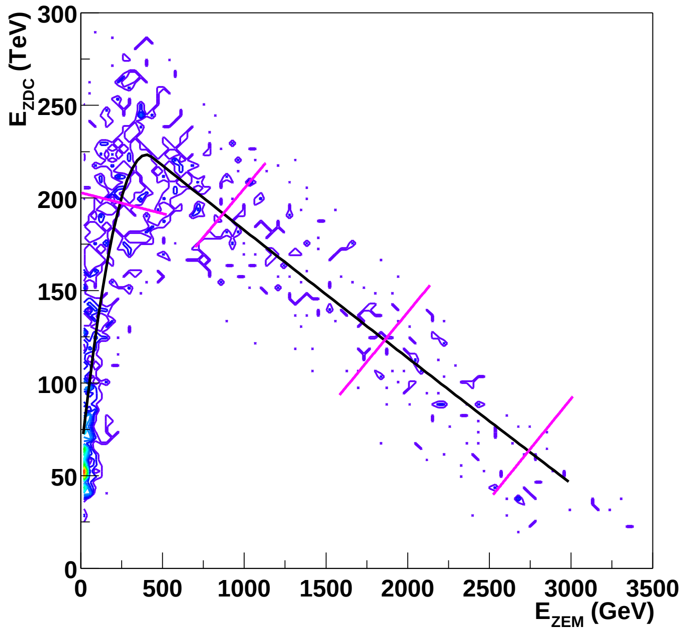

Figure 5.15. Correlation between E_{ZDC} and E_{ZEM} with superimposed the cuts used to define the five centrality classes.

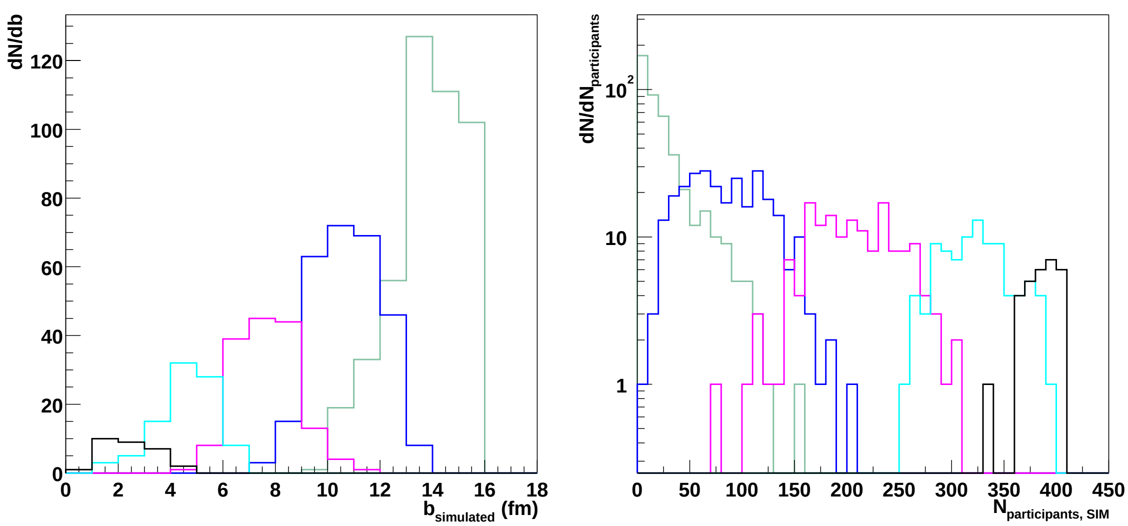

Figure 5.16. Left: centrality classes defined on simulated sample. Right: same centrality classes obtained with event by event reconstruction.

$b_{simulated}$ range	$<b_{sim}>$ (fm)	$<b_{reco}>$ (fm)	$<N^{sim}_{part}>$	$<N^{reco}_{part}>$
0-3 fm	2.1 ± 0.6	2.5 ± 0.9	391 ± 10	385 ± 17
3-6 fm	4.7 ± 0.8	4.6 ± 1.1	323 ± 28	322 ± 33
6-9 fm	7.6 ± 0.9	7.7 ± 1.2	210 ± 35	205 ± 43
9-12 fm	10.6 ± 0.9	10.8 ± 1.3	94 ± 28	84 ± 39
12-16 fm	14.0 ± 1.1	13.8 ± 1.4	18 ± 14	23 ± 25

Table 5.6. Impact parameter and number of spectators reconstructed from the five centrality classes selected in E_{ZDC} vs. E_{ZEM} correlations.

$b_{simulated}$ range	σ(b)/b ev. by ev.	σ(b)/b E_{ZDC} vs. E_{ZEM}	$\sigma(N_{part})/N_{part}$ ev. by ev.	$\sigma(N_{part})/N_{part}$ E_{ZDC} vs. E_{ZEM}
0-3 fm	0.27	0.36	0.04	0.04
3-6 fm	0.25	0.24	0.10	0.10
6-9 fm	0.18	0.16	0.26	0.21
9-12 fm	0.14	0.12	0.49	0.46
12-16 fm	0.09	0.10	1.00	1.00

Table 5.7. Resolution achieved in b and N_{part} reconstruction with the two used methods.

In conclusion, we have two methods to estimate the impact parameter and the number of participants with the ZDC. Both methods are not biased and the results are in relative good agreement. The achieved resolution allows the definition of at least five centrality classes.

5.3 Glauber and Hijing models

The number of participant nucleons as a function of the impact parameter can be estimated by means of Glauber model or using the HIJING event generator. As discussed in section 2.1.1, the results obtained with the two approaches are in agreement; however the HIJING model systematically overestimates the number of participants (see fig. 2.2). In this section I will evaluate if the definition of centrality classes is sensitive to the model used to estimate the number of participants.

For this study a new set of events has been generated with HIJING 1.36. In order to increase the statistic for central collisions, a comparable number of events is produced in fixed impact parameter ranges. The minimum bias distribution can then be built by suitably weighting the simulated events. The weight factors are calculated as the fraction of the total cross section corresponding to the impact parameter ranges chosen for the simulation, normalized to the number of generated event in that range. In table 5.8 the used impact parameter ranges are reported, together with the corresponding fraction of the total geometrical cross section, the number of simulated and of minimum bias events and the calculated weights. Simulated and minimum bias impact parameter distributions are plotted in fig. 5.17.

b range	Fraction of σ_{total}	Number of simulated ev.	Number of MB ev.	Weight factors
0 - 3 fm	3.6%	93	93	1.00
3 - 6 fm	11.0%	100	284	2.84
6 - 9 fm	18.2%	100	470	4.70
9 - 12 fm	25.4%	100	656	6.56
12 - 15 fm	31.9%	200	824	4.12
15 - 18 fm	9.9%	200	256	1.28

Table 5.8. Parameters for the extrapolation of the minimum bias distribution from the simulated events.

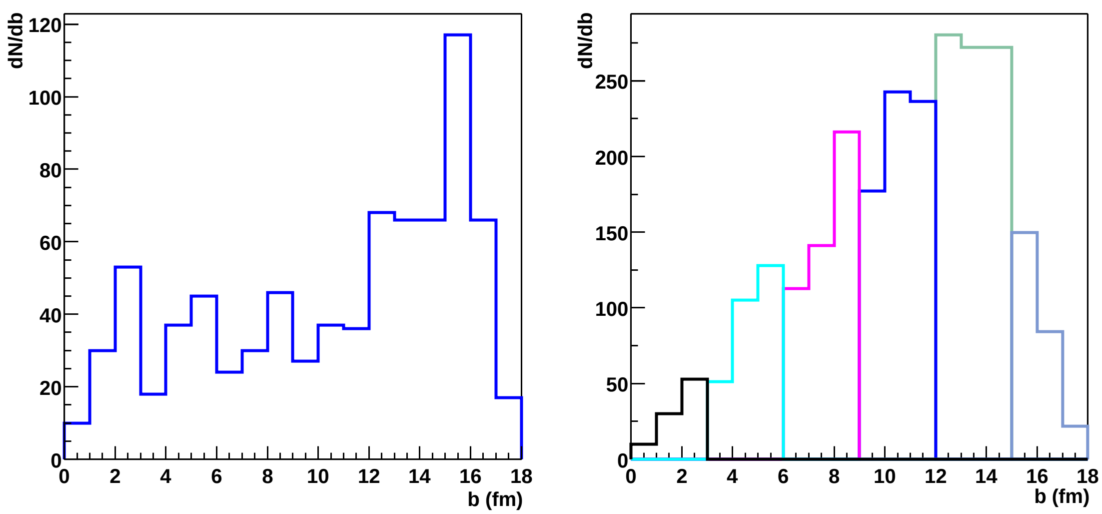

Figure 5.17. Simulated (left) and minimum bias (right) impact parameter distributions.

The correlation between spectators energy detected in hadronic ZDCs and electromagnetic forward energy measured by ZEM is fitted again, since the higher number of events allows a more accurate fit. The five centrality classes previously defined are then selected cutting this correlation as explained before (see fig. 5.18).

The number of participants corresponding to the upper value for each impact parameter interval is evaluated both with the Glauber and with the Hijing model. The resulting values are reported in table 5.9; it can be noticed that there is a systematic difference between the two estimates of about 20 participants.

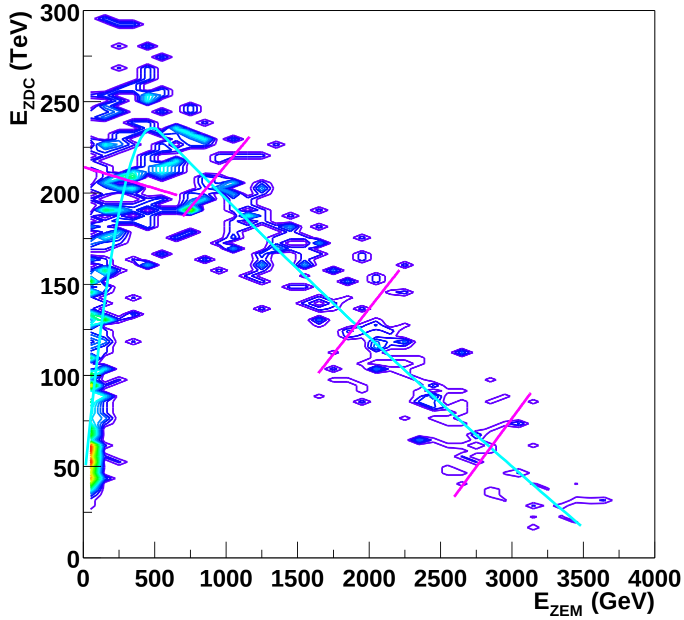

Figure 5.18. Correlation between total energy detected in hadronic ZDCs and energy measured by ZEM. The cuts plotted select the usual centrality classes.

b value	N_{part} from Glauber	N_{part} from HIJING
3 fm	343	361
6 fm	246	271
9 fm	122	151
12 fm	34	46

Table 5.9. Number of spectator for the upper b value of each centrality class.

Using the values provided by the two models, the number of participants is reconstructed in the five centrality classes. Results are plotted in fig. 5.19 and are reported in table 5.10. The results obtained with the two models are comparable. The number of participants evaluated through the HIJING model is always slightly higher compared to the one calculated from the Glauber theory. This discrepancy decreases with increasing centrality, passing from the 20% of the most peripheral class to the 2% of the most central one (results are summarized in table 5.10).

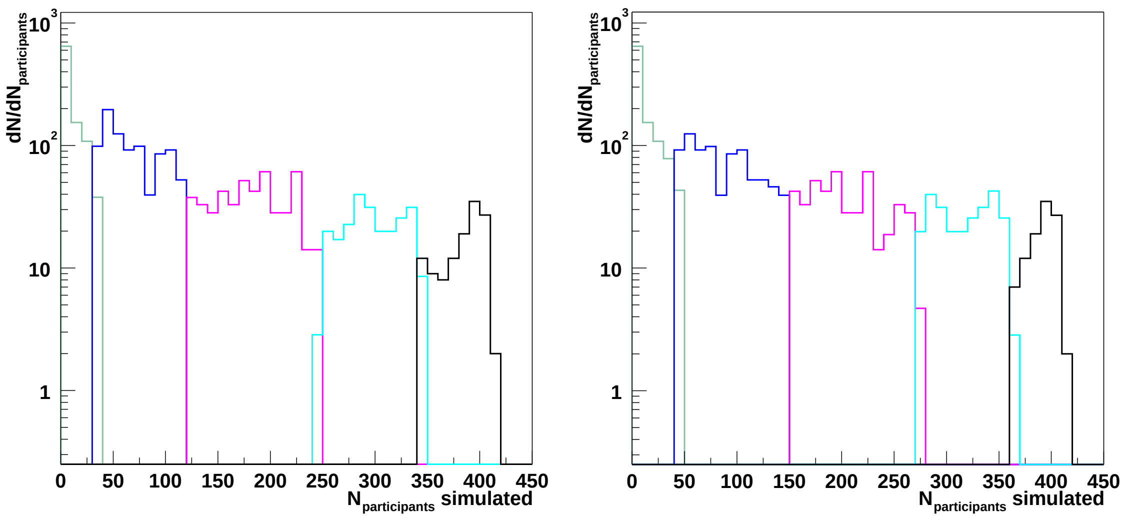

Figure 5.19. Number of participants reconstructed according to Glauber (left) and to HIJING (right) models.

b range (fm)	$<N_{part}^{reco}>$ Glauber	$<N_{part}^{reco}>$ HIJING	$\|\Delta N_{part}^{reco}\|$ normalized
0-3 fm	384 ± 19	392 ± 12	2%
3-6 fm	297 ± 26	317 ± 27	6%
6-9 fm	182 ± 33	204 ± 33	11%
9-12 fm	68 ± 25	86 ± 30	20%
12-18 fm	8 ± 9	10 ± 13	21%

Table 5.10. Mean values of the number of spectators reconstructed using Glauber and HIJING models. The $|\Delta N_{part}^{reco}|$ normalized values are calculated as: $|\Delta N_{part}^{reco}|/(<N_{part}^{reco}>$ HIJING).

Conclusions

Detectors

The design of the Zero Degree Calorimeters for the ALICE experiment has been completed. Their performances have been studied through simulations and the feasibility of the adopted technique for the detection of spectator nucleons at ALICE energies has been demonstrated. Spectator proton losses along the beam line and the production of nuclear fragments have been taken into account in evaluating the detectors acceptance and resolution.

The design of the electromagnetic ZDC has been reviewed and this detector has been shifted from its original position, near the hadronic ZDCs, closer to the interaction point. The reason of this choice is to improve the correlation between the measured energy and the impact parameter of the collision. The new rapidity range covered by the detector assures the complete removal of the ambiguity on centrality determination caused by nuclear fragments production. The use of an air light guide to optically guide the produced Cerenkov light to the photodetector avoids the increase in signal observed in prototypes with fibres tilted at 45°. Results of the test performed on a prototype of the ZEM calorimeter with particle beams have shown that the energy resolution at ALICE energies will be around 2%.

It is important to remind that the information provided by the electromagnetic calorimeters will be used only to discriminate between central and peripheral collisions. The reason for this choice is due to the fact that the correlation between secondaries energy and the impact parameter depends strongly on the model used to describe the interaction. On the contrary the energy carried by spectators measured by the hadronic ZDCs is directly correlated to the geometry of the collision and it is therefore largely model independent.

Centrality determination

Concerning the measurement of centrality with the ZDC, it has been shown that the measurement of spectators energy for both colliding nuclei reduces the fluctuations in the number of spectators and allows the rejection of background. The resolution on centrality measurement has been evaluated taking into account the experimental conditions (namely spectator losses, fragments production and detector resolutions). It has been shown that the resolution does not differ significantly from the intrinsic resolution due to the fluctuations on the number of spectators. This means that the ZDC can provide an unbiased estimation of the centrality of the collision.

The resolution on impact parameter is less than 10% for b>8 fm, it becomes <20% for 3<b<8 fm and is around 55% for the most central collisions with b<3 fm. However the root mean square of the distribution of the reconstructed impact parameter, for a given generated b, is of the order of 1 fm over the whole centrality range. The resolution for most central events is improved if the number of participants is considered instead of the impact parameter. In fact the resolution on the number of participants is less than 10% for N_{part} >250, corresponding, in the Glauber model, to impact parameters b$\lesssim$6.5 fm.

A sample of 1000 Pb-Pb minimum bias events have been produced with HIJING 1.36, using the new code developed for the ZDC simulations. Two methods have been used to reconstruct the impact parameter of the collision and the number of participants from the energy detected in the hadronic ZDCs. The first method provide an event by event estimate of the two quantities. The reconstruction procedure is based on the fit of simulated correlations between the global variables and ZDC energies. In principle the method is sensitive to the model used to describe the interaction. The effect due to background contamination has been evaluated: it is important only for most central collisions and does not strongly affect the centrality determination. The second approach selects centrality classes from the correlation between the total energy measured in hadronic ZDC and the energy detected in the electromagnetic device. Being based on measured quantities, this method has the advantage to be model independent. On the other hand the background contribution due to participants and secondary particles can not be estimated from this correlation. The reconstruction of the centrality of the collisions with both methods gives comparable results. It has been shown that in both cases it is possible to define at least five centrality classes.

The reconstructed number of participants can be sensitive to the model used to estimate N_{part} as a function of centrality. The five centrality classes have been defined using both the Glauber model and the HIJING event generator. The obtained results are comparable, even if HIJING systematically overestimates the number of participants. However the discrepancy is more important for the most peripheral events.